

DISSERTATION

**TiO<sub>2</sub> crystallographic orientation-dependent  
fibrinogen conformation and its effect on  
platelet adhesion and activation**



**FRIEDRICH-SCHILLER-  
UNIVERSITÄT  
JENA**

zur Erlangung des akademischen Grades Doktor-  
Ingenieur(in)(Dr.-Ing.)

vorgelegt dem Rat der Physikalisch Astronomischen  
Fakultät der Friedrich-Schiller-Universität Jena

von M. Sc. Maja Struczyńska (geb. Pieper),  
geboren am 16.06.1994 in Puck, Polen

1. Gutachter: Prof. Klaus D. Jandt

2. Gutachter: Prof. Dr.-Ing. Aldo R. Boccaccini

3. Gutachter: Prof. J. Barbara Nebe

Tag der Disputation: 28.08.2023

*Dedicated to my husband Jakub Struczyński and  
my parents Władysław and Teresa Pieper*



## **Statement of Authorship**

I solemnly declare that I have independently prepared and completed the presented work without undue assistance from third parties or the use of references not cited in literature. Data and ideas which were included directly or indirectly from other sources are cited by referencing the original source.

I did not receive paid assistance or consulting services from PhD consultant or others. Nobody has received direct or indirect monetary benefits for work associated with the content of this submitted thesis.

This work has to date not been submitted domestically or abroad in the current or in a similar version to any other examination board.

I am aware of the applicable regulations for Doctoral Studies of the Faculty of Physics and Astronomy.

I declare on my honor that I have told the truth to the best of my knowledge and have not concealed anything.

Jena, 25<sup>th</sup> March 2023

Signed: Maja Struczyńska



## **Ehrenwörtliche Erklärung**

Ich erkläre hiermit ehrenwörtlich, dass ich die vorliegende Arbeit selbständig, ohne unzulässige Hilfe Dritter und ohne Benutzung anderer als der angegebenen Hilfsmittel und Literatur angefertigt habe. Die aus anderen Quellen direkt oder indirekt übernommenen Daten und Konzepte sind unter Angabe der Quelle gekennzeichnet.

Ich habe hierfür nicht die entgeltliche Hilfe von Vermittlung bzw. Beratungsdiensten (Promotionsberater oder andere Personen) in Anspruch genommen.

Niemand hat von mir unmittelbar oder mittelbar geldwerte Leistungen für Arbeiten erhalten, die im Zusammenhang mit dem Inhalt der vorgelegten Dissertation stehen.

Die Arbeit wurde bisher weder im In- noch im Ausland in gleicher oder ähnlicher Form einer anderen Prüfungsbehörde vorgelegt.

Die geltende Promotionsordnung der Physikalisch-Astronomischen Fakultät ist mir bekannt.

Ich versichere ehrenwörtlich, dass ich nach bestem Wissen die reine Wahrheit gesagt und nichts verschwiegen habe.

Jena, 25th March 2023

Signiert: Maja Struczynska





## Related publications

Within the scope of the present work, several scientific publications were prepared, which have already been published in scientific journals (peer-reviewed) or will be published soon. The following publications have already been published:

1. **M. Struczynska**, I. Firkowska-Boden, K. Scheuer, K. D. Jandt: *Rutile facet-dependent fibrinogen conformation: Why crystallographic orientation matters*, Colloids and Surfaces B: Biointerfaces, 215, 2022, 112506.
2. **M. Struczynska**, I. Firkowska-Boden, N. Levandovsky, R. Henschler, N. Kassir, Klaus D. Jandt: *How crystallographic orientation-induced fibrinogen conformation affects platelet adhesion and activation on TiO<sub>2</sub>*, Advanced Healthcare Materials, 2023, 2202508.

Within the scope of work on related topics, the following publications have been published:

3. I. Firkowska-Boden, C. Helbnig, T. Dauben, **M. Pieper**, K. D. Jandt: *How Nanotopography-Induced Conformational Changes of Fibrinogen Affect Platelet Adhesion and Activation*, Langmuir, 36 (39), 2020, 11573-11580.



## Zugehörige Veröffentlichungen

Im Rahmen der vorliegenden Arbeit wurden mehrere wissenschaftliche Publikationen entstanden, die bereits in wissenschaftlichen Fachzeitschriften (Peer-Reviewed) veröffentlicht wurden bzw. demnächst veröffentlicht wurden. Folgende Publikationen wurden bereits veröffentlicht:

1. **M. Struczynska**, I. Firkowska-Boden, K. Scheuer, K. D. Jandt: *Rutile facet-dependent fibrinogen conformation: Why crystallographic orientation matters*, Colloids and Surfaces B: Biointerfaces, 215, 2022, 112506.
2. **M. Struczynska**, I. Firkowska-Boden, N. Levandovsky, R. Henschler, N. Kassir, Klaus D. Jandt: *How crystallographic orientation-induced fibrinogen conformation affects platelet adhesion and activation on TiO<sub>2</sub>*, Advanced Healthcare Materials, 2023, 2202508.

Im Rahmen der Arbeit verwandter Themen sind folgende Publikationen wurden bereits veröffentlicht:

3. I. Firkowska-Boden, C. Helbnig, T. Dauben, **M. Pieper**, K. D. Jandt: *How Nanotopography-Induced Conformational Changes of Fibrinogen Affect Platelet Adhesion and Activation*, Langmuir, 36 (39), 2020, 11573-11580.



## Abstract

The basic building block of implants, including medical devices, is the biomaterial. The correlation between its structure and properties allows assessment of its potential use in medicine. Material scientists are engaged in studying the structure - property relationship, therefore designing or selecting appropriate biomaterial for implants that perform specific functions. Implant surface deserves special attention, as it is in direct contact with the body fluids, e.g., blood plasma, determining the specificity of the blood components response.

The motivation for the studies presented in this work was an investigation of how the crystallographic orientation, hence the coordination number of surface atoms and their arrangement, affect the biocompatibility of the material. The thrombogenic response of the human body, i.e., the formation of pathological clots on the implant surface, is one of the main problems encountered in biomaterial science for which thrombocytes (platelets) are responsible. It is well known that their adhesion and activation are mediated by proteins, especially human plasma fibrinogen (HPF), containing specific binding sites i.e.,  $\gamma^{400-411}$ . Therefore, strategies to control the HPF conformation upon adsorption on materials, so that specific regions of the protein remain hidden, are constantly being developed.

In the present work, it has been shown that adjustment of the appropriate surface crystallographic orientation, here titanium dioxide (rutile), modulates HPF adsorption in a manner that platelets attach to a lower extent and remain non-active.

The studies were performed on four low-index surfaces of single crystals: (110), (100), (101), and (001). It was observed that despite the similar amount of adsorbed proteins on differently oriented surfaces, various surface atomic structures, and resulting different surface energy and wettability, affected the conformation of HPF. As shown by atomic force spectroscopy (AFM), the low surface energy and hydrophobicity of the (110) surface favored the HPF molecules unfolding, resulting in a trinodular conformation, which is favorable from a thermodynamic point of view. In contrast, the higher undercoordination of atoms on the surfaces (lower coordination number in respect to bulk atoms), and consequently higher surface energy and hydrophilicity, contributed to the HPF adsorption preferentially in a close to native state i.e., globular conformation. Protein conformation-specific reorganization of molecules structure, including the breaking of peptide bonds and the formation of new ones, was confirmed by X-ray photoelectron spectroscopy (XPS). In

addition, the influence of the HPF conformation on the surface energy of the protein-coated substrates was identified, which may find an implication in controlling further processes occurring at the biomaterial - blood interface.

The observed differences in HPF conformation on rutile single crystals suggested a possible different behavior of sequentially attaching platelets. The scanning electron microscope (SEM) visualization, optical microscopy (OM), and analysis of the P-selectin expression levels revealed significantly lower adhesion and activation of platelets on the low energetic and hydrophobic (110) surface compared to other more energetic and therefore hydrophilic surfaces. To explain these observations, the accessibility of the platelet binding sites, depending on the HPF conformation, was investigated. The collected results were the basis for developing a model of the crystallographic orientation-dependent mechanism of platelet adhesion on rutile crystals mediated by HPF. The reduced platelet affinity to the hydrophobic (110) surface was explained by the much lower availability of  $\gamma$ -chains in trinodular HPF than in globular. This indicates the potential antithrombogenicity and biocompatibility of rutile implants with (110) surface crystallographic orientation.

Since the biocompatibility of the material is determined by numerous processes, much remains to be explored in this topic. Therefore, it has been investigated whether polycrystals, which contain multiple differently oriented grains in one sample, can be a relevant and cost-effective alternative for single crystals, in time-consuming studies of crystallographic orientation-dependent biological phenomena. An analysis of HPF adsorption and platelet adhesion on rutile polycrystals was performed, however, this study did not reveal crystallographic orientation-dependent differences in HPF conformation nor platelet activity, which was the case on single crystals. An accurate explanation of these contradictory results was not found during this PhD work, as it requires more extensive characterization of the produced polycrystals and improvement of the polycrystal production method. This leaves it as an open topic for investigation in the future.

To sum up, the studies presented in this work bring numerous valuable information useful for designing highly biocompatible biomaterials for implants, as it provides fundamental insights into crystallographic orientation-dependent platelet - biomaterial interactions. Furthermore, the obtained results point to a new direction of research into the control of cellular response through protein adsorption, to induce specific processes in the human

body. This is a novelty that can significantly contribute to the development of biomedical engineering, as well as improve the effectiveness and safety of currently used implants.





## Zusammenfassung

Die Grundbausteine von Implantaten, einschließlich einiger medizinischer Geräte, sind Biomaterialien. Die Korrelation zwischen der Struktur und den Eigenschaften ermöglicht eine Bewertung des potenziellen Einsatzes in der Medizin. Materialwissenschaftler befassen sich mit der Untersuchung der Beziehung zwischen Struktur und Eigenschaften. Sie entwerfen oder wählen daher geeignete Biomaterialien für Implantate aus, die bestimmte Funktionen erfüllen. Die Implantatoberfläche verdient besondere Aufmerksamkeit, da sie in direktem Kontakt mit den Körperflüssigkeiten, z. B. dem Blutplasma, steht und die Spezifität der Reaktion der Blutkomponenten bestimmt.

Die Motivation für die in dieser Arbeit vorgestellten Studien war eine Untersuchung darüber, wie die kristallografische Orientierung, also die Koordinationszahl der Oberflächenatome und ihre Anordnung, die Biokompatibilität des Materials beeinflussen. Die thrombogene Reaktion des menschlichen Körpers, d.h. die Bildung von pathologischen Gerinnseln auf Implantatoberflächen, ist eines der Hauptprobleme in der Biomaterialwissenschaft, für das die Thrombozyten (Blutplättchen) verantwortlich sind. Es ist bekannt, dass ihre Adhäsion und Aktivierung durch Proteine vermittelt wird, insbesondere durch humanes Plasmafibrinogen (HPF), das spezifische Bindungsstellen, nämlich  $\gamma^{400-411}$ , enthält. Daher werden ständig Strategien entwickelt, um die HPF-Konformation bei der Adsorption an Materialien so zu steuern, dass bestimmte Regionen des Proteins verborgen bleiben.

In der vorliegenden Arbeit wurde anhand von Titanoxid (Rutil) gezeigt, dass die Einstellung der geeigneten kristallografischen Oberflächenorientierung die HPF-Adsorption in einer Weise moduliert, sodass Blutplättchen in geringerem Maße anhaften und inaktiv bleiben.

Die Studien wurden an vier Einkristalloberflächen mit niedrigem Index durchgeführt: (110), (100), (101) und (001). Es wurde beobachtet, dass trotz der ähnlichen Menge an adsorbierten Proteinen auf unterschiedlich ausgerichteten Oberflächen verschiedene atomare Oberflächenstrukturen und die daraus resultierende unterschiedliche Oberflächenenergie und Benetzbarkeit die Konformation von HPF beeinflussen. Mithilfe von Rasterkraftspektroskopie wurde gezeigt, dass die niedrige Oberflächenenergie und Hydrophobizität von der (110) Oberfläche das Entfalten der HPF-Moleküle positiv bedingt.

Dies führt zu einer trinodularen Konformation, welche aus thermodynamischer Sicht günstig ist. Im Gegensatz dazu trug die höhere Unterkoordinierung der Atome auf den Oberflächen (geringere Koordinationszahl im Vergleich zu den Bulk-Atomen) und folglich die höhere Oberflächenenergie und Hydrophilie dazu bei, dass die HPF-Moleküle vorzugsweise in einer nahezu nativen, d.h. globulären Konformation, adsorbiert wurden. Mit Röntgenspektroskopie (XPS) wurde die für die Proteinkonformation spezifische Reorganisation der Molekülstruktur bestätigt, einschließlich des Aufbrechens von Peptidbindungen und der Bildung neuer Bindungen. Darüber hinaus wurde über den Einfluss der HPF-Konformation auf die Oberflächenenergie der proteinbeschichteten Substrate berichtet, was möglicherweise eine Auswirkung auf die Steuerung vieler anderer Prozesse hat, die an der Blut-Biomaterial-Grenzfläche ablaufen.

Die festgestellten Unterschiede in der HPF-Konformation auf Rutil-Einkristallen deuten auf ein mögliches unterschiedliches Verhalten der sequenziellen Anheftung von Blutplättchen hin. Die Visualisierung mit dem Rasterelektronenmikroskop (SEM), dem optischen Mikroskop (OM) und die Analyse der P-Selektin-Expressionsniveaus zeigten eine signifikant geringere Adhäsion und Aktivierung von Blutplättchen auf der (110) Oberfläche im Vergleich zu anderen energetisch höheren und daher hydrophilen Oberflächen. Um dies zu erklären, wurde die konformationsabhängige Sichtbarkeit der primären Bindungsstellen von Blutplättchen untersucht. Die gesammelten Ergebnisse waren die Grundlage für die Erstellung eines Modells des HPF-vermittelten kristallografisch orientierungsabhängigen Plättchen-Adhäsionsmechanismus an Rutil-Einkristallen. Die geringere Affinität der Blutplättchen zur hydrophoben (110) Oberfläche wurde durch die viel geringere Verfügbarkeit von  $\gamma$ -Ketten in trinodularem HPF im Vergleich zu globulärerem erklärt. Dies weist auf die potenzielle Antithrombogenität und Biokompatibilität von Rutil Implantaten mit kristallografischer (110)-Oberflächenorientierung hin.

Da die Biokompatibilität des Materials von zahlreichen Prozessen bestimmt wird, gibt es in diesem Bereich noch viel zu erforschen. Daher wurde untersucht, ob Polykristalle, die mehrere unterschiedlich orientierte Körner in einer Probe enthalten, eine relevante und kosteneffiziente Alternative zu Einkristallen sein können, wenn es um zeitaufwändige Studien von kristallografisch orientierungsabhängigen biologischen Phänomenen geht. Es wurde eine Analyse der HPF-Adsorption und der Thrombozytenadhäsion an Rutil Polykristallen durchgeführt. Diese Studie ergab jedoch im Gegensatz zu Einkristallen

weder kristallografisch orientierungsabhängige Unterschiede in der HPF-Konformation noch in der Thrombozytenaktivität. Eine genaue Erklärung für diese widersprüchlichen Ergebnisse konnte im Rahmen dieser Doktorarbeit nicht gefunden werden, da sie eine umfassendere Charakterisierung der hergestellten Polykristalle und eine Verbesserung der Polykristallherstellungsmethode erfordert. Es bleibt also ein offenes Thema für zukünftige Untersuchungen.

Zusammenfassend lässt sich sagen, dass die in dieser Arbeit vorgestellten Studien zahlreiche wertvolle Informationen liefern, die für die Entwicklung hochgradig biokompatibler Biomaterialien für Implantate nützlich sind, da sie grundlegende Einblicke in die kristallografisch orientierungsabhängigen Wechselwirkungen zwischen Blutplättchen und Biomaterialien bieten. Darüber hinaus weisen die erzielten Ergebnisse auf eine neue Forschungsrichtung hin, die sich mit der Steuerung zellulärer Reaktionen durch Proteinadsorption befasst, um spezifische Prozesse im menschlichen Körper auszulösen. Dies ist eine neue Entdeckung, die wesentlich zur Weiterentwicklung der Biomedizintechnik beiträgt und die Wirksamkeit und Sicherheit der derzeit verwendeten Implantate verbessern kann.



# Table of contents

<b>Statement of Authorship .....</b>	<b>I</b>
<b>Ehrenwörtliche Erklärung.....</b>	<b>III</b>
<b>Related publications .....</b>	<b>V</b>
<b>Zugehörige Veröffentlichungen.....</b>	<b>VII</b>
<b>Abstract.....</b>	<b>IX</b>
<b>Zusammenfassung .....</b>	<b>XIII</b>
<b>Table of contents .....</b>	<b>1</b>
<b>List of Figures.....</b>	<b>5</b>
<b>List of Tables .....</b>	<b>9</b>
<b>List of Abbreviations and Symbols .....</b>	<b>11</b>
<b>1. Introduction .....</b>	<b>13</b>
<b>2. Fundamentals.....</b>	<b>15</b>
2.1. Titanium and its alloys as biomaterials.....	15
2.1.1. Titanium dioxide (TiO <sub>2</sub> ) and its forms .....	15
2.1.2. Crystallographic orientation-dependent physico-chemical properties of rutile surface .....	17
2.2. Fundamentals of the thrombogenic process .....	19
2.2.1. Role of platelets in the material surface-induced thrombogenic process .	20
2.2.2. Role of proteins in the thrombogenic process .....	21
2.2.2.1. Protein structure and adsorption.....	22
2.2.2.2. Blood plasma proteins engaged in a material surface-induced thrombogenic process .....	24
2.2.2.3. Human plasma fibrinogen (HPF) structure .....	25
<b>3. State of the art: Physico-chemical properties of material surface affecting thrombogenic process .....</b>	<b>27</b>
3.1. Impact of physico-chemical properties of a material surface on a protein adsorption.....	28
3.2. Impact of physico-chemical properties of a material surface on HPF conformation and platelet response.....	32

<b>4. Aims of dissertation .....</b>	<b>40</b>
4.1. Open Scientific Questions .....	40
4.2. Hypotheses.....	40
4.3. Objectives .....	41
4.4. Scientific Significance .....	42
<b>5. Crystallographic orientation-dependent HPF adsorption on rutile single crystals.....</b>	<b>43</b>
5.1. Introduction .....	43
5.2. Materials and Methods .....	43
5.2.1. Rutile single crystals .....	43
5.2.2. Protein adsorption .....	44
5.2.3. Colorimetric detection and quantitation of HPF .....	45
5.2.4. Atomic force microscopy analysis (AFM).....	45
5.2.5. X-ray photoelectron spectroscopy (XPS).....	47
5.2.6. Statistical analysis .....	47
5.3. Results and discussion .....	47
5.3.1. Characterization of rutile single crystals.....	47
5.3.2. Analysis of HPF adsorption on rutile single crystals .....	49
5.3.3. XPS analysis.....	55
5.3.4. Surface energy of rutile single crystals after HPF adsorption.....	57
5.3.5. Model of HPF adsorption on rutile single crystals.....	60
5.4. Conclusion.....	61
<b>6. Crystallographic orientation-dependent platelet adhesion and activation on rutile single crystals.....</b>	<b>63</b>
6.1. Introduction .....	63
6.2. Materials and Methods .....	63
6.2.1. Rutile single crystals .....	63
6.2.2. Platelet adhesion on rutile single crystals .....	63
6.2.3. Platelets visualization using scanning electron microscopy (SEM) and optical microscope (OM) .....	64
6.2.4. Immunofluorescence and confocal microscopy .....	64
6.2.5. Statistical analysis .....	65
6.3. Results and Discussion .....	65
6.3.1. Analysis of platelets adhesion and activation .....	65
6.3.2. HPF conformation-dependent visibility of platelet binding sites: Model of crystallographic orientation-dependent platelets adhesion and activation.....	69
6.4. Conclusion.....	71

<b>7. HPF-mediated platelets adhesion and activation on TiO<sub>2</sub> (rutile) polycrystal surface .....</b>	<b>72</b>
7.1. Introduction .....	72
7.2. Materials and Methods .....	74
7.2.1. Rutile polycrystals production and characterization methods .....	74
7.2.2. Protein adsorption studies .....	76
7.2.3. Platelet adhesion and activation analysis .....	76
7.2.4. Statistical analysis .....	77
7.3. Results and Discussion .....	77
7.3.1. Characterization of TiO <sub>2</sub> (rutile) polycrystals .....	77
7.3.2. Crystallographic orientation-dependent platelet adhesion and activation on rutile polycrystal surface .....	79
7.3.3. HPF conformation on thermally etched TiO <sub>2</sub> (rutile) polycrystal .....	82
7.4. Conclusion .....	85
<b>8. Summary .....</b>	<b>86</b>
<b>References .....</b>	<b>88</b>
<b>Acknowledgments .....</b>	<b>106</b>
<b>Appendix .....</b>	<b>107</b>
<b>Curriculum Vitae .....</b>	<b>Fehler! Textmarke nicht definiert.</b>





## List of Figures

**Figure 2.1.** Basic unit cell of rutile with dimensions  $a = b = 0.295 \text{ \AA}$  and  $c = 0.458 \text{ \AA}$  which form slightly distorted octahedra. Blue and yellow balls correspond to titanium and oxygen atoms, respectively. b) Stacking of octahedra in a crystal lattice. Figures were generated using VESTA software.<sup>27</sup>

**Figure 2.2.** Idealized structure of rutile crystal surfaces with (110), (100), (101), and (001) crystallographic orientations. Large blue spheres = titanium cations; small yellow spheres = oxygen anions. Numbers in parentheses indicate coordination numbers of selected surface atoms. Figures were generated using VESTA software.<sup>27</sup>

**Figure 2.3.** Schematic representation of blood - biomaterial interactions showing protein-mediated processes relevant to thrombosis on biomaterials. These processes can interplay with each other.

**Figure 2.4.** Four levels of protein structure. Primary structure specifies the amino acid sequence, i.e., how amino acid residues are connected. Secondary structure defines backbone torsion angles in the amino acid residues. Tertiary structure determines the positions of atoms in a protein in three dimensions. Quaternary structure defines the position and orientation of all proteins in the complex. Molecular structure of proteins taken and adapted from Protein Database (RCSB PDB).<sup>65</sup>

**Figure 2.5.** The major mechanism of platelets adsorption, activation, and aggregation on biomaterials under static conditions (lack of or low blood flow). Resting platelets can bind to available  $\gamma^{400-411}$  sequences in pre-adsorbed HPF. This leads to platelet activation and expression of an activated GP IIb-IIIa receptor. Finally, activated platelets are capable to bind other thrombogenic proteins (RGD sequences) and aggregate.

**Figure 2.6.** Schematic representation of HPF molecule with selected platelet binding sites: primary  $\gamma^{400-411}$  sequences and secondary RGD sequences. Individual hydrophobic D and E domains and hydrophilic  $\alpha C$  parts.  $A\alpha$ ,  $B\beta$ , and  $\gamma$  chains are shown in blue, red, and green colors. Molecular structure of HPF taken and adapted from Protein Database (RCSB PDB).<sup>65</sup>

**Figure 3.1.** Physico-chemical surface properties influencing protein adsorption behavior. Image reproduced from ref.<sup>91</sup>, with permission from Wiley/VCH. Copyright©2017.

**Figure 3.2.** Model of HPF-mediated platelet adhesion and activation on various polymers with different surface wettability. a) Adsorption of HPF by hydrophobic D and E domains to hydrophobic polymers ( $\Theta > 65^\circ$ ) limits the availability of primary platelet binding sites ( $\gamma^{400-411}$ ) for platelets, preventing their adhesion and activation. b) Adsorption of HPF by hydrophilic  $\alpha C$  region to hydrophilic polymers ( $\Theta < 65^\circ$ ) exposes the  $\gamma$ -chain, inducing platelet adhesion and activation. Image reproduced from ref.<sup>155</sup>, with permission from Acta Biomaterialia. Copyright©2017.

**Figure 3.3.** Topography-induced structural changes of HPF. a) HPF orientational and/or conformational changes caused by a) nanofeatures curvature, b) confinement between protrusions, c) nanofeatures edge.

**Figure 3.4.** HPF adsorption and platelet adhesion as a function of the crystal aspect ratio of semicrystalline polymeric surfaces. a) Trinodular conformation observed on lamellar

(LCs) and shish-kebab (SKCs) crystals (aspect ratio > 4), where primary platelet binding sites,  $\gamma^{400-411}$ , are exposed. b) HPF conformation on needle-like (NLCs) crystals (aspect ratio = 1), which enables protein-protein interaction through  $\gamma^{400-405}$  sequences, making only  $\gamma^{406-411}$  sequences accessible to platelets. The aspect ratio of HPF is  $\sim 3$  c) Schematic representation of HPF conformation on semicrystalline polymer surfaces. d) Significantly more pronounced platelet adhesion and activation on LCs and SKCs compared to NLCs due to a higher aspect ratio of the crystalline part than an aspect ratio of HPF. Image reproduced from ref.<sup>139</sup>, with permission of American Chemical Society, 2020.

**Figure 3.5.** a) Schematic representation of grain- and facet-dependent HPF adsorption on strongly thermally etched rutile polycrystal: (i) trinodular conformation of HPF arranged in a ring-like network on a flat stable grain type 1 or single facet wall of grain type 2, (ii) globular assembly on second facet wall of grain type 2, (iii) thin globular layer on irregular less stable grain type 3. b) AFM image of HPF adsorbed on faceted grain type 2 showing HPF molecules in two different conformational states. Image reproduced from ref.<sup>194</sup>, with permission of Acta Biomaterialia.

**Figure 5.1.** a) Raman spectra characteristic for rutile single crystals with a calculated ratio of  $A_{1g}$  to  $E_g$  intensity. b) AFM images of bare rutile single crystals.

**Figure 5.2.** Time- and concentration-dependent HPF adsorption on rutile single crystals. a) AFM visualization of adsorbed HPF on rutile crystals, on the example of the (110) surface. Arrows point out exemplary single proteins. b) Amount of adsorbed HPF determined using BCA assay. Three measurements per sample were performed. Lines next to the bars indicate the statistical differences among groups ( $p > 0.05$ ).

**Figure 5.3.** AFM visualization (200 x 200 nm) of the (110), (100), (101), (001) rutile single crystals with adsorbed HPF. Exemplary molecules are marked with circles. Zoomed images (60 x 60 nm; scale bar 20 nm) in the inset show a single HPF molecule on each surface. Representative profile line of individual molecules supports the visual determination of the protein conformation and allows estimation of its dimensions. A schematic HPF spatial arrangement with marked hydrophobic D and E domains is presented.

**Figure 5.4.** Histogram analysis of the measured HPF length and height distributions adsorbed on rutile single crystals ( $n > 100$ ). A Gaussian-fitted curve overlays each histogram (blue and green curves). The average lengths and heights of the proteins are given above the peaks.

**Figure 5.5.** AFM images (200 nm x 200 nm) of HPF adsorbed on the (110) and (001) rutile single crystals, taken under aqueous conditions. Exemplary molecules are marked with circles.

**Figure 5.6.** Representative survey XPS spectrum of rutile single crystal with marked detected components.

**Figure 5.7.** Deconvolved carbon (C 1s; left images) and nitrogen (N 1s; right images) spectra of HPF-coated (110) and (001) surfaces. Dashed lines correspond to the raw data, while solid lines stand for Gaussian fitting.

**Figure 5.8.** Determined surface energy of rutile single crystals before (yellow color) and after 30 min HPF adsorption (blue color) from solutions with concentrations 0.1 mg/mL and 0.01 mg/mL, respectively. Measurements were performed in air (bars) or aqueous (crosses) conditions. Lines above bars indicate statistical differences ( $p > 0.05$ ) between

§ bare substrates, # HPF-coated substrates (0.1 mg/mL), \* HPF-coated substrates (0.01 mg/mL).

**Figure 5.9.** AFM images (3D) and corresponding adhesion maps of HPF-coated (110) and (001) surfaces. The upper images refer to the (110) surface with marked trinodular proteins and the bottom images to the (001) surface. Images on the right side correspond to represent the adhesion map of single HPF molecules recorded on these surfaces.

**Figure 5.10.** Model of HPF adsorption on rutile single crystals. On low energetic, hydrophobic ( $\Theta \geq 65^\circ$ ) surfaces HPF preferentially adsorb in trinodular conformation, whereas on high energetic, hydrophilic surfaces in globular one. Keep in mind that in the transition water contact angle range for hydrophilicity/hydrophobicity ( $\Theta = 60 - 65^\circ$ ), which applies to (100) and (101) surfaces, HPF adsorbs in both conformations, however, globular structures dominate.

**Figure 6.1.** a) Five morphological forms of platelets observed on rutile single crystals, corresponding to different states of activation, i.e., (i) round, (ii) dendritic, (iii) spread-dendritic, (iv) spread, (v) fully spread. Morphology of platelets after b) 5 min and c) 120 min immersion of rutile crystals in PPP under static conditions.

**Figure 6.2.** Optical microscope images of rutile single crystals immersed in PPP for a) 5 min and b) 120 min. c) Calculated values of surface coverage based on at least four positions per crystal (left axis) and P-selectin expression level obtained by immunochemistry ( $n = 3$ , right axis). d) Visual representation of P-selectin expression (confocal microscopy). Lines above bars indicate statistical differences ( $p > 0.05$ ) in \* surface coverage, and # P-selectin expression level.

**Figure 6.3.** a) Availability of  $\gamma^{400-411}$  sequences in HPF molecules adsorbed on the (110) and the (001) rutile single crystals determined by immunochemistry ( $n = 3$ ).

**Figure 6.4.** Model of HPF-conformation dependent, platelets adhesion and activation on hydrophobic and hydrophilic rutile single crystals. HPF adsorbed by D domains in trinodular conformation on the (110) surface sufficiently limits the visibility of  $\gamma$ -chain (red color), and therefore platelets adhesion and activation. Adsorbed by  $\alpha C$  domains, globular HPF bind and activate platelets due to the accessible  $\gamma$ -chain (green color). Figure not drawn in scale.

**Figure 7.1.** An exemplary method of polycrystal production: a) Powder compression; green-body b) sintering and c) polishing; d) thermal etching.

**Figure 7.2.** Optical microscope image of a thermally etched TiO<sub>2</sub> (rutile) polycrystal surface. Grain size exceeds several tens/hundreds of  $\mu\text{m}$  and grain boundaries are visible. Scale bar represents 500  $\mu\text{m}$ .

**Figure 7.3.** a) Representative SEM image of a thermally etched TiO<sub>2</sub> (rutile) polycrystal surface in an exemplary position. b) EBSD image with a corresponding color-code inverse pole figure map in the inset. (hkl) Miller indices denote lattice planes lying in the macroscopic polycrystal surface. Arrows point to the grains with the (110) and (001) surface crystallographic orientation, which can be recognized in the EBSD image as deep blue and red color. Note, that estimated crystallographic orientations represent the closest approximation to the actual crystallographic orientation of a grain surface.

**Figure 7.4.** Topographic AFM images (200 nm x 200 nm) of bare (110) and (001) grain surface of TiO<sub>2</sub> (rutile) polycrystal.

**Figure 7.5.** SEM images of a) (110) and b) (001) grains surfaces of TiO<sub>2</sub> (rutile) polycrystal exposed to platelets for 120 min under static conditions, taken on three grains marked by the same color, however in various surface positions. Upper images refer to the same grain but show different magnifications.

**Figure 7.6.** Confocal microscope images of expressed P-selectin on (110) and (001) grain surfaces after 120 min exposition of rutile polycrystal for PPP under static conditions.

**Figure 7.7.** EBSD map of TiO<sub>2</sub> (rutile) polycrystal surface in a second exemplary position. As indicated by arrows, the (100), (101), and high-index grains surfaces can be recognized in the EBSD image as green, orange, and bright yellow, respectively. Note, that estimated crystallographic orientations of grains surfaces represent the closest approximation to the actual crystallographic orientation. SEM images of (100), (101), and high-index surfaces exposed to platelets for 120 min under static conditions were taken on two/three grains marked by the same color, however in various surface positions. Upper images refer to the same grain but show different magnifications.

**Figure 7.8.** Distribution of fluorescently-labeled HPF on (110) and (001) grains surfaces of TiO<sub>2</sub> (rutile) polycrystal imaged by confocal microscopy.

**Figure 7.9.** a) AFM images of (110) and (001) grain surfaces of TiO<sub>2</sub> (rutile) polycrystal coated by HPF (C = 0.01 mg/mL, t = 5 min) taken under air conditions. Images show trinodular HPF irrespective of surface crystallographic orientation. b) Confocal microscopy images of available  $\gamma^{400-411}$  on polycrystal grains i.e., sequences available to bind platelets.

**Figure A1.** SEM images of rutile single crystals immersed for a) 5 min and b) 120 min in PPP under static conditions.

## List of Tables

**Table 2.1.** Crystallographic orientation-dependent properties of TiO<sub>2</sub> (rutile) surfaces.

**Table 2.2.** Major platelet receptors for thrombogenic blood plasma proteins and their characteristics.

**Table 5.1.** Crystallographic orientation-dependent properties of rutile single crystals.

**Table 5.2.** Composition of the (110), (100), (101), and (001) rutile single crystals before and after HPF adsorption (5 min, 0.01 mg/mL).

**Table A1.** Elemental composition on rutile single crystals surface after HPF adsorption.



## List of Abbreviations and Symbols

$\alpha$ , $\beta$ , and $\gamma$	Polypeptide chains
$\alpha$ C	Nodules in the D domains
A $\alpha$ <sup>572-574</sup>	572-574 peptide sequences in A $\alpha$ chain
A $\alpha$ 95-97	95-97 peptide sequences in A $\alpha$ chain
$\alpha$ IIb $\beta$ 3	Glycoproteins IIb/IIIa
$\gamma$ 400-411	400-411 peptide sequences in $\gamma$ chain
$\gamma$ 254-256	254-256 peptide sequences in $\gamma$ chain
$\gamma_{\text{tip}}$ and $\gamma_{\text{sample}}$	Surface energy of AFM tip and rutile crystals
$\Gamma$	Interfacial energy
AFM	Atomic force spectroscopy
BCA	Micro Bicinchoninic Acid Protein Assay
BSA	Bovine serum albumin
CH <sub>3</sub>	Methyl groups
C-N	Amine groups
C-NH <sub>3</sub> <sup>+</sup>	Protonated amine groups
C=O	Carbon and oxygen bond
CP	Commercially pure titanium
D and E	D and E domain of fibrinogen
DLC	Diamond-like coatings
DMT	Derjagin-Muller-Toropov model
EBSD	Electron backscatter diffraction
E <sub>g</sub>	A band at 448 cm <sup>-1</sup> in X-ray photoelectron spectroscopy spectrum
Fn	Fibronectin
FITC	Fluorescently-labeled fibrinogen
HOPG	highly ordered pyrolytic graphite
HPF	Human plasma fibrinogen
HSA	Human serum albumin
LCs	Lamellar crystals
Milli-Q water	Pure water with a conductivity of 18.2 M $\Omega$ ·cm <sup>-1</sup>
N-C=O	Peptide groups
NLCc	Needle-like crystals
OM	Optical microscopy
O	Oxygen
O-Ti-O	Bonds between oxygen and titanium
QI mode	Quantitative Imaging mode
PBS	Phosphate-buffered saline solution
pH	Hydrogen ion exponent
PHMS	Polyhydroxymethylsiloxane
PLGA	Poly (lactide-co-glycolic acid)
PMMA	Poly(methyl methacrylate)
PPP	Pooled platelet plasma concentrate

PS	Polystyrene
PU	Polyetherurethanes
PUU	Polyurethaneurea
QI	Quantitative imaging mode
RGD	Arginine, glycine, aspartic acid
$R_q$	Root mean square roughness
SDS	sodium dodecyl sulphate
SEM	Scanning electron microscopy
SKCs	Shish-kebab crystals
THRP2 and R320	Powders used for polycrystals production
Ti	Titanium
$TiO_2$	Titanium dioxide
Ti-6Al-4V	Titanium-Aluminum-Vanadium
UV-Vis	Ultraviolet-visible spectroscopy
$V_n$	Vitronectin
vWF	von Willebrand factor
XPS	X-ray photoelectron spectroscopy



# 1. Introduction

The development of highly biocompatible and safe implants, including medical devices, is essential due to the constantly increasing number of people requiring hospitalization.<sup>1</sup> Biomaterials according to *European Society for Biomaterials Consensus Conference II* are defined as “materials intended to interface with biological systems to evaluate, treat, augment, or replace any tissue, organ, or function of the body”.<sup>2</sup> The appropriate response of the human body to contact with an artificial material is pivotal for successful patient treatment and support of bodily functions.<sup>3</sup> However, currently used in medicine biomaterials still have some shortcomings, for example, limited biocompatibility, which motivates further modifications or design of new ones.

Knowledge of fundamental processes that occur at the blood - biomaterial interface is key for predicting the biocompatibility of implants that would induce a proper host response without any undesired side effects. Within seconds after biomaterial implantation, plasma proteins are adsorbed onto its surface interacting with a previously adsorbed layer of water and inorganic salt ions.<sup>4</sup> Proteins are adhesion initiators and signal mediators for bacteria or cells, which in turn drives further biological processes such as wound healing, infections, inflammation, or thrombosis.<sup>5</sup> Therefore, implant design is a complex process requiring the study of cellular responses to pre-adsorbed proteins. Surface science is one of the indispensable elements that point to the direction of biomaterials development, as it investigates protein-mediated cell attachment concerning surface properties such as material chemistry and topography.

Among the most commonly used materials for the production of bone implants, endoprostheses, mechanical heart valves or biosensors are titanium and its alloys, due to their favorable mechanical properties.<sup>6,7</sup> In addition, their high biocompatibility and good corrosion resistance are ensured by an oxide layer on the surface, mainly titanium dioxide (TiO<sub>2</sub>), which immediately covers titanium implants upon contact with air.<sup>8</sup> Despite these imposing advantages, placement of titanium implants into the human body still carries the risk of complications, mainly related to thrombosis.<sup>9</sup> It is a phenomenon of pathological clot formation on biomaterials surface, which can detach and enter the bloodstream, finally provoking vessel occlusion, patient stroke, or even death.<sup>10</sup> It is widely recognized that clot formation is determined by platelets adhesion and activation,

which in turn is governed by the adsorption of plasma proteins, especially human plasma fibrinogen (HPF).<sup>11</sup> Nevertheless, numerous studies have shown that not the amount, but the conformation of HPF, which decides exposure of platelet binding sites, is a key regulator of blood clotting.<sup>12</sup> This discovery contributed to the widespread interest in the possibility of reducing the risk of pathological clot formation by manipulating the HPF conformation (folding in space), controlled by the physico-chemical parameters of biomaterials surface. Recently, it has been disclosed that surfaces may even hold the key to explaining prothrombotic status in patients with COVID infection.<sup>13</sup>

Materials science is the essence of predicting how structures of materials affect their properties and subsequently performance or applications. This dissertation has been devoted to determining whether TiO<sub>2</sub> (rutile) crystals with specific surface crystallographic orientations can serve as a tool to induce specific characteristics of implants surface to reduce their thrombogenicity.

Characteristics of rutile crystals, HPF structure, and platelets are presented in Chapter 2. Fundamental knowledge about protein adsorption and cellular response, representing the first step of all biological reactions, has been collected. In Chapter 3, the current state of the art in surface-dependent HPF adsorption and platelet adhesion have been reviewed. Collected information provided a background for the formulation of hypotheses and objectives of this work, presented in Chapter 4. Studies results of crystallographic orientation-dependent HPF adsorption and platelets adhesion on the rutile single crystals are presented in Chapters 5 and 6, respectively. Finally, in Chapter 7, the characterization of HPF-mediated platelet behavior on specific grains surfaces of biomedically relevant rutile polycrystals is discussed, and the possibility of its usage for the study of crystallographic orientation-dependent biological phenomena is evaluated.

It is expected that the scope of this work will stimulate further scientific discussion on the attachment of other cells and bacteria to crystalline surfaces and encourage research on this topic. Observations presented here are intended to point to new routes for the design of biointerfaces and surfaces of blood-contacting materials to produce biocompatible implants, that fully perform their intended functions.

## 2. Fundamentals

### 2.1. Titanium and its alloys as biomaterials

Metals have broad potential applications in materials science, tissue engineering, and biomedicine, due to their appropriate mechanical properties that no other class of biomaterials can replicate. Their usage is desirable in particular in the case of medical devices, for example, artificial hearts or ventricular assist devices, requiring high strength, stiffness, or cyclic-loading fatigue resistance.<sup>14</sup> In the 1940s, titanium (Ti) and its alloys were discovered to be valuable materials for a wide range of medical applications and nowadays are at the top of the list of the most common biomaterials used for implants, medical devices, and surgical instruments.<sup>15</sup> The most widespread are commercially pure (CP) titanium or Titanium–Aluminum–Vanadium (Ti–6Al–4V) alloy.<sup>16</sup> More specifically, titanium-based materials have found application in the cardiovascular field, for example as cardiac implants, such as stents, rotor pumps, and heart valve rings.<sup>17</sup> They are also used in dentistry as a component of prosthetic fillers (inlays, crowns, bridges) or in orthopedics as dynamic parts (skeletal prostheses, maxillofacial devices, elements of hip and knee prostheses).<sup>18</sup> Nevertheless, large biocompatibility, chemical inertness, and corrosion resistance of Ti implants are related to spontaneously forming upon contact with air, surface oxide layer, composed mainly of stable and amorphous TiO<sub>2</sub>.<sup>19,20</sup> In addition, numerous methods have been developed, such as surface chemical treatment, coating or anodizing, to form a TiO<sub>2</sub> layer, not only on pure Ti but also on other materials as well.<sup>21,22</sup> Dependent on the manufacturing process and parameters involved, the oxide layer may possess also crystalline microstructure, characterized by strictly defined long-range order, which is not observed in amorphous material. When considering reactions on an atomic scale, the crystalline forms usually serve as a first approximation model to describe biological phenomena occurring at the TiO<sub>2</sub> layer-blood interface.<sup>19</sup>

#### 2.1.1. Titanium dioxide (TiO<sub>2</sub>) and its forms

TiO<sub>2</sub> naturally crystallizes in three major polymorphs: brookite, anatase, and rutile.<sup>23</sup> However, current technology allows only the latter two to be used for medical applications.<sup>23</sup> The substantial attention of researchers has been devoted to rutile due to

its highest stability under physiologic conditions and biocompatibility among others forms.<sup>24</sup> This is essential to ensure constant biological performance and safety of implants in the human body.

A basic rutile unit cell has a tetragonal P4/mm structure with lattice parameters  $a = b = 0.295 \text{ \AA}$  and  $c = 0.458 \text{ \AA}$  as shown in Figure 2.1. a).<sup>25</sup> Ti atoms occupy the body-center and corners of the unit cell. In a bulk, each titanium atom is surrounded by an octahedron of six oxygen (O) atoms. The two bonds between Ti and O are slightly longer than others. As presented in Figure 2.1. b), in crystal lattice neighboring octahedra share one corner along with  $\langle 110 \rangle$  directions and are stacked with their long axis alternating by  $90^\circ$ . The stacking octahedra result in six-fold coordinated Ti and three-fold O atoms in a bulk material.<sup>26</sup>

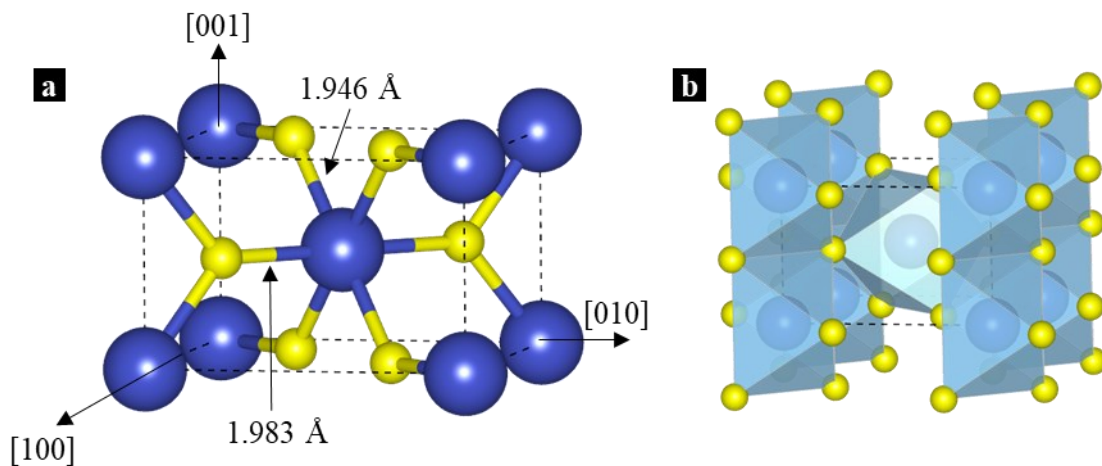


**Figure 2.1.** a) Basic unit cell of rutile with dimensions  $a = b = 0.295 \text{ \AA}$  and  $c = 0.458 \text{ \AA}$  which form slightly distorted octahedra. Blue and yellow balls correspond to titanium and oxygen atoms, respectively. b) Stacking of octahedra in a crystal lattice. Figures were generated using VESTA software.<sup>27</sup>

Although numerous rutile-coated implants are currently available for clinical use, their development still is an active area of research to improve their biological performance. In this dissertation, attention is focused on rutile surface crystallographic orientation, as an important parameter influencing biological reactions.

### 2.1.2. Crystallographic orientation-dependent physico-chemical properties of rutile surface

Since a material surface is in direct contact with blood plasma after implant placement, in-depth knowledge about its atomic structure is key for understanding its unique, physico-chemical properties and determining the appropriate crystal orientation for a particular application. This is a fundamental task for materials scientists.

On a rutile surface, its ordered structure is cut in different ways, resulting in specific patterns of surface atoms coordination (number of atom neighbors) that differ from a bulk. The disruption of intermolecular bonds upon surface creation and the density of undercoordinated (dangling) bonds guide surface physico-chemical properties.<sup>28</sup> In the literature, the structure and properties of the three low-index (110), (100) and (101) surfaces are the most widely described, which due to relatively high stability are preferentially formed during crystal growth and therefore occur most commonly in nature.<sup>23,25</sup> Moreover, despite the instability of the (001) surface, it is frequently studied and taken for comparison due to substantial differences in its structure compared to others, and therefore varying properties. Atomic arrangements on four surfaces of rutile crystal, assuming they are ideal cuts through the rutile structure at the appropriate angle, are presented in [Figure 2.2](#).

As shown in [Table 2.1](#), the coordination number of surface titanium atoms in these rutile crystals is in the range of four to six, while oxygen is two or three. The lower coordination number correlates with higher atoms undercoordination with respect to bulk, a higher number of dangling bonds, and therefore higher surface energy ( $\gamma$ ).<sup>26</sup> Surface energy quantitatively measures the disruption of the intermolecular bond during surface formation, in other words, required work to form a unit area of the surface. Presence of only four coordinated Ti atoms and two coordinated O atoms on the (001) surface results in its highest energy. According to computer simulations, the surface energy of rutile crystals increases in order  $(110) < (100) < (101) < (001)$ , as shown in [Table 2.1](#).<sup>28-30</sup> Keep in mind that the presence of energetically unfavorable dangling bonds on a surface leads to subtle surface atoms relaxation, which refers to a change in surface atoms positions, compared to a bulk crystal structure. Therefore, to evaluate phenomena occurring on the material surface, relaxed surface energy values are considered, which accurately describe

its properties. Values given in Table 2.1., correspond to the relaxed surfaces of rutile crystals.

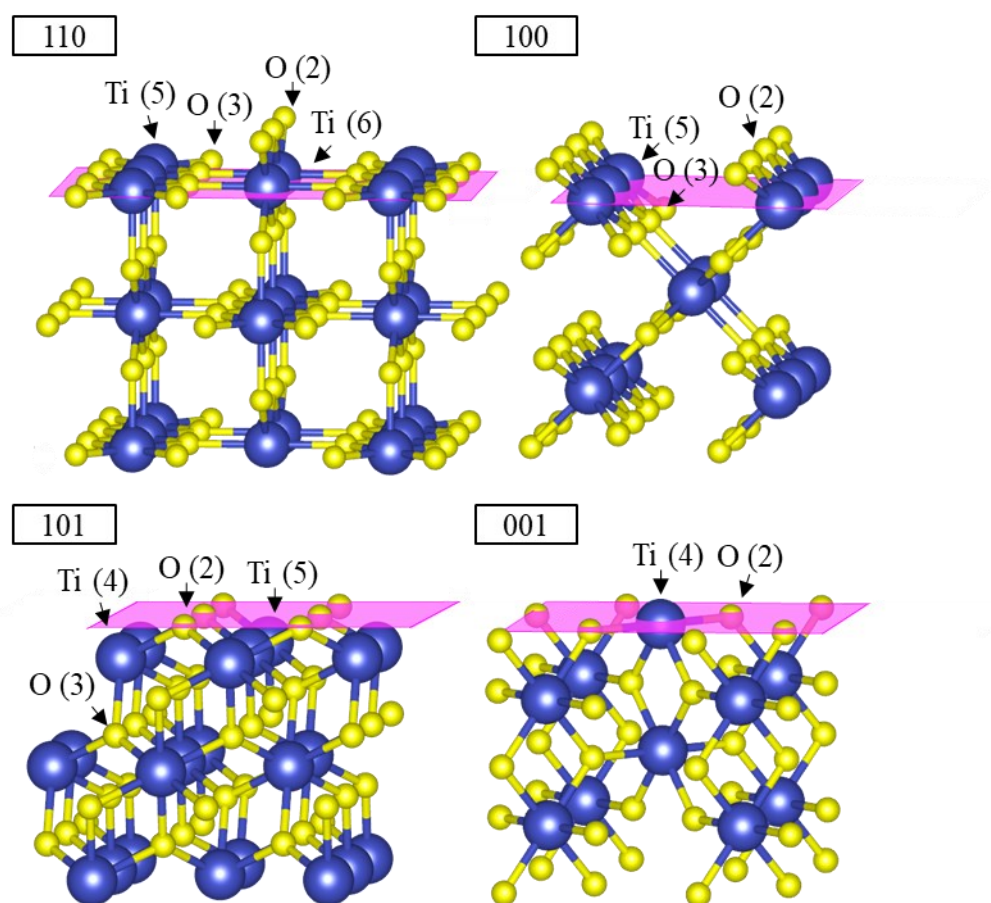


**Figure 2.2.** Idealized structure of rutile crystal surfaces with (110), (100), (101), and (001) crystallographic orientations. Large blue spheres = titanium cations; small yellow spheres = oxygen anions. Numbers in parentheses indicate coordination numbers of selected surface atoms. Figures were generated using VESTA software.<sup>27</sup>

**Table 2.1.** Crystallographic orientation-dependent properties of TiO<sub>2</sub> (rutile) surfaces.

Orientation	Thermodynamic stability	Coordination numbers of surface atoms <sup>29</sup>	Relaxed surface energy [J/m <sup>2</sup> ] <sup>30</sup>	Unsaturation [nm <sup>-2</sup> ] <sup>28</sup>
(110)	Stable	Ti (6,5) O(2,3)	0.96	10.24
(100)	Stable	Ti(5), O(2,3)	1.01	14.47
(101)	Medium	Ti (5,4), O(2,3)	1.41	15.59
(001)	Unstable	Ti(4), O(2)	1.90	18.50

Undercoordination of surface Ti atoms has also an impact on the bonding potential of water molecules and thus determines the nature of their adsorption i.e., dissociative or molecular.<sup>31</sup> The highest density of undercoordinated atoms i.e., the unsaturation of the (001) surface (Table 2.1.), causes the highest probability to dissociate water molecules from an environment and strongly attracts the hydroxyl groups (-OH) via chemisorption.<sup>32</sup> In contrast, the unsaturation of the (110) surface is the lowest, and most of the studies revealed molecular adsorption of water.<sup>33,34</sup> Since a water layer is created on a material surface immediately after implant placement, before the diffusion of proteins or cells, it is a direct mediator of any biological reactions at the blood - biomaterial interface.

This variety of structure-dependent properties of rutile surfaces arouses high interest among material scientists due to their potential multifunctionality. In this dissertation, the possibility of adjusting proper atomic order on the rutile surface to improve the biological performance of implants is investigated.

## **2.2.Fundamentals of the thrombogenic process**

Despite the benefits of coating implants with a TiO<sub>2</sub> layer, thrombosis (blood clotting) at the implant - blood interface is still an unresolved problem.<sup>35</sup> Pathological clot formation is a shortcoming of numerous blood-contacting medical devices such as stents, artificial hearts, intravascular catheters, or valves.<sup>36,37</sup> This is a dangerous phenomenon because dislodged clots can enter the bloodstream and occlude blood vessels, which in turn leads to various complications e.g., myocardial infarction, organ dysfunction, neuropsychological impairment, or even patient death.<sup>38</sup>

Medical device-induced thrombosis occurs as a result of the pathology of blood components (hypercoagulability), impaired blood flow, or specific physico-chemical properties of a material surface.<sup>39</sup> Blood - biomaterial interactions induce a series of complex events responsible for clot formation: adhesion and activation of platelets/leukocytes, and activation of complement/coagulation systems, which are mediated by proteins (Figure 2.3.). Depending on the type of medical device, implant location, or geometry, various biological pathways can interplay, making the thrombogenicity phenomenon even more complex.

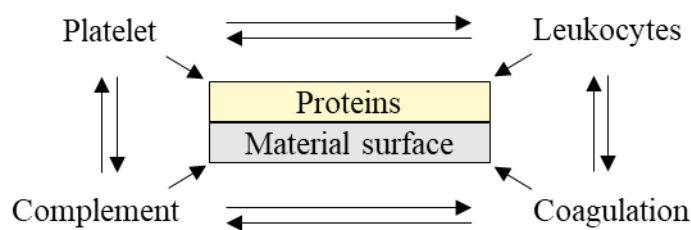


**Figure 2.3.** Schematic representation of blood - biomaterial interactions showing protein-mediated processes relevant to thrombosis on biomaterials. These processes can interplay with each other.

In clinical practice, various drug therapies with anticoagulants and/or antiplatelet agents have been expanded to prevent blood clotting, however, simultaneously multitude of undesirable side-effects have been reported.<sup>40</sup> Moreover, medication does not ensure long-term implant functioning due to anticoagulant depletion after a prolonged usage period.<sup>41</sup> Therefore, other strategies have been developed to prevent blood clotting.

For many years, material scientists have been working on the optimization of material surface properties to control platelets adhesion, which determines the clot formation process.<sup>11</sup> So far, the specific mechanism of platelets attachment is not fully defined, however, it is known that the composition of a pre-adsorbed protein layer and protein conformation are of key importance for signal mediation from the material surface.<sup>42</sup> This dissertation is devoted to understanding the fundamentals of thrombogenic events induced by specific physico-chemical properties of materials surfaces. The following chapter provides a general description of platelets and an overview of plasma proteins engaged in this process.

### **2.2.1. Role of platelets in the material surface-induced thrombogenic process**

Platelets are disc-shaped cells with a diameter of 2 - 3  $\mu\text{m}$ .<sup>43</sup> Their concentration in human blood plasma serves in the range of  $1.5 - 3.5 \times 10^5$  cells/ $\mu\text{L}$  and the main function is the prevention of blood loss upon injury by blood clot formation.<sup>44</sup> Nevertheless, contact of artificial material with blood may lead to uncontrolled clotting, which is manifested by extensive platelet adhesion and activation on a material surface.<sup>45</sup> Platelets normally circulate in the bloodstream in a resting state, where co-exist with other blood components. After biomaterial implantation, platelets do not interact directly with its surface but rather bind to the specific pre-adsorbed proteins through receptors i.e.,



glycoproteins (GP), protruding from the above cell membrane.<sup>46</sup> The major receptors, their content per platelet, and ligands are listed in [Table 2.2](#).

**Table 2.2.** Major platelet receptors for thrombogenic blood plasma proteins and their characteristics.<sup>47</sup>

Glycoprotein	Copies per platelet	Ligand	Comments
GP IIb-IIIa ( $\alpha_{IIb}\beta_3$ )	80 000	HPF, vWF, Fn, Vn	key role in clot formation, binding only after platelet activation (except HPF), aggregation
GP Ib-IX-V	50 000	vWF	arresting flowing platelets under high blood shear rates
GPIc/IIa ( $\alpha_5\beta_1$ )	2 000	Fn	supporting role in clot formation, stabilizing thrombus growth
$\alpha_v\beta_3$	100	HPF, vWF, Fn, Vn	supporting role in clot formation, stabilizing thrombus growth

The most abundant is GP IIb-IIIa (half of all receptors). Its ligands can be found in a structure of proteins such as fibronectin (Fn), vitronectin (Vn), von Willebrand factor (vWF), or human plasma fibrinogen (HPF).<sup>48</sup> However, binding to those proteins usually requires the prior activation of platelets.<sup>49</sup> Unique is HPF as it has the potential to bind platelets regardless of their state. Moreover, it can initiate the activation process.<sup>46</sup> The latter is accompanied by a release of the platelets' interior content (e.g. P-selectin) to a membrane, which consequently leads to the cell morphological changes.<sup>47</sup> Activation is characterized by an increase in size and rearrangement of the cytoskeletal, which is manifested by a change of shape, from discoidal to spread, with the appearance of appendages, termed pseudopods.<sup>50</sup> Consequently, platelets start to communicate with each other, form aggregates and subsequently blood clots, therefore these phenomena are the main indicators of biomaterials thrombogenicity. Furthermore, it has been found that other, mentioned in [Table 2.2.](#), receptors play a supportive role in clot formation.<sup>51</sup> In an attempt to understand how proteins mediate the behavior of platelets, it is necessary to thoroughly familiarize with their structure and functionalities at the molecular level.

### 2.2.2. Role of proteins in the thrombogenic process

Protein adsorption is initiated several seconds after biomaterial implantation, outpacing platelets adhesion.<sup>52</sup> This is the first stage of biological response, following interaction with water and ions from body fluids. Adsorbed proteins are the mediators of various

molecules, cells, and bacteria adhesion.<sup>53</sup> Therefore, a protein layer is a key element for proper tissue development, while in the case of blood-contacting medical devices, may initiate thrombosis.

Adsorption process for each type of protein proceeds differently due to characteristic diffusion rates, affinity to a substrate, as well as a relative concentration in blood.<sup>54</sup> Each protein has unique functions, which are correlated with its structure. Specific regions can be recognized by cells, yet their accessibility depends on the spatial arrangement of a protein.<sup>55</sup> The susceptibility of proteins to structural reorganization is determined by their stability. The control and prediction of protein structure upon adsorption are primary and the most important steps in the study of biological responses to contact with biomaterial.

### **2.2.2.1. Protein structure and adsorption**

Proteins are complex biopolymers composed of 20 amino acids occurring as monomeric units with a multitude of additional side chains, which define the primary structure (Figure 2.4).<sup>56</sup> As a result of intramolecular hydrogen bonds, the secondary structure of a protein ( $\alpha$ -helix,  $\beta$ -harmonica) is formed, while ionic, hydrophobic interactions and sulfide bridges are responsible for the tertiary structure. Due to interactions between polypeptide chains, each having a specific 1<sup>st</sup>, 2<sup>nd</sup>, and 3<sup>rd</sup> order structure, a quaternary structure is formed.<sup>57</sup> Finally, each folded protein contains characteristic regions with hydrophobic or hydrophilic, positively or negatively charged moieties.<sup>58</sup> This unique diversity of basic building blocks contributes to the complexity of the protein structures and functions. The role of proteins in the human body are: 1) growth and maintenance of tissues, 2) transport 3) nutrition and storing, 4) biochemical reaction catalysis (enzymes), 5) regulation and coordination of chemical processes in cells and tissues (hormones), 6) tissue contractile or motility, and 7) defense (immune proteins).<sup>59</sup>

Complicated structure makes an issue of protein adsorption on biomaterials difficult to model. This process is protein type-specific and involves many aspects such as transport (diffusion), adsorption/desorption steps, orientational and conformational changes, as well as protein-protein interactions.<sup>60,61</sup> Conformational changes i.e., spatial restructuration due to a movement of certain groups of atoms in relation to others, are associated with loss of secondary structure and depend on protein dimension, composition, and stability.<sup>62</sup> Small and “rigid” proteins, e.g. albumin, have a lower tendency to conformational changes compared to larger, “soft” ones, such as

immunoglobulin G or fibrinogen.<sup>63</sup> Finally, conformational changes have a direct impact on the number of interaction points and thus bond strength between protein and material surface.<sup>53</sup> It has been widely recognized that the process of a protein layer formation depends on the nature of a protein, physico-chemical properties of an adhesive surface, and environmental factors.<sup>64</sup>

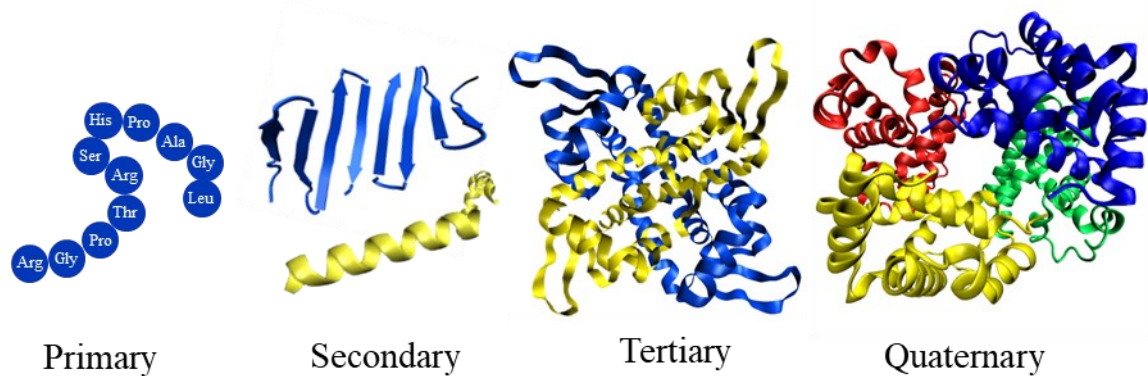


**Figure 2.4.** Four levels of protein structure. Primary structure specifies the amino acid sequence, i.e., how amino acid residues are connected. Secondary structure defines backbone torsion angles in the amino acid residues. Tertiary structure determines the positions of atoms in a protein in three dimensions. Quaternary structure defines the position and orientation of all proteins in the complex. Molecular structure of proteins taken and adapted from Protein Database (RCSB PDB).<sup>65</sup>

A protein layer formed on a material surface is a dynamic unit that evolves over time and its final stable composition differs from the initial one. Blood plasma contains as many as 4500 different proteins and peptides, that compete for the possibility of adsorption.<sup>66</sup> Biomaterial surface is coated firstly with the fastest diffusing proteins, such as albumin, due to their low molecular weight and high concentration in blood plasma.<sup>60</sup> However, these initially adsorbed proteins are usually displaced by larger ones (e.g. fibrinogen), which have more binding sites to interact with surfaces and in turn higher potential to be adsorbed on a biomaterial surface.<sup>67,68</sup> This phenomenon is called Vroman effect.<sup>69</sup> Finally, the high energy required to break all contact points between protein and surface makes the protein adsorption irreversible. Since the adsorption process is surface-dependent and involves many displacements/replacement steps, modeling a protein layer composition remains a challenge. A protein layer on biomaterial converts it into biologically recognizable material, thus understanding the role of an individual protein in biological response is essential background for designing biocompatible implants.

### 2.2.2.2. Blood plasma proteins engaged in a material surface-induced thrombogenic process

The functionality of a protein is strictly determined by specific regions recognizable by distinct cells. As it was mentioned above (Chapter 2.2.1.), platelets interact with proteins such as Fn<sup>70</sup>, Vn<sup>71</sup>, vWF<sup>72</sup>, and HPF<sup>73</sup> containing specific ligands, in particular, Arg-Gly-Asp (RGD) amino acid sequences. However, in a resting platelet state, the most abundant GP IIb-IIIa integrins are bent, and therefore the RGD sequences are unable to establish initial contact with sufficiently high affinity to bind the platelets.<sup>74</sup> Binding by RGD ligands requires prior platelet activation inducing GP IIb-IIIa rearrangement.<sup>46</sup> Until recently, it was not fully understood how non-activated platelets in the blood can detect the adsorbed protein layer, although it was known that it is associated with adsorbed HPF.<sup>75</sup> It was highlighted in the study by Tsai *et al.*, where platelet adhesion to biomaterials preadsorbed by afibrinogenemic plasma was limited, however, greatly increased if exogenous purified HPF was added.<sup>70</sup> Similar observations were not reported for other thrombogenic proteins (vWF, Fn, or Vn).<sup>75</sup> This extraordinary function of HPF turned out to be due to its bifunctionality, i.e. the presence of additional binding sequences  $\gamma^{400-411}$  in its structure (see Chapter 2.2.2.3.).<sup>76</sup> HPF-mediated clot formation mechanism is schematically presented in [Figure 2.5](#). It has been found that after HPF-induced platelets adhesion and activation, an expression of functionally competent GP IIb-IIIa allows for full utilization of its binding potential through multiple focal contacts with HPF and other thrombogenic proteins by RGD sequences.<sup>49</sup> Additionally, activated platelets can bind thrombogenic proteins from plasma, amplify an activation of other platelets, and finally, aggregate.<sup>46</sup> Since HPF has been identified as a prominent component of the adsorbed protein layer due to its high affinity to various materials, it can be considered a major indicator of thrombogenic events.<sup>77,78</sup> Keep in mind that, under high shear rates conditions ( $>1000\text{ s}^{-1}$ ) induced by blood circulation, vWF and binding by GP Ib-IX-V are essential to pre-arrest flowing platelets.<sup>78</sup>

Notwithstanding, information about platelets adhesion via protein functional sites is still only partially understood, thus clot formation process on biomaterials is not yet conclusive. Collection of detailed knowledge about HPF structure, e.g., size, charge, hydrophobicity, structural stability, and its behavior upon adsorption on a material surface, facilitates the prediction of platelet binding sites availability and thus an occurrence of thrombogenic phenomena.

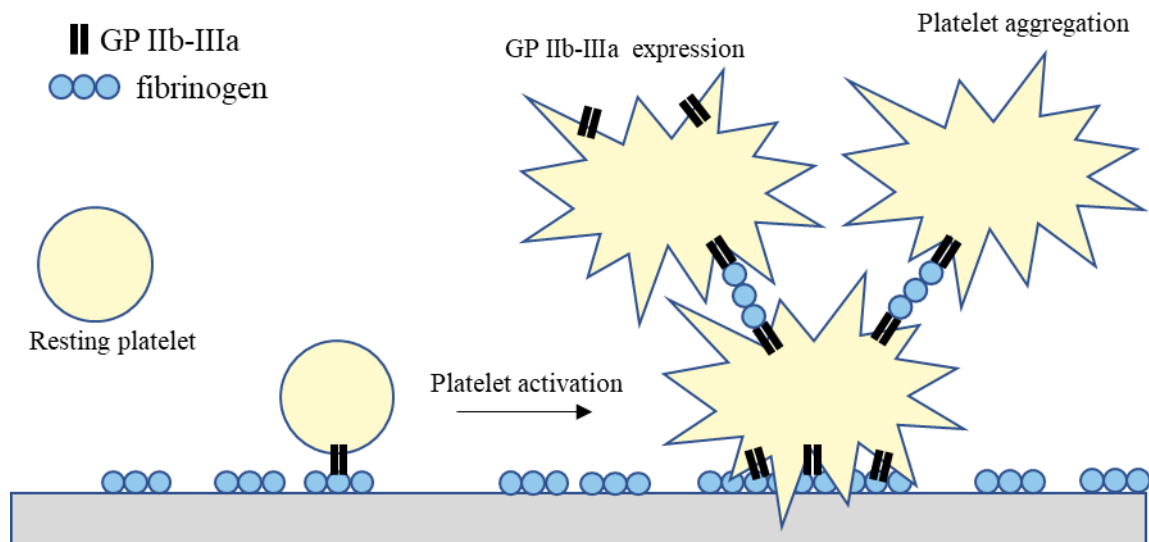


**Figure 2.5.** The major mechanism of platelets adsorption, activation, and aggregation on biomaterials under static conditions (lack of or low blood flow). Resting platelets can bind to available  $\gamma^{400-411}$  sequences in pre-adsorbed HPF. This leads to platelet activation and expression of an activated GP IIb-IIIa receptor. Finally, activated platelets are capable to bind other thrombogenic proteins (RGD sequences) and aggregate.

### 2.2.2.3. Human plasma fibrinogen (HPF) structure

Human plasma fibrinogen (HPF) is a rod-shaped plasma protein with a molecular weight of 340 kDa, which circulate in blood at the concentration of 2 - 4 mg/mL.<sup>79</sup> Microscopic analysis and crystallographic studies revealed that a single HPF molecule, as shown in [Figure 2.6.](#), consists of two sets of three polypeptide chains ( $\alpha$ ,  $\beta$ , and  $\gamma$ ) folded into three negatively charged (at pH = 7.0) and hydrophobic domains i.e., two globular-shaped D domains on the ends, and one central positioned E - domain.<sup>80</sup> Those domains are linked together by more hydrophilic, triple-stranded, helical coiled coils. The positively charged (at pH = 7.0), hydrophilic  $\alpha$ C - termini extend from two distal D domains because  $\alpha$  - chains are slightly longer than  $\beta$  and  $\gamma$ .<sup>81</sup> Elongated HPF has 47.5 nm in length and 6 nm in width.<sup>82</sup>

Due to the high proportion of hydrophobic and negatively charged aminoacids, an overall molecule has a net hydrophobic nature and negative charge.<sup>83</sup> Nevertheless, due to the presence of different types of functional groups, it can be considered an amphiphilic molecule.<sup>84</sup> In blood, HPF is folded in a globular structure, with non-polar hydrophobic parts located in the core, hidden from a hydrophilic medium, which ensures structural stability in an aqueous solution. Upon implant placement, the diversity of protein residues influences specific structural rearrangements that enable its adsorption on a material

surface. This process depends on numerous factors, especially environmental (temperature, pH, ionic strength, etc.) and physico-chemical material surface characteristics.<sup>85</sup> Depending on an obtained conformation, the ligands for platelets GP IIb-IIIa may be hindered or become exposed. In HPF, three types of ligands have been identified, which are located in:

- D - domains of the gamma chain: dodecapeptide ( $\gamma^{400-411}$ )
- $\alpha$ C - termini: RGDS ( $A\alpha^{572-575}$ )
- coil - coiled regions: RGDF sequence ( $A\alpha^{95-98}$ ).<sup>86</sup>

While RGDs are common for numerous proteins,  $\gamma^{400-411}$  is unique for HPF and is therefore considered the primary ligand for platelet adhesion.<sup>87</sup> Location of  $\gamma$ -chain after HPF adsorption is critical in platelet adhesion.<sup>87</sup> In solutions,  $\gamma^{400-411}$  sequences are hidden in the core of an HPF molecule and thus interactions with platelets are impossible i.e., HPF is “inactive”.<sup>88</sup> However, adsorption-induced unfolding can sufficiently reveal hidden sites, which dictates the degree of platelets adhesion and activation. The conformation of adsorbed HPF is strictly surface-dependent. In the following chapter, the current state of the art in manipulating the adsorption behavior of HPF and platelets adhesion on biomaterials, by controlling physico-chemical surface properties, has been reviewed.

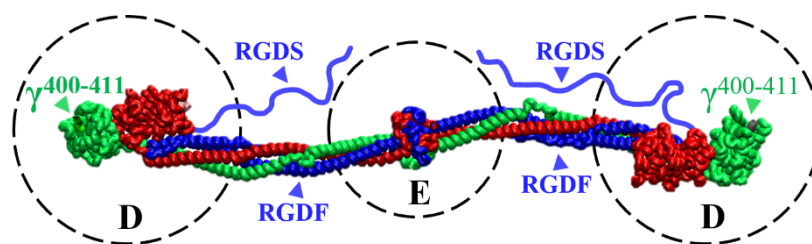


**Figure 2.6.** Schematic representation of HPF molecule with selected platelet binding sites: primary  $\gamma^{400-411}$  sequences and secondary RGD sequences. Individual hydrophobic D and E domains and hydrophilic  $\alpha$ C parts.  $A\alpha$ ,  $B\beta$ , and  $\gamma$  chains are shown in blue, red, and green colors. Molecular structure of HPF taken and adapted from Protein Database (RCSB PDB).<sup>65</sup>

### **3. State of the art: Physico-chemical properties of material surface affecting thrombogenic process**

Numerous studies on protein adsorption have been conducted since the 1970s, as it has been recognized as a major determinant of biological phenomena, such as blood clotting.<sup>89</sup> Comprehensive attempts have been made to explain thrombogenic phenomena at the biomaterial - blood interface by characterization of platelets adhesion in relation to surface-dependent protein behavior.

It has been found that a multitude of factors influences protein adsorption, introduced by hydrophobic interactions, electrostatic attraction (Coulomb's force), hydrogen bonding, or weak forces, such as Van der Waals' forces, between protein and biomaterial.<sup>90</sup> Surface wettability, chemistry, and topography are important parameters determining protein layer composition and structure, as it is schematically illustrated in [Figure 3.1](#).<sup>91</sup> Based on thermodynamics, it is known that the main driving forces for protein adsorptions are the minimization of energy and entropy gain within a surface-protein-water system.<sup>92</sup> The latter arise from surface dehydration, redistribution of charged groups in the biomaterial - blood interface, and conformational changes of proteins.<sup>61</sup> Modulation of protein and thus cellular response, by adjustment of a material surface properties is a promising strategy for the development of antithrombogenic biomaterials because it does not change bulk material properties while preserving its functions.<sup>73,93-97</sup> However, a comprehensive explanation of how surface properties correlate with protein response on the implanted biomaterial is still missing. Therefore, this chapter presents the current state of the art regarding the influence of material surface properties on protein adsorption, especially HPF, and subsequent platelet adhesion, which was the starting point for studies presented in this thesis.



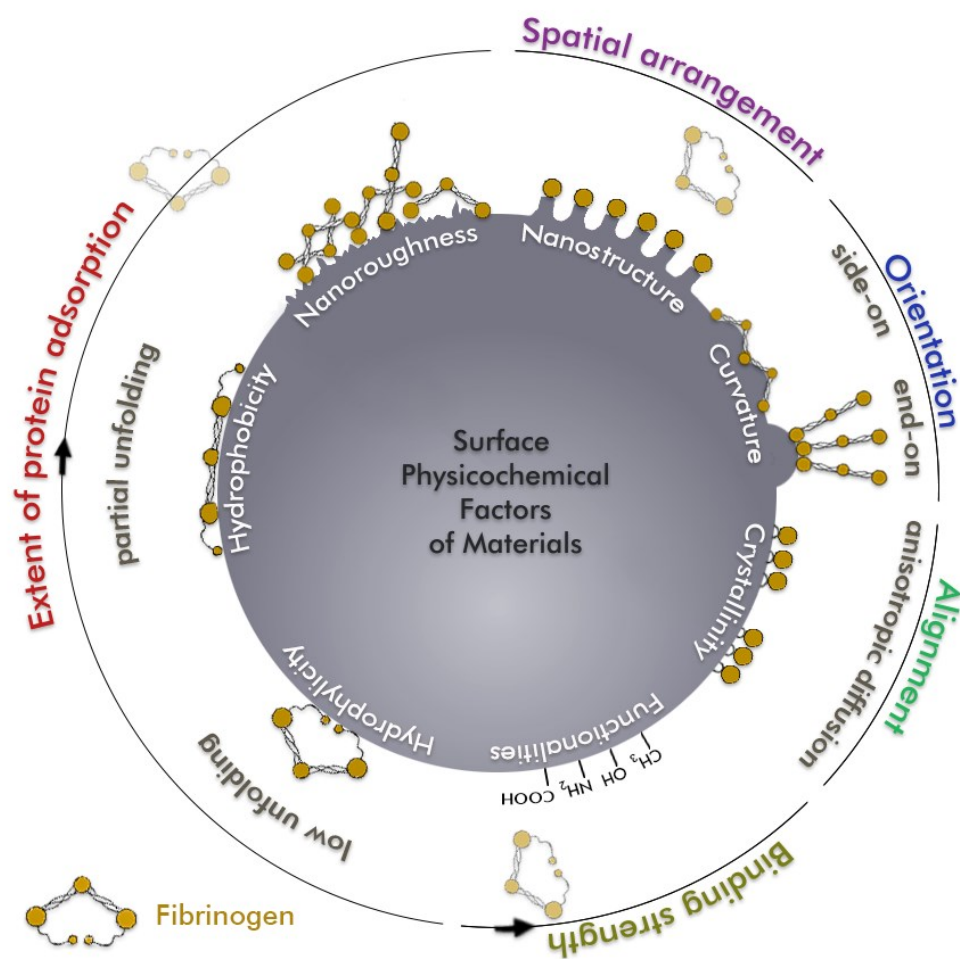


**Figure 3.1.** Physico-chemical surface properties influencing protein adsorption behavior. Image reproduced from ref.<sup>91</sup>, with permission from Wiley/VCH. Copyright©2017.

### 3.1. Impact of physico-chemical properties of a material surface on a protein adsorption

Hydrophobic interactions are fundamental for maintaining protein tertiary and secondary structure, which correspond to the minimum energy state, and are a major factor guiding protein behavior after implant placement.<sup>92</sup> In polar, hydrophilic solvents, including blood plasma, hydrophilic residues of HPF are directed toward water, while forming hydrophobic cores inside, which result in HPF folded globular structure.<sup>64</sup> This equilibrium state is disrupted when proteins encounter an implant.<sup>64</sup> It is widely documented that proteins e.g., HPF, attach extensively and experience pronounced conformational changes on hydrophobic surfaces due to the low energy required for the displacement of loosely bounded water molecules.<sup>98-100</sup> It is energetically favorable as



surface dehydration and protein adsorption minimize free energy due to contact reduction of the hydrophobic surface with water, whereas HPF unfolding leads to entropy gain. In contrast, during adsorption on hydrophilic surfaces, protein-surface interactions are limited due to the strongly adsorbed water layer.

According to a well-known paradigm, the limit value of the water contact angle  $\Theta = 90^\circ$  differentiates material surfaces as hydrophilic ( $\Theta < 90^\circ$ ) or hydrophobic ( $\Theta > 90^\circ$ ). However, in numerous studies, including Yoon *et al.* it was observed that long-range hydrophobic (attractive) forces, promoting protein adsorption and unfolding, are present on surfaces with a water contact angle  $\Theta > 62.4^\circ$ .<sup>101,102</sup> In contrast, strongly bound water on surfaces with a water contact angle  $\Theta < 62.4^\circ$  induces repulsive solvation forces, and therefore surface dehydration by proteins is unfavorable.<sup>102,103</sup> Berg *et al.* defined a limit value of water contact angle  $\Theta = 65^\circ$  for the presence of long-range attractive forces on surfaces.<sup>104</sup> A new limit of hydrophilicity/hydrophobicity has been defined and is equal not  $\Theta = 90^\circ$ , but  $\Theta = 65^\circ$ , which quantitatively defines the terms "hydrophilicity" and "hydrophobicity" of a material surface in the context of protein adsorption. Therefore, in the following part of this dissertation surfaces exhibiting water contact angle  $\Theta < 65^\circ$  are classified as hydrophilic, and hydrophobic if  $\Theta > 65^\circ$ .<sup>101</sup>

Moreover, Vogel *et al.* observed that strong changes in proteins behavior occur on surfaces with a water contact angle  $\Theta \approx 60 - 65^\circ$ , and established this range as the criterion for distinguishing a surface as "protein-adherent" or "protein-non-adherent".<sup>103</sup>

Since hydrophobic surfaces are usually non-polar, hydrophobic interactions are recognized as major driving forces, triggering a protein adsorption process on hydrophobic surfaces. However, especially on hydrophilic and charged surfaces, other interactions i.e., electrostatic and van der Waals forces, as well as hydrogen bonds, may take over the primary role.<sup>105</sup> Therefore, controlling protein adsorption is also possible by the introduction of specific functional groups or manipulation of surface charge.

Studies carried out until the beginning of the 21<sup>st</sup> century allowed drawing groundbreaking conclusions and proposing the so-called "Whiteside's rules", which are still the basis for the design process of the protein-repellent surface.<sup>106,107</sup> These surfaces are characterized by four features: 1) hydrophilicity (presence of polar functional groups), 2) presence of hydrogen-bonds acceptors and 3) lack of hydrogen-bonds donors, and 4) electrical neutrality.<sup>108</sup> The first three rules are associated with water retention on a

material surface, which acts as a barrier for protein adsorption.<sup>109–111</sup> Lack of hydrophobic forces and presence of only weak interactions between proteins and biomaterial surface, such as hydrogen bonds and van der Waal's interactions, leads to reduced protein adsorption strength and minimizes perturbation of their structure.<sup>112</sup>

Since all proteins contain both positively and negatively charged amino acids, which are typically located on the outside of molecules, biomaterial surface charges determine the amount of adsorbed proteins and steer their conformation.<sup>113</sup> Proteins expose positively or negatively charged regions to oppositely charged surfaces, which is accompanied by a rearrangement of their structure.<sup>114,115</sup> It has been recognized that negatively charged proteins such as HPF, interact more strongly with positively charged surfaces, than with negatively charged ones.<sup>116</sup> However, it is important to note that proteins bearing an overall negative charge still may adsorb on negatively charged surfaces to some extent, due to their amphiphilic nature (presence of positively charged regions).<sup>117,118</sup> Thus, charge-neutral surfaces are recognized to be the most protein-repellent.<sup>106,108,119</sup> Charge neutrality limits the induction of additional forces i.e., electrostatic forces, which rather enhance the protein adsorption. Rodrigues *et al.* reported a linear decrease of HPF adsorption, as well as platelet adhesion and activation with an increased level of charge-neutral OH in relation to negative CH<sub>3</sub> groups on surfaces.<sup>120</sup>

Inspired by collected results, numerous attempts have been made to chemically modify the surface of implants, which alter their wettability and charge, to reduce the probability of clot formation. Substantial research has been devoted to creating uniformly coated surfaces with functionalities that control the binding strength of protein adsorption and provide bioinert surfaces.<sup>61,121</sup>

Physical modification of a material surface is also a promising way of controlling medical device-induced thrombogenic reactions. The importance of nanotopography in steering cellular response, by pre-adsorbed proteins has been underlined by Lim *et al.*, who found that cell adhesion remains rather unaltered by surface nanotopography in the absence of blood plasma.<sup>122</sup> This observation pioneered a new research strategy to design biomaterial surfaces in terms of proteins, not cells, to induce the desired response of the human body to implant.

It is widely accepted, that nanofeatures, especially with a size compatible with the physical dimensions of proteins i.e., ranging between 10 nm and 100 nm, may impact

protein behavior upon adsorption.<sup>123</sup> However, numerous inconsistencies remain in this topic and need to be explored in the future. According to studies by Han *et al.*, surface roughness in the range of 5 - 60 nm has little effect on the amount or structure of the adsorbed proteins.<sup>124</sup> Similar conclusions were drawn by studying the adsorption of HPF on nanorough titanium films with a roughness of 2 - 21 nm.<sup>125</sup> In contrast, Rechendorff *et al.* demonstrated an enhancement of HPF adsorption on tantalum surfaces with an increase in roughness ranging from 2 nm to 32.9 nm, attributed to the more efficient packing of HPF molecules.<sup>126</sup> This was later confirmed by Dolatshahi-Pirouz *et al.* on platinum surfaces, where higher surface roughness, in a range of 1.5 nm to 9 nm, induced a greater HPF adsorption compared to more smoothly shaped surface features.<sup>127</sup> In an other study, higher levels of surface nanoroughness contributed to significantly lower HPF adsorption than surfaces with lower roughness.<sup>128</sup> The possible explanation of this mechanism is limited contact between protein solution and material, to the top of protrusions due to air entrapment between the protrusions, leading to an overall reduction in surface area for protein adsorption.<sup>128</sup>

These contradictory results indicated the existence of multiple factors influencing the protein adsorption process, and mechanism dependent on the characteristics of the nanostructures. Furthermore, modeling protein adsorption on nanostructured surfaces is still challenging due to the interplay of physical and chemical properties of a material surface, acting synergistically or antagonistically.<sup>8,129</sup> On the one side, physical modification (topography changes) provides a more accessible contact area for proteins and enhances biological properties that originate from surface chemistry.<sup>130</sup> On the other side, modification of a surface topography may alter its wettability, energy, charge distribution, or chemical homogeneity.<sup>131,132</sup> It has been also revealed that morphological features may create confined spaces, which restrict protein exchange between protein and solution, leading to topography-dependent variations in adsorbed protein species.<sup>133,134</sup>

It can be concluded that combined modulation of surface chemistry and topography may alter the final pathway of biological reactions, compared to considering the effects of surface features individually. Hence, thorough control of overall surface parameters is an essential way to design highly biocompatible materials.

### 3.2. Impact of physico-chemical properties of a material surface on HPF conformation and platelet response

Despite numerous studies, no biomaterial with complete protein resistance is known, and it has been found that an extremely low amount of adsorbed HPF ( $\sim 5 \text{ ng/cm}^2$ ) is enough to fully initiate a clot formation process.<sup>70</sup> Therefore, the idea of designing antifouling surfaces to limit thrombogenic phenomena failed. Biomaterials that resist blood clotting despite high HPF adsorption have attracted the interest of researchers, and efforts have been made to explain this. Numerous studies have suggested that the major determinant of cellular response may be protein conformational state, rather than the amount of adsorbed proteins. Therefore the modulation of platelet adhesion through surface-induced HPF conformational changes seems to be a promising strategy to limit thrombogenic reactions.<sup>135</sup>

A propensity of proteins to structural changes, guiding platelet response to blood-contacting biomaterial was emphasized for the first time by Lindon *et al.* in the 1990s.<sup>136</sup> Observation of platelet behavior on various HPF-coated polymer surfaces allowed for a statement that the platelet adhesion is closely correlated with the conformational state of HPF, regardless of its amount in the pre-adsorbed protein layer.<sup>137</sup> This finding was later confirmed by numerous other groups and explained by HPF conformation-dependent availability of platelet binding sites, especially  $\gamma^{400-411}$ , as it is the primary ligand for platelet adhesion.<sup>12,54,95,138,139</sup>

Since HPF adsorbs thorough hydrophilic ( $\alpha$ C) and hydrophobic (D and E) domains to alike surfaces, one of the major factors influencing its conformation is surface wettability.<sup>140</sup> Numerous studies showed that hydrophobic surfaces tend to induce stronger HPF unfolding compared to hydrophilic ones.<sup>53,141-144</sup> Moreover, platelet adhesion is correlated with a degree of adsorption-induced unfolding, yet there are numerous contradictory reports on the topic. Most researchers observed that characteristic for hydrophobic surfaces HPF unfolding, and thus adsorption in trinodular conformation, promoted platelet adhesion and activation.<sup>93,120,145-149</sup> However, the same phenomenon was also reported on hydrophilic surfaces, where HPF kept a folded, close to native, globular conformation.<sup>150</sup> This implies that HPF unfolding is not obligatory to promote a clot formation process. These inconsistencies can be explained by analysis of the conformation-dependent localization of  $\gamma^{400-411}$  primary platelet binding sites in the adsorbed HPF molecule that binds to platelet receptors GP IIb-IIIa. A comparison of

numerous studies allows for a statement that the availability of  $\gamma^{400-411}$  is HPF unfolding degree independent.<sup>137,151,152</sup> Based on this knowledge, comprehensive studies on surfaces with different wettability have been recently performed.

Cihova *et al.* found a favorable HPF conformation for preventing platelet adhesion and spreading on hydrophilic metal, titanium, compared to more hydrophobic palladium, as adsorption of HPF, in close to the native state, resulted in lower availability of  $\gamma^{400-411}$  for platelets.<sup>153</sup> This was also reported by Zhao *et al.*, who conducted a study on native and fucoidan-modified TiO<sub>2</sub> surface, which showed that surface hydrophilicity induced by surface treatment, limited HPF unfolding,  $\gamma^{400-411}$  exposition, and thus inhibited platelets adhesion.<sup>154</sup>

In contrast, Zhang *et al.* observed lower platelets adhesion and activation on hydrophobic polymers ( $\Theta > 65^\circ$ , see Berg limit in Chapter 3.1.), than on hydrophilic ones, because adsorption of trinodular HPF via hydrophobic D and E domains rendered the  $\gamma^{400-411}$  to be hidden from the environment.<sup>150</sup> They proposed a model of HPF-mediated platelet adhesion mechanism for polymeric surfaces with various hydrophilicity, which is presented in Figure 3.2.

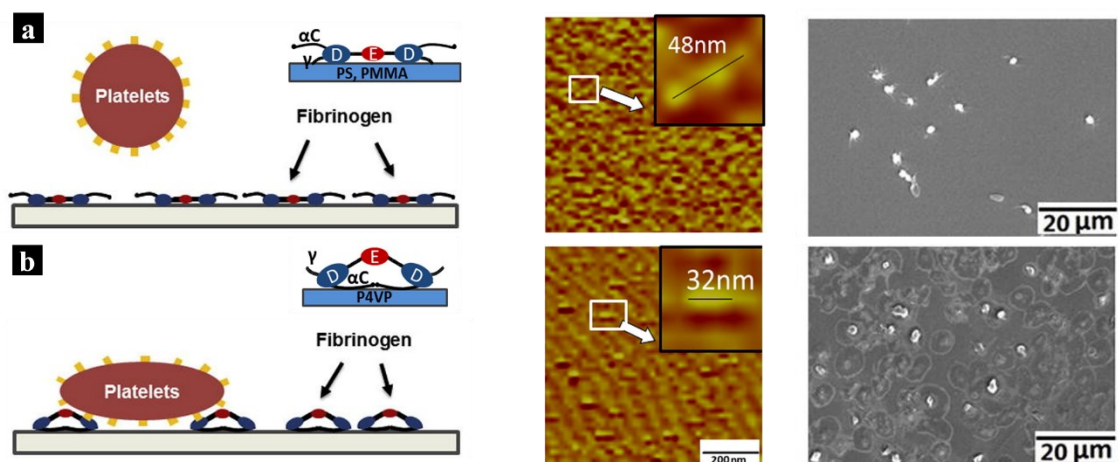


**Figure 3.2.** Model of HPF-mediated platelet adhesion and activation on various polymers with different surface wettability. a) Adsorption of HPF by hydrophobic D and E domains to hydrophobic polymers ( $\Theta > 65^\circ$ ) limits the availability of primary platelet binding sites ( $\gamma^{400-411}$ ) for platelets, preventing their adhesion and activation. b) Adsorption of HPF by hydrophilic  $\alpha C$  region to hydrophilic polymers ( $\Theta < 65^\circ$ ) exposes the  $\gamma$ -chain, inducing platelet adhesion and activation. Image reproduced from ref.<sup>155</sup>, with permission from Acta Biomaterialia. Copyright©2017

Cihova *et al.* suggested that those inconsistent results may come from differences in material classes, which emphasizes the importance of a complex consideration of physico-chemical surface properties, beyond surface wettability, in the evaluation of material thrombogenicity.<sup>153</sup>

Platelet adhesion and activation on biomaterials can also be controlled by surface topography. Nevertheless, in this case, the effect of physical modification on HPF conformation, as well as platelets adhesion should be considered, as both proteins and cells are able to sense the topographical features. Keep in mind that proteins and cells respond to features with a size comparable to their physical dimension.<sup>156,157</sup>

It has been widely recognized that surface nanostructuring modifies an orientation and conformation of protein upon adsorption, which recognizes surface curvature (Figure 3.3. a), may be trapped between protrusions (Figure 3.3. b)<sup>158</sup> or reorganize its structure on the edges of protrusions (Figure 3.3. c).<sup>159,160</sup> Numerous researchers characterized the influence of surface curvature on proteins distribution and structural distortions (loss of secondary structure).<sup>159,161,162</sup> For instance, Roach *et al.* investigated the HPF adsorption on silica nanospheres with a diameter in the range of 15 - 165 nm. They observed that a high surface curvature, of 15 nm silica nanospheres, promoted end-on adsorption, higher denaturation, and structural destabilization of HPF molecules, while on 165 nm nanoparticles, HPF preferred side-one orientation (Figure 3.3. a).<sup>163</sup> In addition, recent studies showed strong interactions between D domains of HPF and nanoparticles having dimensions comparable to its physical size i.e., 38 nm limits the  $\gamma$ -chain visibility, in contrast when HPF is adsorbed on smaller (16 nm) or bigger (68 nm) one's nanoparticles.<sup>164</sup> Therefore, surface curvature may change the functionality of a protein, which may contribute to changes in cellular adherence behavior.<sup>159,164-166</sup> However, no studies exist on the effect of nanoparticle curvature on platelet behavior mediated by HPF.

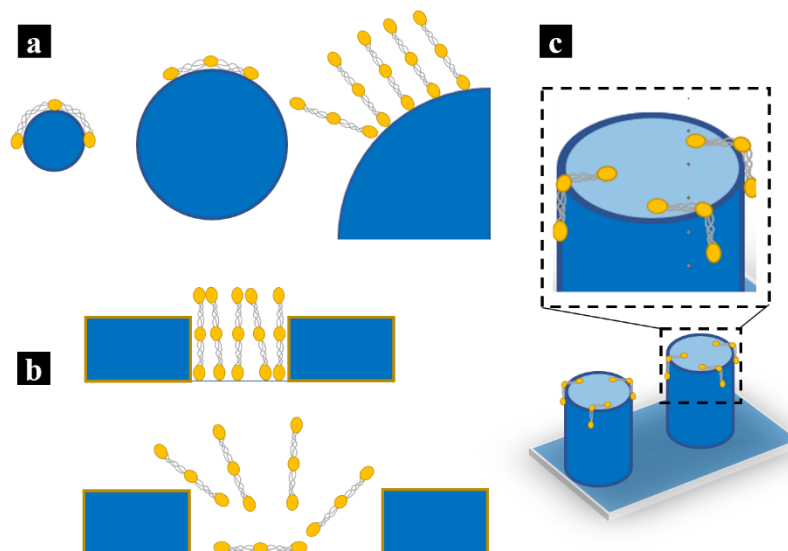


**Figure 3.3.** Topography-induced structural changes of HPF. a) HPF orientational and/or conformational changes caused by a) nanofeatures curvature, b) confinement between protrusions, c) nanofeatures edge.

Recently, Wang *et al.* reported that it is possible to limit the accessibility to unfolded HPF molecules on a hydrophobic surface of poly(methyl methacrylate) (PMMA) by their entrapment in pores smaller than their hydrodynamic diameter i.e.,  $< 50$  nm (Figure 3.3. b)). It was shown that nanopores in this size were effective in dictating protein quantity and spatial distribution, thus limiting the exposure of an entire HPF molecule to the environment.<sup>167</sup>

Although major research has been devoted to significant steps forward and understanding HPF adsorption on nanostructured surfaces, the linkage of the observed HPF-induced conformational changes with differences in platelet response has been poorly studied. An idea of controlling platelets adhesion and activation to surface nanotopography through conformational changes of HPF molecules, for the first time, was speculated by Sutherland *et al.* in 2001.<sup>168</sup> However, so far only a few studies present experimental data on HPF conformation and its relation to topographical features. Nandakumar *et al.* showed that nanopatterned diamond-like coatings (DLC) with nanoroughness in the range of 5 - 8 nm may sufficiently reduce the potential of HPF activating platelets, as proteins were adsorbed between grooves in altered conformation, reducing the availability of platelet binding sites.<sup>169</sup> Recently, our group proposed a new possibility to control the HPF conformation-dependent platelet response by fabricating semicrystalline hydrophobic polymers with different sizes of crystalline parts.<sup>139</sup> As HPF has a higher

affinity for crystalline moieties, it adopted specific conformations depending on crystal dimensions, which is schematically displayed in [Figure 3.4. a\) and b\)](#). Spatial arrangement on lamellar (LCs) and shish-kebab (SKCs) crystals with an aspect ratio (length-to-width)  $> 4$ , i.e., higher than that specified for a single HPF molecule ( $\sim 3.4$ ), allowed the primary platelet binding sites ( $\gamma^{400-411}$ ) to be available, stimulating platelets adhesion and activation ([Figure 3.4. d\)](#)). In contrast, for needle-like crystals (NLCc), an aspect ratio = 1 induced a specific HPF arrangement in which proteins interacted with each other (end-to-end interaction), blocking the partial exposition of the  $\gamma$ -chain ([Figure 3.4. a\) and b\)](#)). This limited platelet adhesion and activation ([Figure 3.4. d\)](#)).

In other studies, significant differences in platelets behavior on titania nanotubes (50 - 120 nm) as compared to smooth titanium surfaces were reported.<sup>170-172</sup> HPF molecules located at nanotubes edges experienced conformational rearrangement ([Figure 3.3. c\)](#)), thus lost the ability to bind platelets, however, at the same time enhanced their activation, which finally was correlated to partial shielding of platelet binding sites.<sup>172</sup> However, it has been suspected that the influence of nanotubes on platelet response could be magnified by the direct effect of surface topography on the cells themselves.



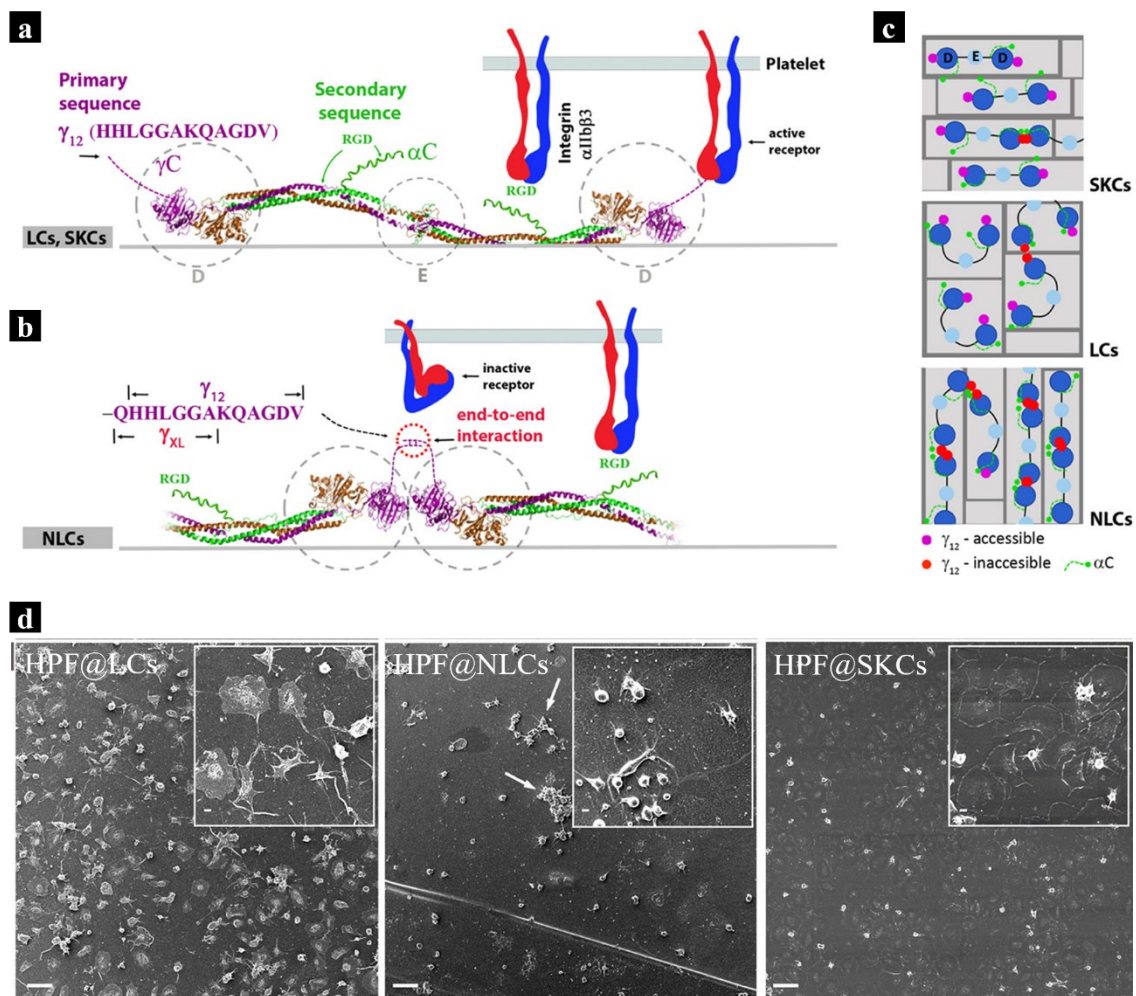


**Figure 3.4.** HPF adsorption and platelet adhesion as a function of the crystal aspect ratio of semicrystalline polymeric surfaces. a) Trinodular conformation observed on lamellar (LCs) and shish-kebab (SKCs) crystals (aspect ratio  $> 4$ ), where primary platelet binding sites,  $\gamma^{400-411}$ , are exposed. b) HPF conformation on needle-like (NLCs) crystals (aspect ratio = 1), which enables protein-protein interaction through  $\gamma^{400-405}$  sequences, making only  $\gamma^{406-411}$  sequences accessible to platelets. The aspect ratio of HPF is  $\sim 3$  c) Schematic representation of HPF conformation on semicrystalline polymer surfaces. d) Significantly more pronounced platelet adhesion and activation on LCs and SKCs compared to NLCs due to a higher aspect ratio of the crystalline part than an aspect ratio of HPF. Image reproduced from ref.<sup>139</sup>, with permission of American Chemical Society, 2020.

Several researchers noted a direct effect of surface topography on cells regardless of a previously adsorbed protein layer. Nevertheless, this phenomenon has been observed especially in a microscale or hundred nm and is associated with changes in cell adhesion, contact guidance, cytoskeleton organization, or apoptosis.<sup>173</sup> It has been recognized that effective features to stimulate platelet behavior have dimensions in the range of physical size of platelets or smaller, but not as small as sub-100 nm, which is less than pseudopods of activated platelets.<sup>174,175</sup> Reduced platelets adhesion, spreading, or activation originate

from the inability of platelets to form stable contact with a surface due to reduced area for multivalent adhesive interactions.<sup>176–186</sup> Of note, platelet response depends on interspacing, width, and height (i.e., aspect ratio) of nanofeatures. A detailed study by Koh *et al.* on pillared poly(lactic-co-glycolic-acid) (PLGA) films revealed that the following parameters of surface features are desirable to effectively limit the adhesion and activation of platelets: interspacing = < 200 nm, height = 300 - 800 nm, width = 100 - 200 nm (aspect ratio 3 - 5).<sup>176</sup> An interspace smaller than 200 nm prevents the platelet entrapment and thus limits its activation due to low contact with a surface.<sup>184–186</sup> Moreover, if the feature is as narrow as ~100 nm and the height is 3 - 5 times greater, platelets interact only with their tips and can be dislodged from a surface due to unstable adhesion.<sup>176,177</sup> These results indicate that the impact of physical material surface modification on HPF-mediated platelets adhesion, but also platelets themselves, should be considered.

This dissertation addresses the crystallographic orientation of a material surface as a potential factor modulating the HPF conformation, and therefore adhesion and activation of platelets. The arrangement of atoms on a material surface, and their coordination number are closely correlated with surface energy, which in turn is relevant when material comes into contact with liquid or another material. Since the beginning of the 19th century, it was known that surface energetics dictates interactions with water, therefore surface wettability. Surface energy has been expressed by Young equation and a series of empirical models such as Fowkes, Owens-Wendt-Rabel-Kaelble, or van Oss *et al.* theory.<sup>187,188</sup> In addition, numerous studies have shown that typical hydrophobic materials have low surface energy. A low number of broken bonds during the formation of such surface, and hence low density of dangling bonds and reduction in coordination number of surface atoms, subsequently leads to weaker adsorption of water molecules.<sup>189</sup> This suggests that the crystallographic orientation-dependent biological response may be indirectly linked to the different surface energy and wettability of crystals.<sup>190,191</sup>

Recently, preliminary reports describing the effect of surface crystallographic orientation on protein or cell behavior appeared.<sup>192–194</sup> Cai *et al.* observed that crystallographic orientation-dependent functionality of adsorbed fibronectin on rutile single crystals affects surface bioactivity. More specifically, it modulates a biomineralization process of implant surfaces.<sup>192</sup> In contrast, surface crystallographic orientation had no effect on hepatocyte adhesion on the same rutile crystals.<sup>193</sup> In an other study, Keller *et al.* reported

grain and facet-dependent HPF conformational changes on a surface of strongly thermally etched rutile polycrystals (Figure 3.5).<sup>194</sup> Network of trinodular proteins or thin globular protein layers were observed on surfaces depending on local surface energy and wettability. Nevertheless, in this study, a faceting phenomenon prevented a detailed evaluation of the crystallographic orientation of each grain/facet wall.

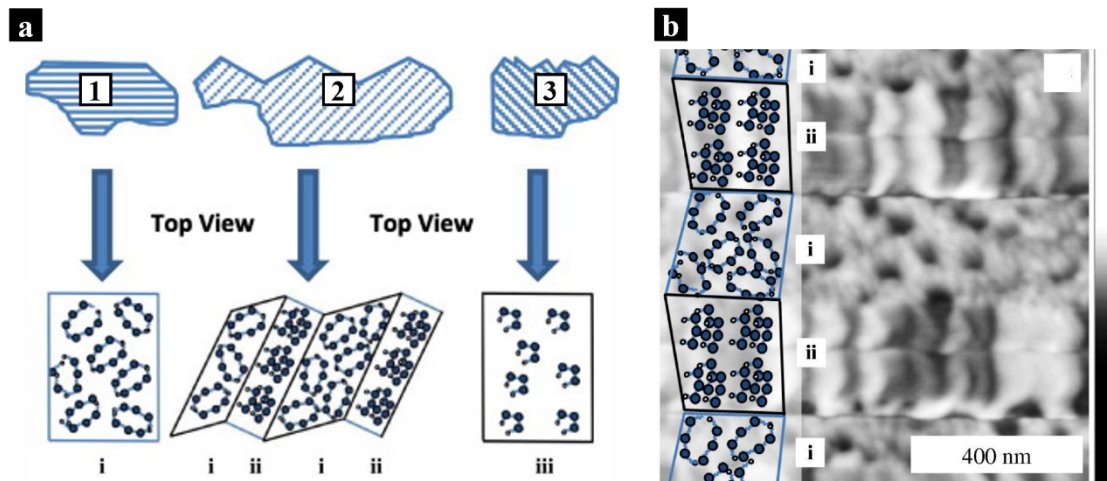


**Figure 3.5.** a) Schematic representation of grain- and facet-dependent HPF adsorption on strongly thermally etched rutile polycrystal: (i) trinodular conformation of HPF arranged in a ring-like network on a flat stable grain type 1 or single facet wall of grain type 2, (ii) globular assembly on second facet wall of grain type 2, (iii) thin globular layer on irregular less stable grain type 3. b) AFM image of HPF adsorbed on faceted grain type 2 showing HPF molecules in two different conformational states. Image reproduced from ref.<sup>194</sup>, with permission of Acta Biomaterialia.

Nevertheless, systematic studies regarding crystallographic orientation-dependent cellular adhesion mediated by protein are still missing. This encourages a deeper understanding of this topic concerning the design of biointerfaces and biocompatible material surfaces for medical applications. The challenge of investigating and proposing a desirable surface crystallographic orientation of rutile to prevent pathological clot formation on the biomaterial surface was addressed in this work and results are described in the following chapters.

## 4. Aims of dissertation

### 4.1. Open Scientific Questions

Currently available production methods for TiO<sub>2</sub> coatings in rutile form, allow controlling the formation of surfaces with preferred crystallographic orientation.<sup>23</sup> Researchers have demonstrated that an adsorption behavior of proteins and/or cells is unique for specific rutile surfaces depending on crystallographic orientation.<sup>192–194</sup> An explanation is the various atomic arrangement, coordination numbers, density of unsaturated (dangling) bonds on a surface, and a tendency for defects formation, which directly affects the surface energy and adsorptive behavior of water molecules (molecular or dissociative). Inspired by these unique phenomena, the following questions were posed for this dissertation:

- I. Can the arrangement and coordination of titanium and oxygen atoms on rutile surfaces play a significant role in the adsorption and conformational changes of HPF?
- II. Can a surface crystallographic orientation control the adhesion and activation of platelets as mediated by pre-adsorbed HPF?
- III. How does crystallographic orientation-dependent HPF conformation control platelet response to rutile surfaces?
- IV. Are rutile polycrystals a universal tool for studying biological phenomena that depend on a grain surface crystallographic orientation?

### 4.2. Hypotheses

In this thesis, four hypotheses have been tested:

- I. The amount and conformation of the adsorbed HPF depend on the crystallographic orientation of TiO<sub>2</sub> (rutile) crystal surfaces.
- II. The surface energy of protein-coated substrates depends on protein conformation.
- III. Platelets adhesion and activation are guided by crystallographic orientation-dependent HPF conformation.
- IV. Crystallographic orientation-dependent structure and functionality of adsorbed HPF and platelets are comparable on both rutile single crystals and polycrystals.

### 4.3.Objectives

This work aimed to gain in-depth insight into the thrombogenicity of TiO<sub>2</sub> (rutile) crystals and to propose material surface characteristics for a reduction of surface-induced blood clotting. For the investigation of hypotheses I – III, studies were performed on rutile single crystals and the following objectives have been defined:

**Objective I:** Characterize the rutile single crystals' surface topography and surface energy using AFM.

**Objective II:** Determine the structure and wettability of rutile single crystals surface using Raman spectroscopy and sessile drop method, respectively.

**Objective III:** Determine the amount of adsorbed HPF on rutile single crystals using BCA™ Protein Assay Kit and colorimetric quantification method.

**Objective IV:** Investigate crystallographic orientation-dependent conformation of adsorbed HPF using AFM in air and aqueous environment.

**Objective V:** Detect the HPF conformational changes by XPS and AFM analysis of adhesion forces between AFM tip and protein-coated substrates.

**Objective VI:** Characterize the HPF conformation-dependent availability of platelets binding sites and its' impact on platelets adhesion and activation using SEM, confocal and optical microscopy, as well as immunofluorescence technique.

**Objective VII:** Develop a model explaining TiO<sub>2</sub> crystallographic orientation-dependent HPF conformation and its effect on platelet adhesion and activation.

To investigate hypothesis IV, studies were performed on rutile polycrystals, and the following objectives have been defined:

**Objective VIII:** Produce polycrystalline substrates by rutile powder compaction, sintering, polishing, and thermal etching.

**Objective IX:** Determinate the surface crystallographic orientation of grains surface using electron backscatter diffraction (EBSD).

**Objective X:** Characterize the surface topography of selected grains using AFM.

**Objective XI:** Determine HPF distribution and conformation on the surface of selected grains using confocal microscopy and AFM.

**Objective XII:** Determine the morphology and activation state of the adhered platelets using SEM and confocal microscopy.

**Objective XIII:** Explain platelet behavior on the surface of individual grains with a defined surface crystallographic orientation and compare it with the response of platelets on single crystals.

#### **4.4. Scientific Significance**

Research into a cellular response to biomaterials through protein adsorption is essential for an in-depth understanding of biomaterial – blood interactions. Adjusting the crystallographic orientation of the TiO<sub>2</sub> surface may provide a new opportunity for designing biomaterials with improved biocompatibility, bioactivity, and performance. This perspective motivates interdisciplinary research on differently-oriented crystals. In addition, TiO<sub>2</sub> coatings with desirable properties can significantly reduce the costs of manufacturing conventional implants, which will not require additional surface modification. The possibility of using polycrystalline substrates instead of single crystals in biological studies can make an experimental procedure cheaper and faster. This will significantly accelerate the development of implantology, thereby improving the efficiency and comfort of patient treatment.

Results presented in this dissertation will provide comprehensive information on surface-protein-cell interactions and knowledge of the controlled cellular response on blood-contacting materials, with potential practical applications in medicine.

## **5. Crystallographic orientation-dependent HPF adsorption on rutile single crystals**

### **5.1. Introduction**

Atomically flat TiO<sub>2</sub> (rutile) single crystals with (110), (100), (101), and (001) crystallographic orientations were used to study the effect of surface crystallographic orientation on HPF adsorption. Based on the literature describing the structure of rutile surfaces and preliminary reports considering crystallographic orientation-dependent water and protein molecules adsorption (Chapter 2.1.2), it has been hypothesized that HPF amount and conformation depend on a material surface properties dictated by different arrangements and coordination of titanium and oxygen atoms. Water contact angle that defines the wettability of crystals surfaces was measured. Then, the amount of absorbed HPF from low and highly concentrated solutions i.e., 0.01 mg/mL and 0.1 mg/mL, was analyzed using BCA™ Protein Assay Kit (BCA). The dominant HPF conformation on rutile single crystals was determined by atomic force spectroscopy (AFM) visualization of single HPF molecules. Before and after HPF adsorption, X-ray photoelectron spectroscopy (XPS) analysis of the surface composition was performed. In addition, the surface energy of the protein-coated rutile crystals was established based on adhesion curves collected by AFM to investigate the second hypothesis that the surface energy of protein-coated substrates is protein conformation-dependent.

Results presented in this chapter highlight the importance of surface crystallinity in the modulation of protein behavior, which has implications for biological processes that occur at the biomaterial - blood interface.

### **5.2. Materials and Methods**

#### **5.2.1. Rutile single crystals**

High-quality (99% purity), one-side epi-polished (root mean square roughness  $R_q < 0.2$  nm) rutile single crystals (5 x 5 x 0.5 mm) with (110), (100), (101), and (001) crystallographic orientations were purchased from Crystal GmbH (Berlin, Germany). Before and after each experimental step, substrates were thoroughly washed with ethanol and Milli-Q water in an ultrasonic bath for 15 minutes each.

Raman spectra of rutile crystals were recorded in a wavelength range of 70 to 1555  $\text{cm}^{-1}$  using a Raman microscope SENTERRA (Bruker, Germany) equipped with OLYMPUS BX51 confocal microscope and laser wavelength  $\lambda=532$  nm. At least two spectra per crystal were collected. The analysis particularly concerned two, specific for rutile, peaks at 448  $\text{cm}^{-1}$  and 610  $\text{cm}^{-1}$  and their intensity ratio, which was used to differentiate crystals (if necessary) during further experimental procedures.

The sessile drop method was used to determine a static water contact angle of bare rutile single crystals. Images of distilled water drops were recorded and shape of the axisymmetrical menisci was analyzed by DSA10 drop shape analysis system (Kruss GmbH, Hamburg, Germany).

### 5.2.2. Protein adsorption

Before an adsorption procedure, crystals, and phosphate-buffered saline (PBS) were heated to 37 °C. HPF stock solution (Calbiochem, Merck, Darmstadt, Germany) was prepared by dissolving proteins in PBS at 37 °C. The concentration  $C$  was analyzed using a UV-Vis spectrophotometer (LAMBDA 35 UV/Vis, PerkinElmer, Waltham, USA) and calculated based on Beer-Lambert law:

$$C = \frac{A_{280} \cdot 10}{\epsilon_{\%} \cdot l} \quad (1)$$

, where  $A_{280}$  is the mean absorbance measured at 280 nm ( $n = 3$ ),  $\epsilon_{\%}$  is the mass extinction coefficient expressed in  $(\text{mg/mL})^{-1}(\text{cm})^{-1}$  which for HPF is 15.1, and  $l$  is the path length in cm (length of the cuvette). Finally, the stock solution was diluted to the desired concentration.

Rutile crystals were immersed in 2 mL of prepared protein solutions and kept in the oven at 37 °C under a parafilm cover. Subsequently, the supernatant was removed, and samples were washed once in PBS and twice in Milli-Q water to remove loosely bound proteins. In the end, samples were left to dry in an ambient atmosphere and followed by AFM, colorimetry, and XPS analysis. One set of samples was directly used, without drying, for AFM protein molecules characterization under aqueous conditions.



### **5.2.3. Colorimetric detection and quantitation of HPF**

Micro BCA Protein Assay Kit (Thermo Scientific, Rockford, IL, USA) was used to evaluate the amount of adsorbed HPF on rutile single crystals from solutions with concentrations 0.1 and 0.01 mg/mL for 5 min and 30 min. The experiment was performed according to the manufacturer's instructions. Briefly, previously adsorbed proteins were detached from substrates by incubation in 2 mL of 1% sodium dodecyl sulphate (SDS) for 30 min. Nine bovine serum albumin (BSA) standards with known concentrations (0 µg/mL - 200 µg/mL) were prepared. To 150 µL of each standard and 150 µL of each HPF sample, 150 µL of working solution (Reagent A: Reagent B: Reagent C mixed in the ratio of 25: 24: 1) was added and stirred for 30 s at 600 rpm. Next, mixtures were incubated for 2 h at 37 °C in 96-well plates. After this time, the absorption at 562 nm was measured using Power Wave XS plate reader (BioTek Germany, Bad Friedrichshall, Germany). The BSA concentration-absorbance standard curve was determined, which enables further estimating of HPF concentration. Measurements were performed three times.

### **5.2.4. Atomic force microscopy analysis (AFM)**

Before and after protein adsorption, samples were analyzed using NanoWizard 4 (JPK BioAFM, Bruker, Berlin, Germany) and Multimode (Bruker, Veeco, Santa Barbara, CA) equipped with a nanoscope IV controller. Measurements under air conditions were performed using a standard silicon cantilever (RTESPA 300, Bruker, Santa Barbara, CA) with a resonance frequency in the range of 315 - 364 kHz, and spring constant in the range of 20 - 80 N/m. Images were analyzed using Gwyddion software.

Topography and root mean square roughness ( $R_q$ ) of bare crystals were determined from at least four  $1000 \times 1000 \text{ nm}^2$  images taken in AFM tapping mode.

AFM imaging was also performed to determine adsorption parameters, i.e., HPF solution concentration and incubation time, suitable for incomplete and full surface coverage. Proteins adsorbed from solutions with concentrations of 0.01 and 0.1 mg/mL, by 5 min and 30 min were analyzed. Single HPF molecules were visualized at a solution concentration of 0.01 mg/mL after 5 min adsorption, while higher concentrations or longer adsorption periods were required for full surface coverage.

Surface energy was determined for bare and fully HPF-covered rutile single crystals. This study was conducted to evaluate HPF conformation-dependent surface energy changes after protein adsorption. The resulting surface energy values of bare single crystals were used as a reference. Then, HPF was adsorbed from solutions with a concentration of 0.01 mg/mL and 0.1 mg/mL for 30 min. Adhesion forces between AFM tips and samples were measured in Quantitative Imaging (QI) mode in an air conditions, using a silicon tip (SCAN ASYST - AIR) with a radius of 2 - 12 nm and a spring constant of 0.4 N/m. Force-distance curves for each sample were recorded in at least three separate areas consisting of  $1000 \times 1000 \text{ nm}^2$  and  $256 \times 256$  pixels, which corresponds to more than 65 000 individual force curves per image. The loading force was set to 1 nN. Interfacial energy was determined based on Derjagin-Muller-Toropov (DMT) model and its correlation with measured adhesion value by formulas:

$$F = 2\pi r\Gamma \quad (2)$$

$$\Gamma = 2 (\gamma_{\text{sample}} \times \gamma_{\text{tip}})^{\frac{1}{2}} \quad (3)$$

, where  $F$  is adhesion force,  $r$  is tip radius,  $\Gamma$  is the interfacial energy between a tip and sample surface,  $\gamma_{\text{sample}}$  and  $\gamma_{\text{tip}}$  are surface energies of a sample surface and silicon tip, respectively. The mean tip radius (6 nm) specified by the manufacturer was used for calculations. The surface energy of the silicon tip was taken as  $\gamma_{\text{tip}} = 1.240 \text{ J/m}^2$ .<sup>192</sup> Finally, the surface energy of samples was determined:

$$\gamma_{\text{sample}} = \frac{F^2}{16\pi^2 r^2 \gamma_{\text{tip}}} \quad (4)$$

Adhesion forces measurements were also used to create the adhesion force map of HPF-coated (0.01 mg/mL, 5 min) surfaces, which supported the detection of single HPF molecules and identification of their spatial arrangement. Before measurement AFM tip was subjected to UV-cleaning, making it superhydrophilic.

HPF molecules visualization and surface energy experiments were additionally performed under aqueous conditions without previous samples drying after the adsorption procedure. The same adsorption parameters as for imaging under air conditions were applied. Standard sharp silicon nitride cantilevers (SNL-10, Brucker, Santa Barbara, CA) with a resonance frequency in the range 50 - 80 kHz, spring constant 0.175 - 0.7 N/m,

and a mean tip radius of 6 nm were used. Measurements were performed in QI mode with a loading force of 1 nN.

### **5.2.5. X-ray photoelectron spectroscopy (XPS)**

Before and after HPF adsorption (5 min, 0.01 mg/mL) surface chemistry was determined by XPS measurements performed with Quantum 2000 system (PHI Co., Chanhassen, MN, USA) equipped with monochromatic AlK $\alpha$  source (250 W,  $h\nu = 1486.6$  eV). Multipak software was used for peak identification and quantification. High-resolution spectra C 1s, N 1s, and O 1s were obtained using an analyzer pass energy of 58.7 eV. A binding energy scale was referenced to C 1s peak set at 285.0 eV. For a detailed analysis of bond reconstruction in HPF molecules after adsorption, deconvolution of C 1s and N 1s was performed using curve-fitting analysis and Gaussian–Lorentzian curve fitting procedure in OriginPro 2020 software.

### **5.2.6. Statistical analysis**

The results are presented as mean values with  $\pm$  standard deviations. Statistical analysis in a given group was performed by One-Way analysis (ANOVA) with Turkey test ( $p < 0.05$ ) using Origin software.

## **5.3. Results and discussion**

### **5.3.1. Characterization of rutile single crystals**

Raman spectra of (110), (100), (101), and (001) rutile single crystals are presented in [Figure 5.1. a](#)). Two major vibration modes were recorded, E<sub>g</sub> at 448 cm<sup>-1</sup> and A<sub>1g</sub> at 610 cm<sup>-1</sup>, which corresponds to an asymmetric bending of O–Ti–O bonds by oxygen atoms and symmetric stretching of O–Ti–O bonds, respectively.<sup>195</sup> The ratio of A<sub>1g</sub> to E<sub>g</sub> intensity for each surface was calculated. Since anisotropic scattering of rutile crystals is determined by crystallographic structure, this ratio has been used to distinguish crystals in the subsequent experimental procedure, if necessary.<sup>192</sup>

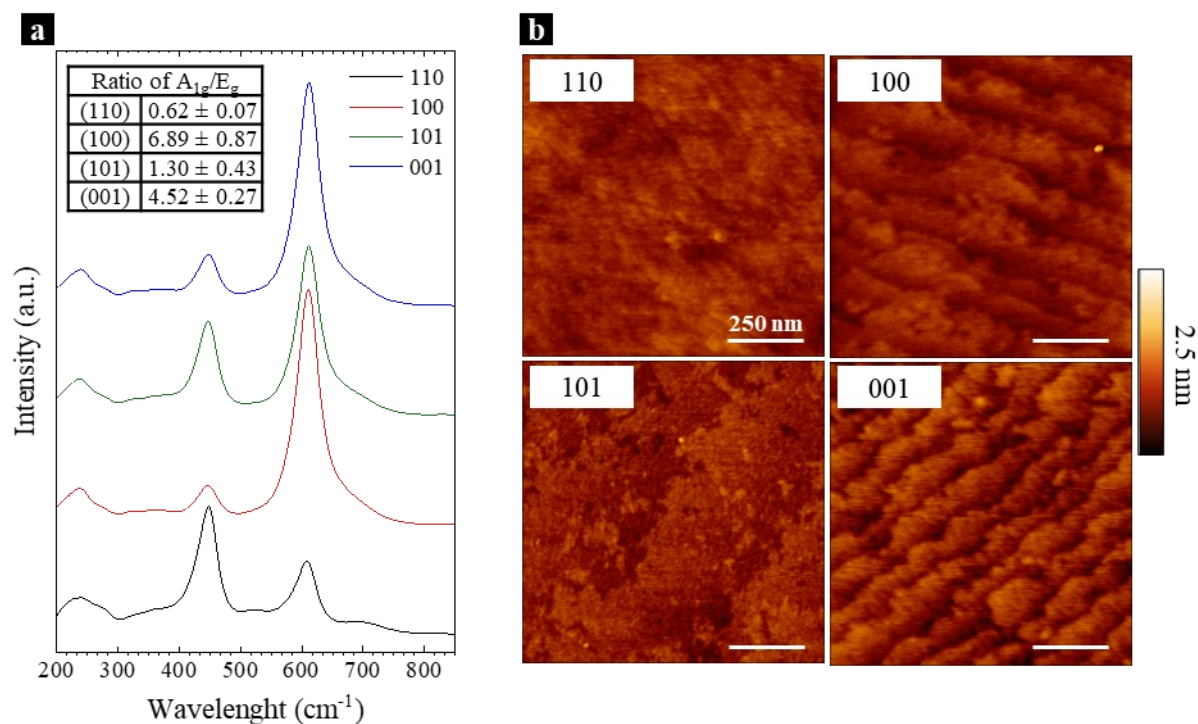


**Figure 5.1.** a) Raman spectra characteristic for rutile single crystals with a calculated ratio of  $A_{1g}$  to  $E_g$  intensity. b) AFM images of bare rutile single crystals.

Figure 5.1. b) shows topographies of bare rutile single crystals visualized by AFM. Based on at least four 1000 nm x 1000 nm images, the root mean square roughness ( $R_q$ ) parameter of surfaces was calculated and the results are presented in Table 5.1. All values are below 0.15 nm, therefore surfaces can be considered atomically flat. According to the literature, this allows us to exclude roughness as a parameter affecting protein adsorption in this study.<sup>38,125</sup>

**Table 5.1.** Crystallographic orientation-dependent properties of rutile single crystals.

Orientation	$R_q$ (nm)	Water contact angle ( $^\circ$ )
(110)	$0.119 \pm 0.004$	$65.2 \pm 0.7$
(100)	$0.081 \pm 0.006$	$59.6 \pm 1.4$
(101)	$0.144 \pm 0.006$	$61.3 \pm 0.4$
(001)	$0.130 \pm 0.003$	$58.0 \pm 0.7$

Since different arrangements, coordination of surface atoms, and density of dangling bonds determine surface energy and wettability (see Chapter 2.1.2.), these factors were considered potential determinants of crystallographic orientation-dependent biological reactions. It is known that the surface energy of rutile increases proportionally to a degree

of undercoordination of surface atoms (compared to bulk atoms), i.e. in the following order: (110) < (100) < (101) < (001).<sup>28,196</sup> Moreover, the wettability of rutile single crystals was measured using the sessile drop method. The water contact angle ( $\Theta$ ) on all crystal surfaces is below 90.0°, suggesting their hydrophilicity (Table 5.1.). However, the highest angle value  $65.2 \pm 0.7^\circ$  was found for the (110) surface and the lowest  $58.0 \pm 0.7^\circ$  for the (001) surface. These differences can be attributed to crystallographic orientation-dependent variations in rutile surface structure, which can affect the nature of water adsorption (molecular or dissociative).<sup>197</sup> It is known that water dissociation dominates on the (001) surface due to a large number of dangling bonds per unit area, resulting in a high probability of chemisorption of hydroxyl (-OH) groups.<sup>32</sup> This makes the (001) surface more hydrophilic compared to the others, especially the (110) surface where molecular adsorption tends to occur.<sup>33,34</sup>

It is widely recognized that differences in surface energy and therefore wettability are major parameters controlling the amount and conformation of proteins.<sup>198</sup> Therefore, it is worth studying whether the adsorption behavior of HPF varies on the investigated rutile single crystals.

### 5.3.2. Analysis of HPF adsorption on rutile single crystals

To explore the effect of the surface crystallographic orientation on the adsorption behavior of HPF, rutile single crystals were incubated in solutions 0.01 mg/mL and 0.1 mg/mL at 37 °C. After 5 min and 30 min, time- and concentration-dependent surface coverage was analyzed (Figure 5.2.). Firstly, AFM imaging in an air condition, shown in Figure 5.2. a), enabled determination of adsorption parameters, a concentration of 0.01 mg/mL, and an adsorption period of 5 min, necessary for single protein visualization. Higher concentration or longer adsorption time contributed to full surface coverage, which is in agreement with the literature.<sup>194,199</sup> These observations were further confirmed by quantitative evaluation of the amount of adsorbed proteins using BCA assay. Results presented in Figure 5.2. b) indicate a lack of statistical differences in the amount of protein on all crystals after 30 min of adsorption regardless of solution concentration. This implies full surface coverage by HPF. Nevertheless, 5 min adsorption from a 0.01 mg/mL solution resulted in a statistically significant lower amount of adsorbed HPF on the (001) surface compared to the others, pointing to the lowest affinity of HPF to this surface. This

phenomenon was not observed after 5 min of adsorption from 10 times higher concentrated solution i.e., 0.1 mg/mL, suggesting fast full coverage of crystals surface by HPF at biologically relevant concentrations.

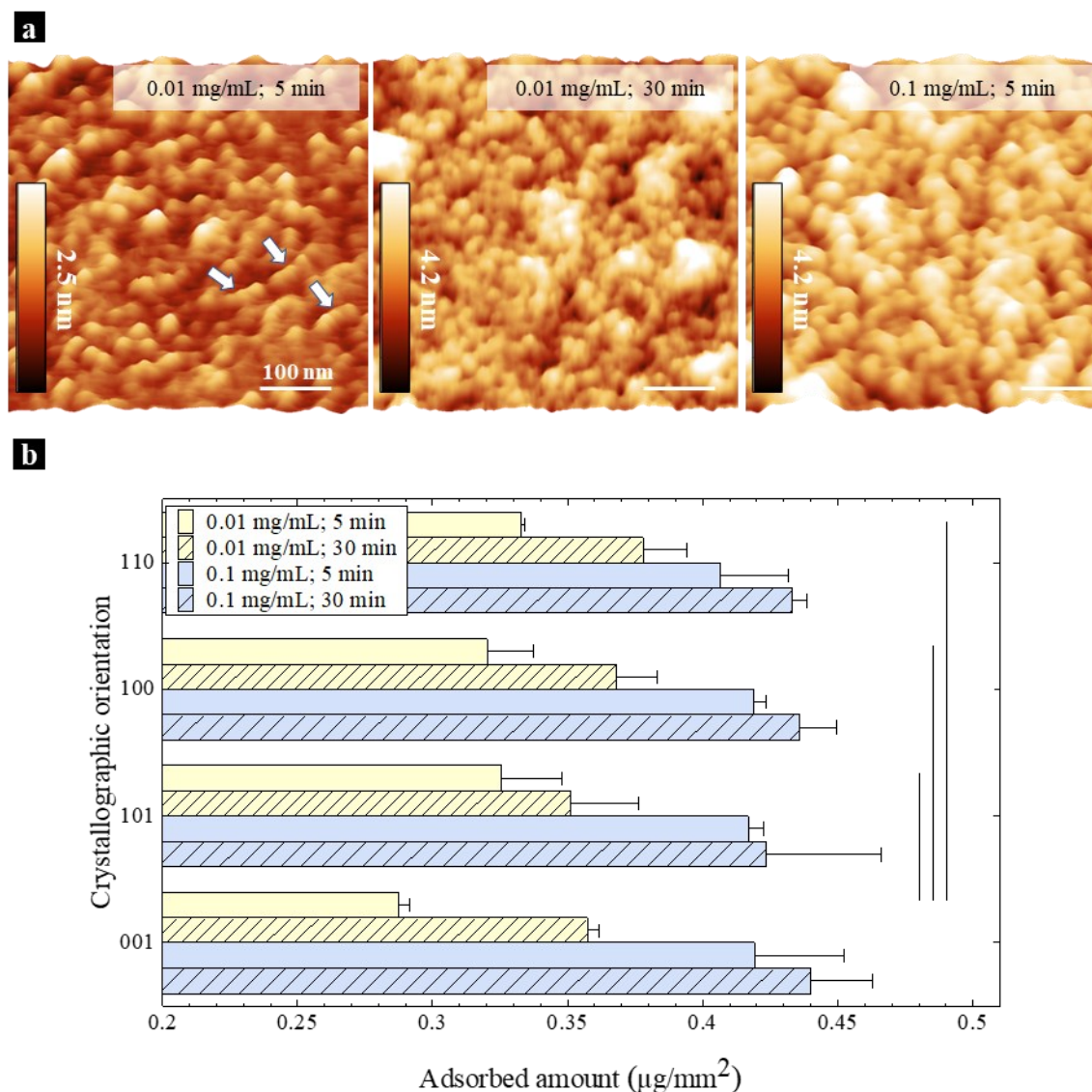


**Figure 5.2.** Time- and concentration-dependent HPF adsorption on rutile single crystals. a) AFM visualization of adsorbed HPF on rutile crystals, on the example of the (110) surface. Arrows point out exemplary single proteins. b) Amount of adsorbed HPF determined using BCA assay. Three measurements per sample were performed. Lines next to the bars indicate the statistical differences among groups ( $p > 0.05$ ).

Based on these results and a well-known structure of HPF (schematic sketch presented in [Figure 2.6.](#)), the conformation of HPF was analyzed using AFM images of samples exposed to 0.01 mg/mL solution for 5 min. Protein conformation turned out to be different on various surfaces, as shown in [Figure 5.3. \(left site\)](#). Three individual, one central, and

two distal nodes of HPF are distinguishable on the (110) surface, which can be ascribed to hydrophobic E and D domains. In contrast, on the (001) surface, HPF appears as a single globule. On the other two i.e., (100) and (101) surfaces, both (trinodular and globular) conformations are detectable, however, globular molecules dominate.

Visual assessment of HPF conformation was confirmed by analysis of height profile lines of individual HPF molecules adsorbed on each rutile crystal and enabled the evaluation of protein dimensions. Representative single-molecule profile lines are shown in [Figure 5.3. \(right site\)](#). Based on at least 100 measurements the histograms of length and proteins height distributions were created and are shown in [Figure 5.4](#). The greatest mean length and the lowest mean height were determined for trinodular HPF adsorbed on the (110) surface i.e.,  $46 \pm 4$  nm and  $1.6 \pm 0.2$  nm, respectively, due to the high molecules unfolding. Similar structures were previously reported for HPF adsorbed on hydrophobic substrates such as highly ordered pyrolytic graphite (HOPG)<sup>200</sup>, titanium dioxide (TiO<sub>2</sub>)<sup>38</sup>, poly(methyl methacrylate) (PMMA)<sup>100</sup>. In contrast, globular HPF molecules on the (001) surface were significantly shorter ( $21 \pm 2$  nm) but at the same time had higher mean height i.e.,  $3.1 \pm 0.4$  nm. This is consistent with the HPF dimensions observed on hydrophilic surfaces such as mica or silicon surfaces.<sup>152,201,202</sup>

The heterogeneity of HPF conformation on the other two (100) and (101) surfaces is manifested by the presence of more than one band in the length distribution histogram, which is not the case for (110) and (001) surfaces. On the (101) surface the shortened i.e., partially unfolded HPF molecules, with a length of  $\sim 30$  nm, are present in 15%. 12% of the molecules have an average length of  $45 \pm 3$  nm, which relates to HPF in trinodular conformation. The remaining 73% of proteins have  $22 \pm 2$  nm and this is ascribed to globular proteins. The diversity of molecules conformations contributes to a broad distribution of their heights.



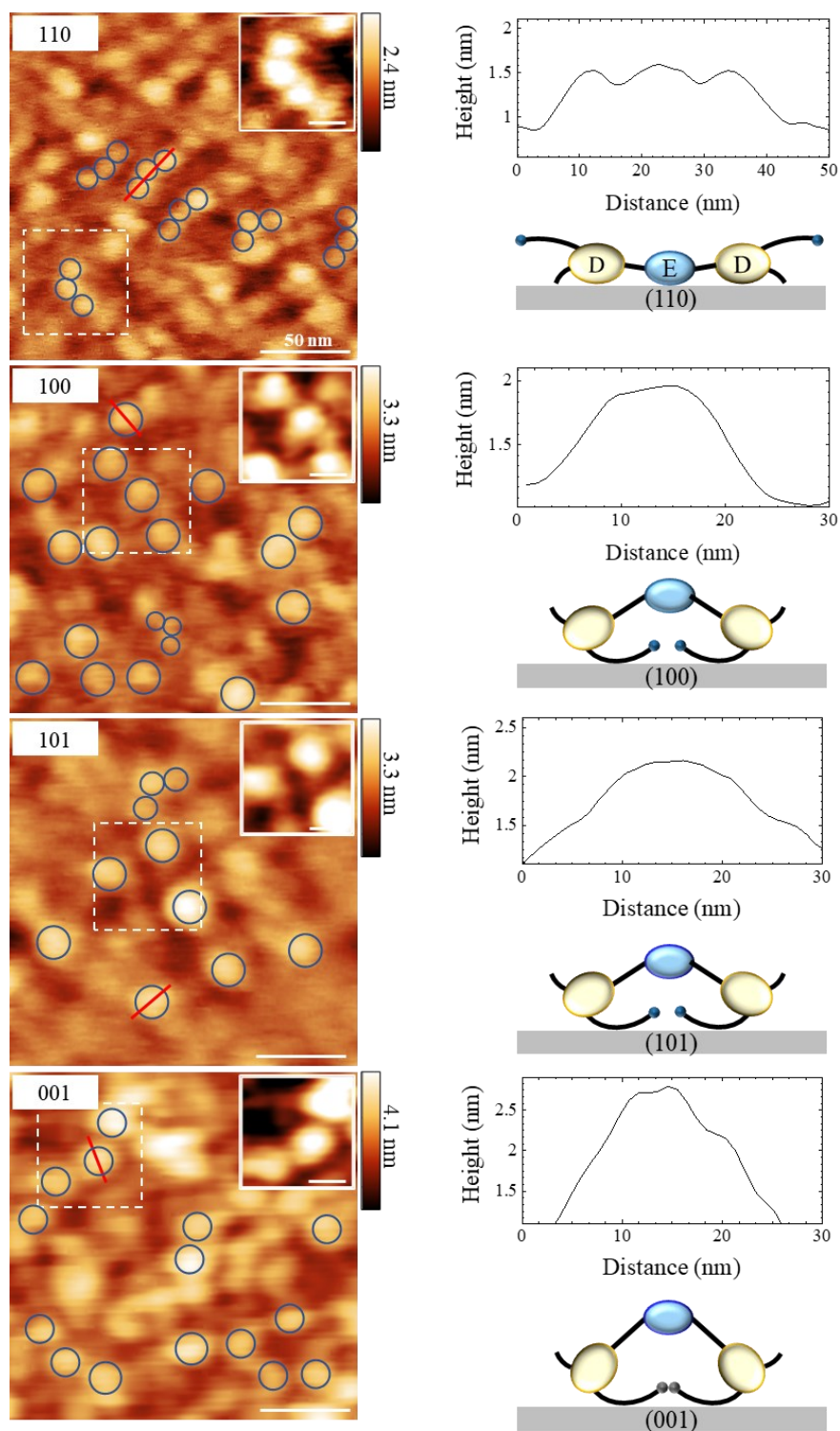


**Figure 5.3.** AFM visualization (200 x 200 nm) of the (110), (100), (101), (001) rutile single crystals with adsorbed HPF. Exemplary molecules are marked with circles. Zoomed images (60 x 60 nm; scale bar 20 nm) in the inset show a single HPF molecule on each surface. Representative profile line of individual molecules supports the visual determination of the protein conformation and allows estimation of its dimensions. A schematic HPF spatial arrangement with marked hydrophobic D and E domains is presented.



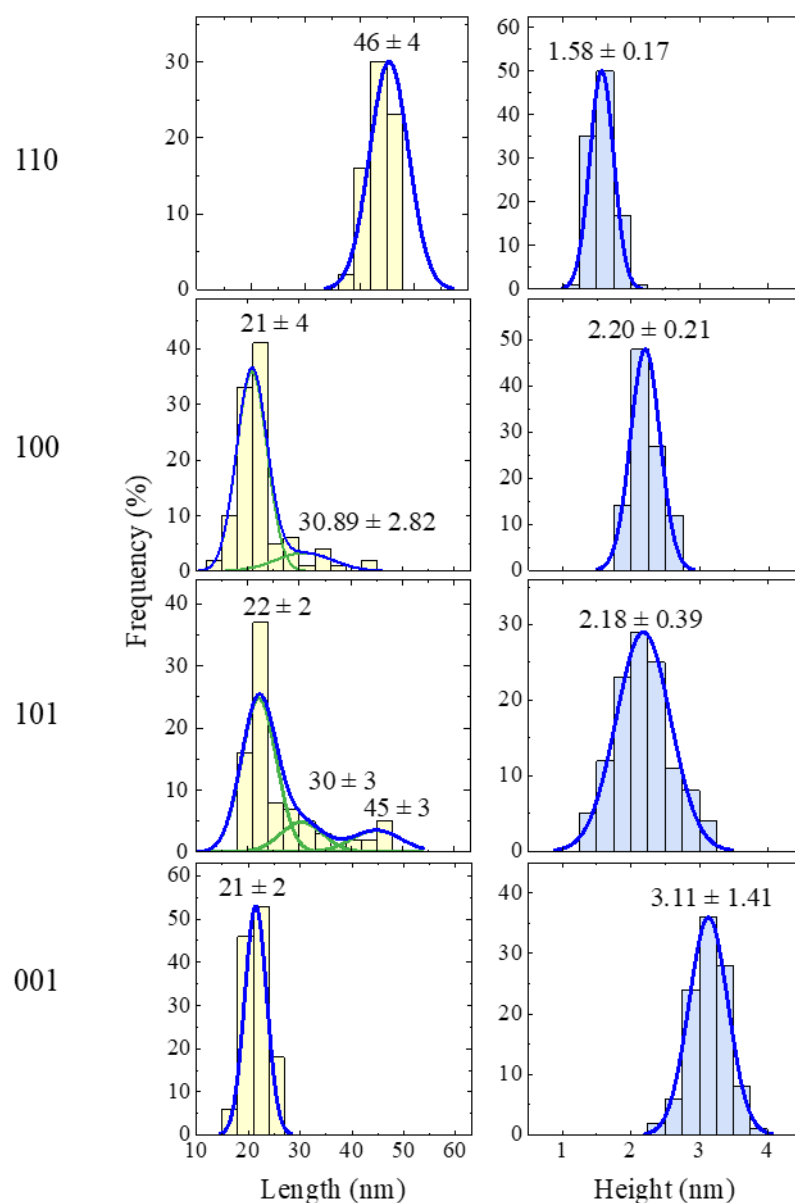


**Figure 5.4.** Histogram analysis of the measured HPF length and height distributions adsorbed on rutile single crystals ( $n > 100$ ). A Gaussian-fitted curve overlays each histogram (blue and green curves). The average lengths and heights of the proteins are given above the peaks.

Since a liquid is a biologically relevant environment, the dependence of HPF conformation on rutile single crystals was also studied under aqueous conditions. By means of AFM, HPF molecules adsorbed on the (110) and (001) surfaces were visualized under water conditions (Figure 5.5.). Substantial similarity in the appearance of HPF structures on the given crystals to those observed in an air was detected. This indicates that HPF conformations detected during measurements in an air may correspond to those present upon material contact with body fluids i.e., blood plasma.

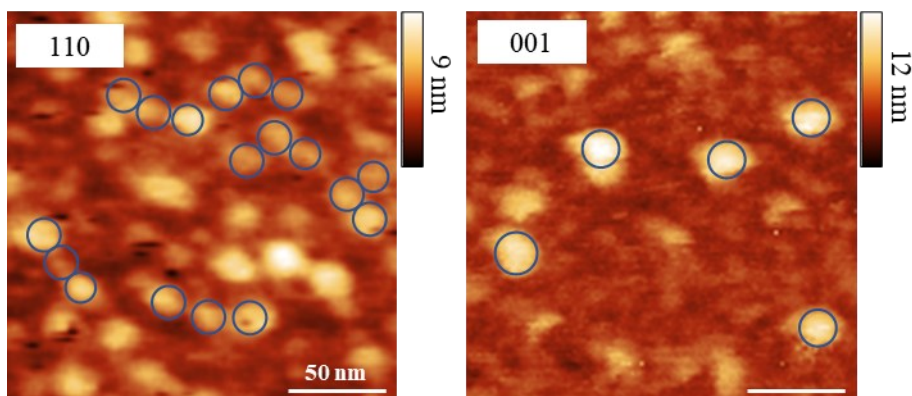


**Figure 5.5.** AFM images (200 nm x 200 nm) of HPF adsorbed on the (110) and (001) rutile single crystals, taken under aqueous conditions. Exemplary molecules are marked with circles.

An explanation for these crystallographic orientation-dependent differences in HPF adsorption behavior can be inferred by analyzing water contact angles of the rutile surfaces and the nature of individual HPF domains. Generally, material surfaces are considered hydrophobic if  $\Theta > 90^\circ$ , whereas hydrophilic if  $\Theta < 90^\circ$ . Nevertheless, Berg *et al.* defined a new hydrophobicity/hydrophilicity limit i.e., water contact angle  $\Theta = 65^\circ$ , in the context of protein adsorption.<sup>104</sup> According to this concept, surfaces with a water contact angle value  $\Theta \geq 65^\circ$  are hydrophobic due to a weak attraction of water molecules, and the presence of hydrophobic forces that promote protein adsorption and unfolding.<sup>111,203</sup> This is energetically favorable since surface dehydration and protein adsorption minimize the contact of the hydrophobic surface with water, whereas protein unfolding leads to entropy gain. This refers to the (110) rutile single crystal (see Table 5.1.). It is widely recognized that on hydrophobic materials HPF adsorbs via hydrophobic E and D domains, which is accompanied by HPF unfolding and trinodular conformation.<sup>98-100</sup> Other rutile single crystals ( $\Theta < 65^\circ$ ) can be considered hydrophilic as strongly bounded water molecules limit protein-surface interactions on such surfaces, which promotes the occurrence of HPF in a globular conformation.<sup>199</sup> HPF adsorb via hydrophilic  $\alpha$ C domains on such surfaces.

Moreover, Vogler *et al.* recognized that large changes in protein behavior tend to occur if a water contact angle of a material surface is in the range of  $\Theta \sim 60 - 65^\circ$ .<sup>103</sup> A detailed review of numerous reports allowed them to distinguish surfaces as a "protein adherent" and "non-adherent" depending on water contact angle value above or below this borderline, respectively. This explains the existence of both trinodular and globular HPF

molecules on the (100) and (101) surfaces, as their water contact angle lies in this transition range.

### 5.3.3. XPS analysis

For a better understanding of the crystallographic orientation-dependent conformational changes of HPF, XPS measurements were performed before and after HPF adsorption. [Figure 5.6](#) shows a representative survey spectrum of a bare rutile substrate. The lack of components other than those corresponding to TiO<sub>2</sub> and carbon from the air suggests an absence of impurities on investigated crystals.<sup>204</sup>

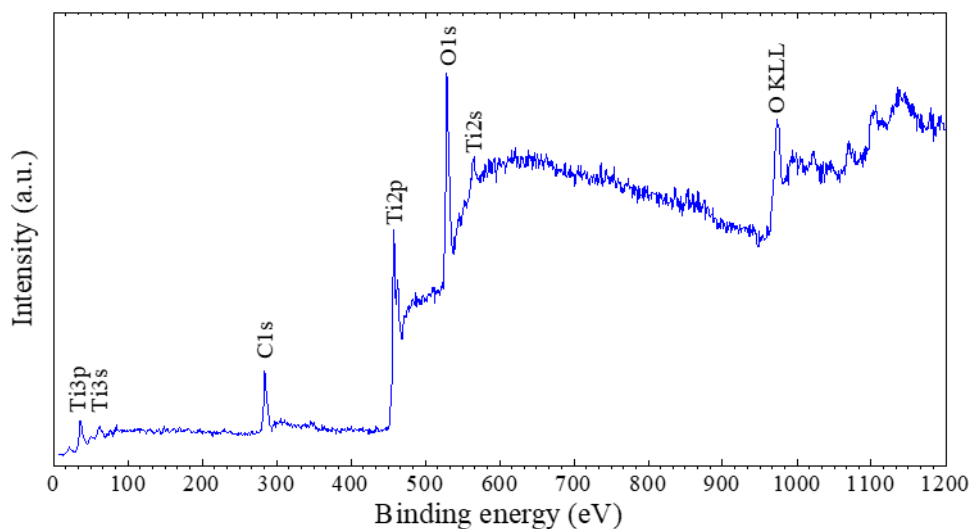


**Figure 5.6.** Representative survey XPS spectrum of rutile single crystal with marked detected components.

Further detailed analysis of high-resolution spectra enabled quantitative evaluation of surface atomic compositions. Results are presented in [Table 5.2](#). After 5 min HPF adsorption from a 0.01 mg/mL solution, the lowest nitrogen content and suppression of the TiO<sub>2</sub>-derived signal (Ti:C) were found for the HPF-coated (001) surface, which indicates the smallest amount of absorbed HPF and confirms BCA results within the measurement accuracy.

**Table 5.2.** Composition of the (110), (100), (101), and (001) rutile single crystals before and after HPF adsorption (5 min, 0.01 mg/mL).

Sample	Orientation	N (at%)	Ti: C
BARE	(110)	-	0.46
	(100)	-	0.43
	(101)	-	0.56
	(001)	-	0.41
HPF	(110)	6.22	0.40
	(100)	7.35	0.29
	(101)	9.66	0.23
	(001)	5.81	0.41

In addition, deconvolution of the carbon (C 1s) and nitrogen (N 1s) high-resolution spectra were conducted to gain deeper insight into the nature of the bonds in the HPF molecules. Results are shown in Figure 5.7. and Table A1.

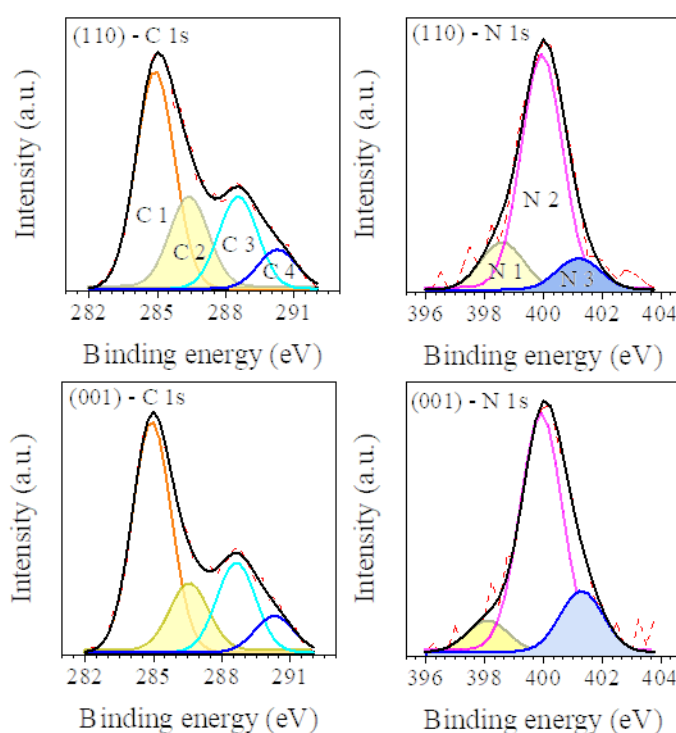


**Figure 5.7.** Deconvoluted carbon (C 1s; left images) and nitrogen (N 1s; right images) spectra of HPF-coated (110) and (001) surfaces. Dashed lines correspond to the raw data, while solid lines represent Gaussian fitting.

The deconvoluted carbon band revealed four peaks marked as C1 - C4. The C2 and C3 are specific for proteins and are attributed to amino (C-N) and peptide (HN-C=O) groups, respectively.<sup>205</sup> For the nitrogen band, three peaks appeared, i.e., N1, N2, and N3 referring

to amino (C-N), peptide (N-C=O), and protonated amino (C-NH<sub>3</sub><sup>+</sup>) groups, respectively.<sup>205,206</sup> Significant differences in the level of amino- and protonated amino groups were detected between (110) and (001) surfaces. This is manifested in smaller C2 and N1 band areas, while simultaneously higher N3 band area on the (001) surface. The diversity of emerging groups and their content on HPF-coated rutile surfaces is correlated with an adsorption-induced peptide bond breaking and HPF structure rearrangement which level determines the type and the number of newly formed bonds. This is dependent on HPF conformation, which supports the AFM observations.

#### **5.3.4. Surface energy of rutile single crystals after HPF adsorption**

Observed crystallographic orientation-dependent HPF conformational changes indicate a rearrangement of hydrophilic/hydrophobic groups and suggest that exposure to a medium of specific HPF regions may determine the surface energy of a material.

Before and after HPF adsorption, interaction strength (adhesion forces) between hydrophilic AFM tip and rutile single crystals was measured in an air condition, and surface energy was calculated in a manner described in the methodology part. Determined surface energies of bare rutile single crystals were used as a reference for studies of surface energy changes after HPF adsorption. As presented in [Figure 5.8](#). (yellow bars), their surface energy increases in the order of (110) < (100) < (101) < (001), which is consistent with theoretical values estimated based on computer simulations ([Table 2.1](#).) and the measurements of Cai *et al.* with minor discrepancies, which may come from the tip geometry used for the study.<sup>28,29,192,207</sup> The strongest interactions were detected between a hydrophilic AFM tip and a hydrophilic (001) surface.

Striking results were found after 30 min HPF adsorption from 0.01 mg/mL solution (full surface coverage). Values of the surface energy of all surfaces (measured in the air) decreased up to an order of magnitude and followed an inverse trend compared to bare substrates, i.e., (110) > (100) > (101) > (001) (see [Figure 5.8](#)).

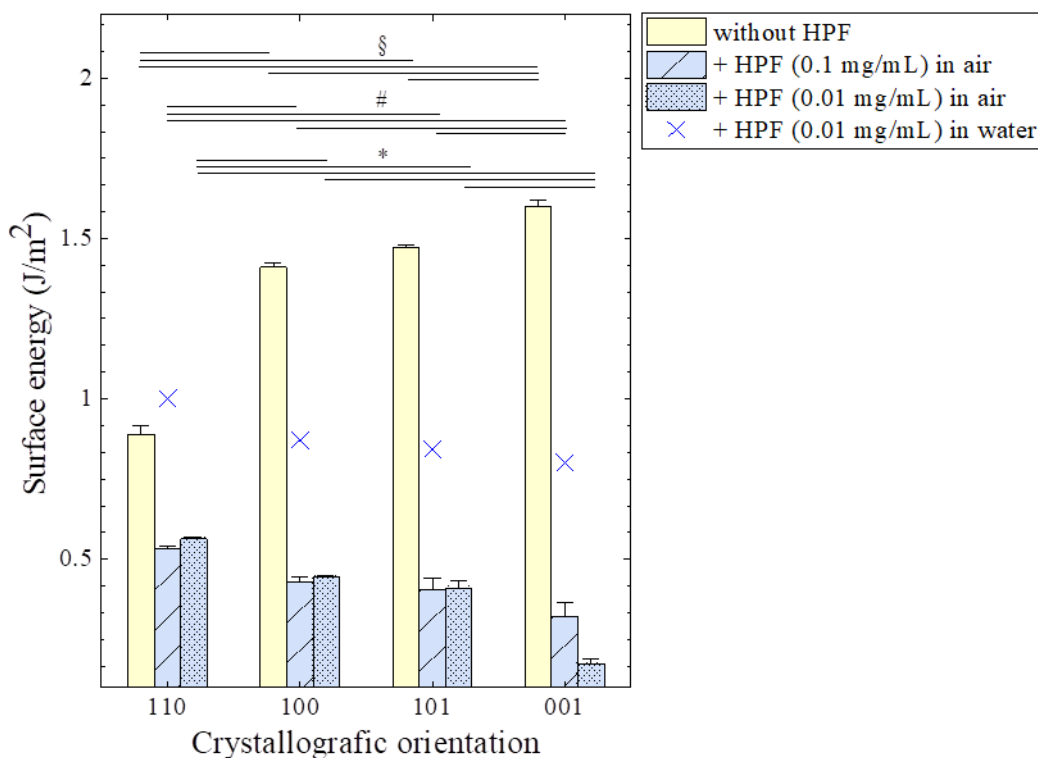


**Figure 5.8.** Determined surface energy of rutile single crystals before (yellow color) and after 30 min HPF adsorption (blue color) from solutions with concentrations 0.1 mg/mL and 0.01 mg/mL, respectively. Measurements were performed in air (bars) or aqueous (crosses) conditions. Lines above bars indicate statistical differences ( $p > 0.05$ ) between § bare substrates, # HPF-coated substrates (0.1 mg/mL), \* HPF-coated substrates (0.01 mg/mL).

Supported by AFM imaging, analysis of interactions between a hydrophilic AFM tip and exposed specific HPF regions with hydrophilic/hydrophobic nature, contributes to a better understanding of protein behavior in a hydrophilic blood environment. It is widely recognized that protein adsorption occurs when it is accompanied by a net decrease in the energy of the surface-protein-medium system. The stronger protein adsorption and unfolding are typically observed on hydrophobic substrates to limit undesired hydrophobic-hydrophilic interactions between material surface and medium.<sup>98–100</sup> Moreover, generation of a surface-protein interface is associated with simultaneous generation of a protein-medium interface. HPF adsorption via hydrophobic domains on hydrophobic surfaces, such as rutile (110) surface, allows hydrophilic regions to strongly interact with hydrophilic AFM tip and medium. In contrast, HPF adsorption on hydrophilic surfaces, such as (001) surface, through hydrophilic groups, triggers simultaneous hydrophobic-hydrophilic interactions at the protein-medium interface. This is energetically less favorable and prevents further protein molecules unfolding and

results in a globular HPF conformation.<sup>112</sup> It can be stated that an analysis of surface energy differences after coverage by proteins allows to observe their adsorption-induced conformational changes. Moreover, the same findings were observed on rutile surfaces exposed to HPF solution with a biologically more relevant concentration i.e., 0.1 mg/mL (Figure 5.8. blue bars) and conducting AFM measurements in aqueous conditions (Figure 5.8. crosses), which validates the relevance of these observations in vivo regardless of protein concentration.

It is worth mentioning that crystallographic orientation-dependent differences in the surface energy after protein adsorption were also observed by Cai *et al.* who studied fibronectin adsorption on rutile single crystals.<sup>192</sup> However, in this case, reported values were higher than for bare substrates and followed the reversed order i.e., (110) < (100) < (101) < (001) compared to HPF. These distinct results point out the specificity of surface energy variations for a given type of protein.<sup>208</sup> In addition, it has been found that the phenomenon of surface energy changes after protein adsorption may be one of the factors influencing subsequent processes at the biomaterial - blood interface such as biomineralization.<sup>192</sup>

The AFM measurements of adhesion forces between the AFM tip and proteins also enabled the creation of an adhesion force map that supports protein detection and identification of their conformations. Before measurements, AFM tip was subjected to UV cleaning, making it superhydrophilic. Adhesion force maps recorded for HPF-coated (110) and (001) surfaces are presented in Figure 5.9.

Due to the significant differences in interaction forces between superhydrophilic tip-HPF and superhydrophilic tip - rutile crystal, the identification of proteins and their conformations could be observed, which was an alternative to the usual AFM topography imaging. In addition, the future subject of our research is high-resolution AFM adhesion force mapping, which provide also an opportunity to analyze the exposure of hydrophilic/hydrophobic groups of proteins to the medium at the atomic scale. This would show a full picture of proteins' adsorption mechanism, their spatial arrangement, and the availability of specific regions for successively attaching cells.<sup>209</sup>



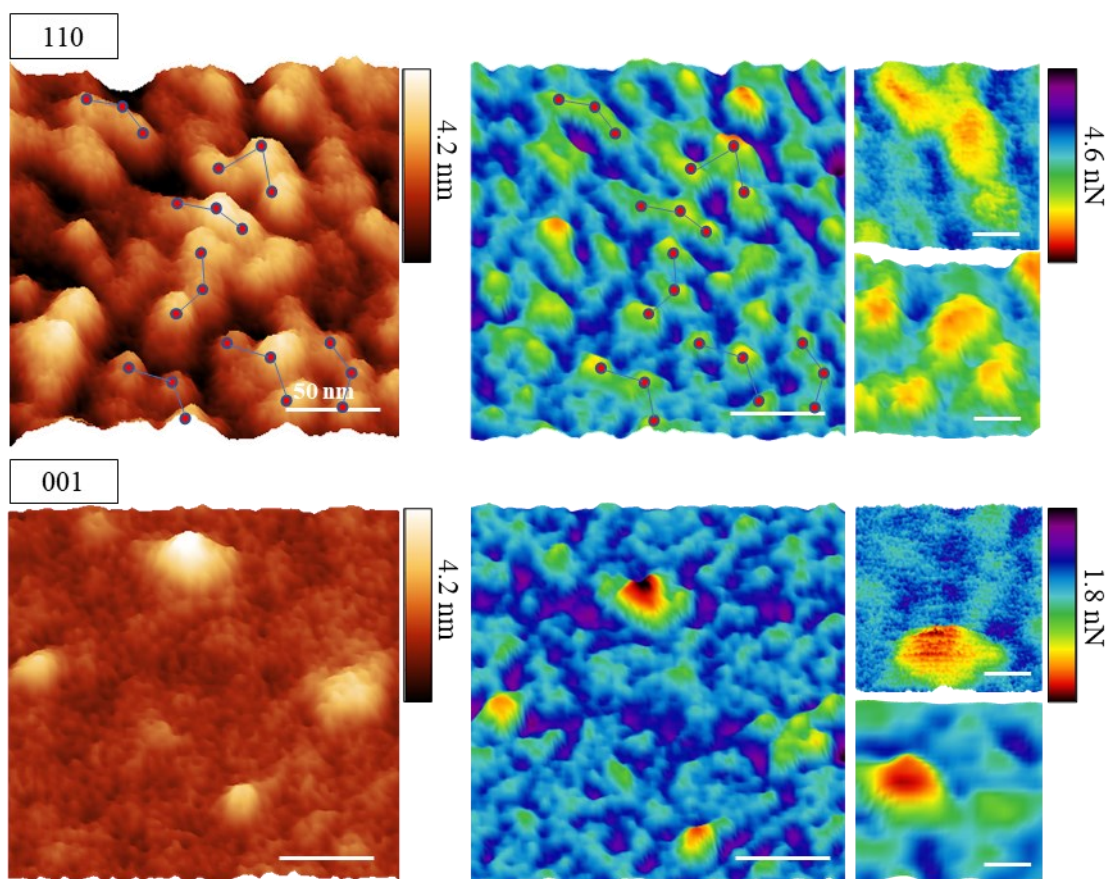


**Figure 5.9.** AFM images (3D) and corresponding adhesion maps of HPF-coated (110) and (001) surfaces. The upper images refer to the (110) surface with marked trinodular proteins and the bottom images to the (001) surface. Images on the right side correspond to represent the adhesion map of single HPF molecules recorded on these surfaces.

### 5.3.5. Model of HPF adsorption on rutile single crystals

Structure analysis of HPF molecules adsorbed on rutile single crystals allowed to model crystallographic orientation-dependent HPF adsorption mechanism. In [Figure 5.10.](#), a relationship between surface atomic structure, its properties, and resulting HPF conformation is schematically summarized. As the coordination number of surface atoms is reduced i.e., surface unsaturation increases due to broken bonds upon its formation, surface energy increases, which leads to its hydrophilicity and consequently minimizes the tendency of HPF molecules to unfold upon adsorption.

More specifically, in the case of (110) surface, presence of six coordinated Ti atoms (as in bulk) alternated by five coordinated Ti atoms, and three coordinated O atoms (as in bulk) alternated by two coordinated O atoms, leads to its low energy and imparts its hydrophobicity. Therefore, HPF easily displaces weakly bound water molecules and



adsorbs in trinodular conformation. For other surfaces, in particular (001) surface, higher undercoordination of surface atoms and higher density of dangling bonds increases surface energy and hydrophilicity, which in turn increases the probability of HPF adsorption in a globular conformation. Since HPF conformation determines the availability of platelet binding sites, in the following chapter the HPF conformation-dependent response of platelets to rutile single crystals will be described.

(110)	(100)	(101)	(001)
$\gamma_{110} = 0.96 \text{ J/m}^2$	$\gamma_{100} = 1.01 \text{ J/m}^2$	$\gamma_{101} = 1.41 \text{ J/m}^2$	$\gamma_{001} = 1.90 \text{ J/m}^2$
hydrophobic	hydrophilic	hydrophilic	hydrophilic

**Figure 5.10.** Model of HPF adsorption on rutile single crystals. On low energetic, hydrophobic ( $\Theta \geq 65^\circ$ ) surfaces HPF preferentially adsorb in trinodular conformation, whereas on high energetic, hydrophilic surfaces in globular one. Keep in mind that in the transition water contact angle range for hydrophilicity/hydrophobicity ( $\Theta = 60 - 65^\circ$ ), which applies to (100) and (101) surfaces, HPF adsorbs in both conformations, however, globular structures dominate.

## 5.4. Conclusion

In conclusion, this chapter provides evidence to accept the hypothesis that the crystallographic orientation of  $\text{TiO}_2$  (rutile) crystal surfaces determines the conformation of the adsorbed HPF molecules. However, an impact on the amount of absorbed protein was not observed.

AFM visualization of the (110), (100), (101), and (001) rutile single crystals revealed adsorption of HPF in a trinodular conformation on low energetic and hydrophobic (110) surface, while in globular one on more energetic and hydrophilic surfaces, in particular (001) surface. In addition, the hypothesis that the surface energy of protein-coated substrates is protein conformation dependent has been accepted. Observed phenomena are relevant in vivo regardless of protein concentration.

Results presented here suggest that HPF conformation may be a major determinant of subsequent cellular response. This motivates investigations into whether the high biocompatibility and antithrombogenicity of implants can be achieved by designing a rutile surface with a preferred crystallographic orientation.

## **6. Crystallographic orientation-dependent platelet adhesion and activation on rutile single crystals**

### **6.1. Introduction**

In the previous chapter, the influence of rutile crystallographic orientation on HPF conformation was confirmed. Since HPF is a major initiator of thrombogenic events, this was the basis for a hypothesis that observed crystallographic orientation-dependent HPF conformational changes may affect platelet adhesion and activation. Therefore, platelets behavior on rutile single crystals with (110), (100), (101), and (001) crystallographic orientations was characterized by scanning electron microscopy (SEM) and optical microscope (OM). Platelet activity was additionally examined with the usage of fluorescent antibodies, detectable by confocal microscopy and immunofluorescence technique. Finally, it has been investigated whether observed platelet behavior is correlated with the availability of primary platelet binding sites in HPF molecules. Obtained results provide a deep insight into the mechanism of HPF-mediated, platelet adhesion on rutile single crystals.

### **6.2. Materials and Methods**

#### **6.2.1. Rutile single crystals**

To examine crystallographic orientation-dependent platelets adhesion, the same type of epi-polished rutile single crystals (5 mm x 5 mm x 0.5 mm), as for protein adsorption experiments (see Chapter 5.2.1.) were used. Briefly, studies presented in this chapter were performed on crystals with (110), (100), (101), and (001) crystallographic orientations. Before experiments, all substrates were thoroughly sterilized in ethanol.

#### **6.2.2. Platelet adhesion on rutile single crystals**

Pooled platelet plasma concentrate (PPP,  $2.7 \times 10^8$  platelets per mL) was obtained from four buffy coats of voluntary whole blood donors after informed consent. Then, 0.5 mL of PPP was added to each rutile substrate placed in 24-well plates and kept in an oven

with 5% CO<sub>2</sub> for 5 min or 120 min at 37 °C. Then the samples were thoroughly washed with PBS and subjected to further experiments.

### **6.2.3. Platelets visualization using scanning electron microscopy (SEM) and optical microscope (OM)**

Before SEM imaging, platelets were fixed on substrates by immersion in 2.5% glutaraldehyde overnight at T = 4 °C. Then, samples were washed with PBS and dehydrated with graded ethanol series (10% - 100%, each step for 10 min). Subsequently, ethanol was partially replaced by hexamethyldisilane (HDMS ≥ 98% from GC, Carl Roth, Germany) in steps 25, 50, and 75% HDMS, until the final step 100% HDMS. Samples were left to dry overnight in ambient conditions and afterward sputtered with tungsten. In the end, the platelets morphology was examined by SEM (Auriga 60® CrossBeam Workstation, Carl Zeiss Jena GmbH, Jena, Germany) at an accelerating voltage of 5 kV.

Platelets coverage of each rutile surface was assessed using an optical microscope (Leica DM2700M) and evaluated with ImageJ software at a minimum of four positions per sample (n > 4). Each OM image was converted to an 8-bit image and then to a binary image. Afterward, a threshold was adjusted, and the area occupied by platelets was calculated.

### **6.2.4. Immunofluorescence and confocal microscopy**

P-selectin is a marker of platelet state due to its expression on the platelet membrane only after platelet activation.<sup>210</sup> It can be identified by specific fluorescently labeled antibodies detectable by immunochemistry and confocal microscopy. For those experiments, adhered platelets were fixed on substrates with paraformaldehyde (4% in PBS) overnight at T = 4 °C. Subsequently, samples were blocked with 1% BSA for 1 h at 37 °C and then immersed in 600 µL of primary mouse monoclonal P-selectin antibodies (diluted 1: 300 in PBS, antibodies-online GmbH) for 1 h at T = 37 °C. After washing five times in PBS, the secondary Alexa Fluor® 488 conjugated goat anti-mouse IgG antibody (diluted 1: 300 in PBS, Abcam, Cambridge) for confocal microscopy and HRP conjugated goat anti-mouse IgG antibody (diluted 1: 1000 in PBS; Abcam, Cambridge) for immunochemistry were added. Finally, samples were rinsed five times in PBS and one set was directly used

for visualization of expressed P-selectin using confocal microscopy. At least four images per crystal were recorded.

The second set of the samples, for immunochemistry, was additionally immersed in 150  $\mu\text{L}$  of TMB solution for 20 min at  $T = 37\text{ }^\circ\text{C}$  in the dark. To stop the reaction, 50  $\mu\text{L}$  of 1 M  $\text{H}_2\text{SO}_4$  was added. A 130  $\mu\text{L}$  of each reaction mixture was pipetted and placed in 96-well plates. Absorbance was measured at 450 nm with a PowerWave XS plate reader (BioTek Germany, Bad Friedrichshall, Germany). All samples were examined in triplicate and background fluorescence was subtracted.

The conformation-dependent availability of the primary platelet recognition sites  $\gamma^{400-411}$  in HPF molecules was determined also by immunochemistry. The same procedure as for P-selectin expression measurements was used, however, a mouse monoclonal anti-human HPF  $\gamma$ -chain antibody (diluted 1:300 in PBS, Bio-Techne GmbH, Germany) was used as a primary antibody.

### **6.2.5. Statistical analysis**

Results are presented as mean values with  $\pm$  standard deviations. Statistical analysis in a given group was performed by One-Way analysis (ANOVA) with Turkey test ( $p < 0.05$ ) using Origin software.

## **6.3. Results and Discussion**

### **6.3.1. Analysis of platelets adhesion and activation**

Platelet pooled plasma (PPP) used in this study contained a certain amount of protein, including HPF at a concentration of about 0.3 mg/mL. In the previous chapter, it was described that such a concentration is sufficient for full coverage of rutile surfaces in a short time, therefore it can be assumed that in this study HPF layer guides the behavior of the subsequently attaching platelets.

Four rutile single crystals with (110), (100), (101), and (001) conformations were immersed in PPP. After 5 and 120 min, differences in the amount and morphology of platelets were determined using SEM. The latter enabled a visual assessment of the activation state of platelets. It is widely recognized that resting platelets resemble a disk

shape, while during activation their size increases, and numerous filopodia appear i.e., finger-like projections, which extend from cell periphery.<sup>211</sup> According to Goodmann's theory, the degree of activation can be divided into five stages based on changes in morphology: round (R), dendritic (D), spread-dendritic (SD), spread (S), and fully spread (FS).<sup>212</sup> All of the aforementioned structures were found in this study and are shown in [Figure 6.1. a](#)).

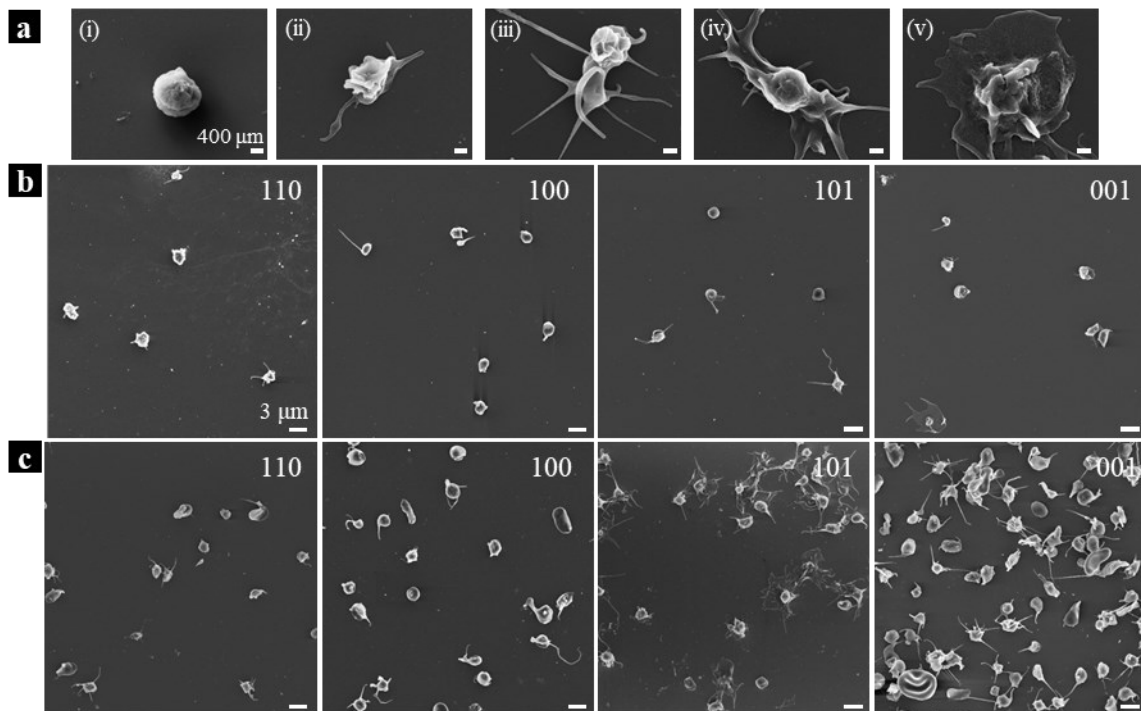


**Figure 6.1.** a) Five morphological forms of platelets observed on rutile single crystals, corresponding to different states of activation, i.e., (i) round, (ii) dendritic, (iii) spread-dendritic, (iv) spread, (v) fully spread. Morphology of platelets after b) 5 min and c) 120 min immersion of rutile crystals in PPP under static conditions.

After 5 min of adhesion, a small number, and mostly round platelets were detected on all surfaces, indicating their resting state ([Figure 6.1. b](#)). No significant crystallographic orientation-dependent differences in platelet morphology were observed, however, more active forms i.e., spread-dendritic and spread also appeared on (101) and (001) surfaces to a small extent. Subsequently, an adhesive behavior of platelets was examined on rutile single crystals immersed for 120 min in PPP, as numerous implants and medical devices are exposed to a blood environment for a longer period. Although activation typically requires seconds to minutes, absorbed platelets can trigger a cascade of attachment and activation of new ones ([Figure 2.5](#)).<sup>46,153</sup> As demonstrated in [Figure 6.1. c](#)), strong

differences in the amount and platelet morphology were observed on investigated rutile surfaces. Minimal platelet adhesion, which preserved their round shape was found on the (110) surface. On the (100) surface adhesion increased, and platelets with dendritic structure dominated. Nevertheless, the lack of dendritic-spread nor more active forms on both (110) and (100) surfaces indicate non-activity or only the early stage of platelet activation. In contrast, a more extensive attachment and reorganization of platelet structure were noticed for the other two (101) and (001) surfaces. Platelets appeared in all five activation states, with a predominance of active spread-dendritic and spread forms. In the end, the largest surface area was occupied by platelets on the (001) surface (Figure 6.1. b) and Figure A1).

The visual observations were supported by quantitative analysis of surface coverage by platelets using optical microscope images ( $n > 4$ ), presented in Figure 6.2. a) and b). Calculated values are collected in Figure 6.2. c) (left axis). It has been found that after 5 min of adhesion, platelets occupied less than 2% of a surface regardless of crystallographic orientation. The increase in platelets adhesion was more prominent and crystallographic orientation-dependent, upon longer exposure of substrates on PPP (120 min). Still, coverage in 9% and 12% on the (110) and (100) surfaces, respectively, can be considered minimal, which proves a low adherence of non-activated platelets. On the other hand, the (101) surface occupancy reached 18%, while on the (001) increased up to 47%. The increase in surface coverage in the order of  $(110) < (100) < (101) < (001)$  is associated with both, an increase in the number and activation of platelets.

The latter was quantitatively determined using P-selectin, which is a component secreted from the interior to platelet membrane after their activation.<sup>210</sup> Quantitative analysis was performed by measurement of light absorbance by P-selectin conjugated fluorescent agent, using an immunochemistry technique. Results presented in Figure 6.2. c) (right axis) validate the visual SEM assessment of platelets activation. The lowest absorbance was detected on the (110) surface, while the highest on the (001) surface, which was subsequently visualized by confocal microscopy. As presented in Figure 6.2. d), significantly less secreted P-selectin was detected on the (110) compared to the (001) surface.

To sum up, a detailed analysis of the platelet adhesion and activation on rutile single crystals showed a crystallographic orientation-dependent relationship and an increase in the order of  $(110) < (100) < (101) < (001)$  upon their prolonged exposure to PPP. Since

platelet adhesion determines a clot formation process, it can be speculated that rutile surfaces with the (110) crystallographic orientation could be the most effective in reducing the risk of thrombogenic phenomena on biomaterials. Nevertheless, additional studies conducted under in vivo conditions, particularly in presence of high shear forces induced by blood flow, are essential to fully assess the surface-induced clotting on rutile single crystals.

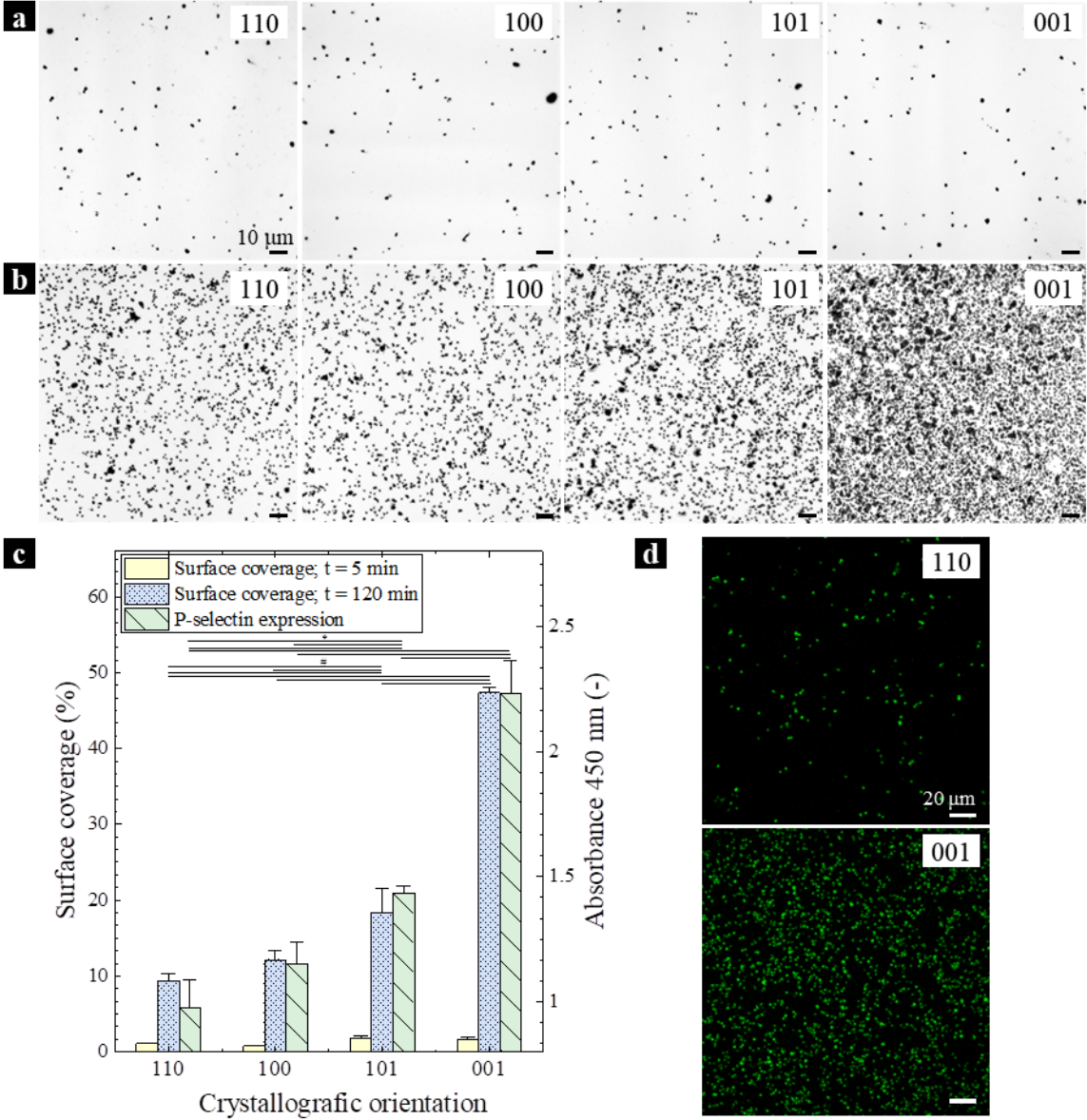


**Figure 6.2.** Optical microscope images of rutile single crystals immersed in PPP for a) 5 min and b) 120 min. c) Calculated values of surface coverage based on at least four positions per crystal (left axis) and P-selectin expression level obtained by immunochemistry (n = 3, right axis). d) Visual representation of P-selectin expression (confocal microscopy). Lines above bars indicate statistical differences ( $p > 0.05$ ) in \* surface coverage, and # P-selectin expression level.



### 6.3.2. HPF conformation-dependent visibility of platelet binding sites: Model of crystallographic orientation-dependent platelets adhesion and activation

The cellular response is closely correlated with the layer of preadsorbed proteins, the main one being thrombogenic HPF. A hypothesis has been posed, that observed platelet behavior on rutile single crystals is guided by crystallographic orientation-dependent HPF conformation. Furthermore, it is known that a minimal amount of adsorbed HPF is sufficient to fully activate platelets.<sup>70</sup>

HPF contains three pairs of platelets binding sites i.e., two secondary RGD sequences in the A $\alpha$  chain (RGDF at 95–98 and RGDS at 572–575) and one in the  $\gamma$ -chain, HHLGGAKQAGDV at 400–411, primary sequence.<sup>213,214</sup> RGDs sequences are common for other proteins, while the  $\gamma^{400-411}$  is unique for HPF and is the only one able to bind non-active platelets from the bloodstream.<sup>76</sup> Therefore, HPF conformation-dependent visibility of  $\gamma^{400-411}$  sequences, on protein-coated rutile single crystals was quantified. The  $\gamma$ -chain antibodies conjugated with a fluorescent agent, detectable by immunochemistry technique, were used. Results presented in Figure 6.3. imply significantly higher availability of  $\gamma^{400-411}$  in HPF molecules adsorbed on the (001) compared to the (110) surface.

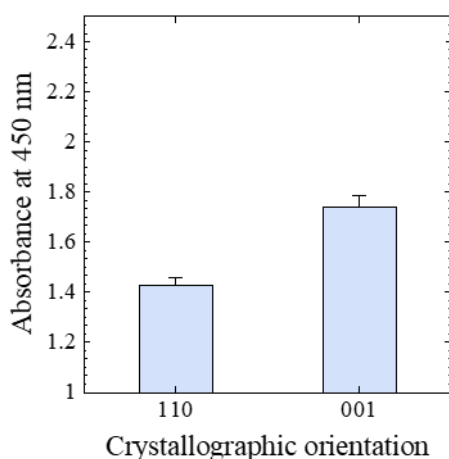


**Figure 6.3.** a) Availability of  $\gamma^{400-411}$  sequences in HPF molecules adsorbed on the (110) and (001) rutile single crystals determined by immunochemistry (n = 3).

Supported by AFM visualization of HPF molecules (Chapter 5.3.2.), a model of HPF conformation-dependent platelets adhesion mechanism is proposed here and is

schematically shown in Figure 6.4. On low energy and hydrophobic surfaces, such as the (110) surface, HPF adsorption by hydrophobic D and E domains results in a trinodular conformation and directs  $\gamma$ -chains toward a surface, which limits the availability of primary binding sites for platelets. Therefore, low adhesion of non-activated platelets was observed on this type of surface. In contrast, due to hydrophilic  $\alpha$ C-regions adsorption on more hydrophilic surfaces, HPF appears in the globular conformation, repulsing  $\gamma$ -chains, which consequently leads to strong  $\gamma^{400-411}$  accessibility. This stimulates extensive platelet adhesion and activation.

It can be stated that platelet adhesion and activation, and therefore the probability of clot formation increases in the order of (110) < (100) < (101) < (001), which is closely correlated with an involvement of HPF absorbed in globular conformation. These results underline the strong influence of surface energy and wettability, guided by crystallographic orientation, on the thrombogenicity of a material surface.

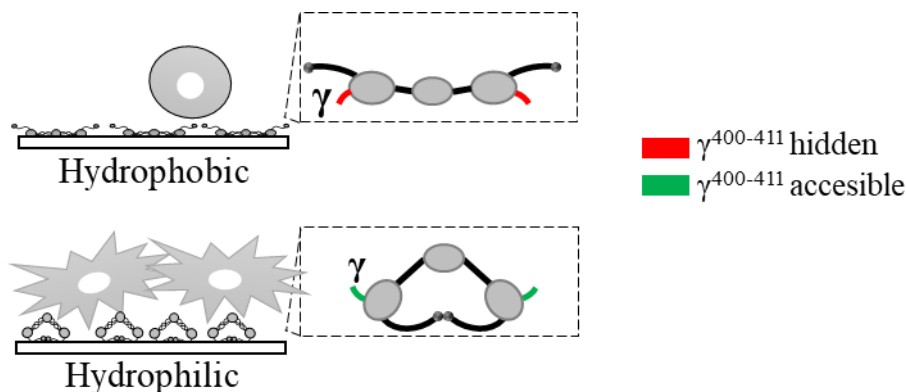


**Figure 6.4.** Model of HPF-conformation dependent, platelets adhesion and activation on hydrophobic and hydrophilic rutile single crystals. HPF adsorbed by D domains in trinodular conformation on the (110) surface sufficiently limits the visibility of  $\gamma$ -chain (red color), and therefore platelets adhesion and activation. Adsorbed by  $\alpha$ C domains, globular HPF bind and activate platelets due to the accessible  $\gamma$ -chain (green color). Figure not drawn in scale.

Since it is known that HPF regulates an adhesion of other cells and bacteria as well, the potential to modulate surface-related coagulation and bacterial attachment is anticipated.<sup>192,193,215</sup> Present work and the possibility of adjusting the crystallographic orientation of an implant surface, highlight a new direction for future research into the manipulation of other biological processes mediated by proteins.

It should be mentioned that Zhao *et al.* reported the phenomenon of fibrogenesis on hydrophobic surfaces exposed to HPF concentrations of 4 mg/mL, i.e., higher than those used in this study.<sup>150</sup> Since in human blood plasma HPF concentration is in the range of 2 - 4 mg/mL, it carries the risk of nanofiber formation on the (110) surface, which may promote clot formation. Nevertheless, researchers suggested that rutile surfaces pre-coating with a monomeric HPF layer, by immersion in HPF solution with lower concentration i.e., 0.1 mg/mL, can effectively prevent this phenomenon occurrence. This makes rutile, with (110) crystallographic orientation, a promising antithrombogenic biomaterial.<sup>214</sup>

Keep in mind that the results presented in this chapter, concern quite well-defined single crystal surfaces. Since TiO<sub>2</sub> crystals commonly used in medicine have typically a less ordered polycrystalline nature, with a higher density of structural defects, it is necessary to check, if the same crystallographic orientation-dependent HPF and platelet behavior will be observed also in that case. This issue is covered in the following chapter. Subsequently, the next task will be a limitation of material imperfections, and engineering of rutile polycrystals with the highest extent of preferably oriented grains.

## 6.4. Conclusion

In conclusion, this chapter provides evidence allowing to accept the hypothesis that platelet adhesion and activation are guided by crystallographic orientation-dependent conformation of adsorbed HPF on rutile surfaces. Studies were performed on rutile single crystals with (110), (100), (101), and (001) crystallographic orientations. Low platelet adhesion and activation were observed on the low energetic and hydrophobic (110) surface, which is associated with trinodular conformation of pre-adsorbed HPF and thus limited visibility of primary platelet binding sites. In contrast, HPF in globular conformation, present on more energetic and hydrophilic surfaces (in particular (001) surface), promoted platelets binding through the  $\gamma^{400-411}$  and their subsequent enhanced activation. In the end, a mechanism guiding platelet behavior on rutile single crystals is proposed. It determines the fate of material in contact with blood. This study contributes to a better understanding of the human body's response to implanted biomaterials and highlights the possibility of controlling the cellular response mediated by proteins by adjusting the crystallographic orientation of a rutile surface.

## 7. HPF-mediated platelets adhesion and activation on TiO<sub>2</sub> (rutile) polycrystal surface

### 7.1.Introduction

In the previous chapters, it has been observed that the behavior of proteins and cells, and therefore the course of biological reactions occurring at the biomaterial - blood interface, varies depending on the crystallographic orientation of a material surface. These studies were carried out using high-quality polished single crystals, which eliminates an influence of other variables on the process due to continuous, uniform, and highly-ordered structure. However, large-scale production of single-crystalline implants is rather challenging.<sup>216,217</sup> Therefore, commercially available implants are mainly polycrystalline.

Rutile polycrystals used for observation of crystallographic orientation-dependent biological processes can be self-produced, for example by powder compaction, sintering, and polishing, which is schematically shown in Figure 7.1. a) – c).

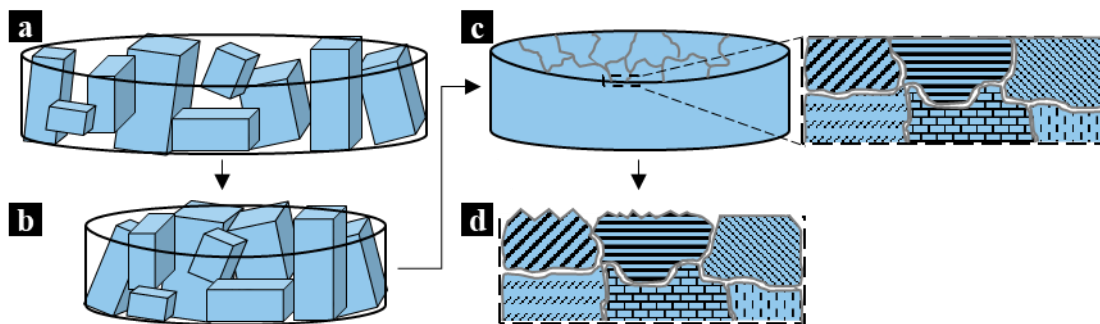


**Figure 7.1.** An exemplary method of polycrystal production: a) Powder compression; green-body b) sintering and c) polishing; d) thermal etching.

Usage of polycrystals for research purposes reduces the cost of experiments and allows for multiple grains investigation with different surface crystallographic orientations in a single experiment under the same conditions. On the other side, the production of polycrystals without any defects is impossible, which impacts overall surface properties and may introduce some inconsistencies in results. For example, to limit the influence of imperfections on a cellular response, surfaces with large grains without closed porosity are preferred. Additional effort in the usage of polycrystals for research is microscopic observation and characterization of individual grains, requiring substrate thermal etching

to visualize grain boundaries.<sup>218</sup> The side effect of this treatment may be the minimization of surface energy and changes in its physico-chemical properties. Thermal etching leads to grain-specific surface reconstructions due to the local diffusion of surface atoms.<sup>219</sup> Crystallographic orientation-dependent susceptibility of surface atoms to reorganization affects the faceting process, which locally creates areas inclined in relation to a macroscopic substrate surface.<sup>25</sup> This is schematically shown in [Figure 7.1. d](#)). Detailed evaluation of the crystallographic orientation of a single facet wall is limited by electron microscopy resolution. Nevertheless, it is widely recognized that the degree of faceting depends on thermal treatment conditions e.g., temperature and duration of etching. Therefore, it is worth investigating whether a reduction of those parameters to a minimum will sufficiently limit the level of structural changes on the surface, to properly interpret crystallographic orientation-dependent biological reactions. This would enable the usage of polycrystalline substrates, produced in laboratory conditions, as reference samples for the study of designed biomaterials biocompatibility, which will improve the process of implant development.<sup>220</sup>

Since this dissertation is devoted to thrombogenic phenomena and the mechanism of HPF conformation-dependent platelet adhesion on rutile single crystals is already described in previous chapters, here:

- 1) crystallographic orientation-dependent HPF adsorption and platelets adhesion on different grains of rutile polycrystal surfaces are described,
- 2) results obtained on single crystals and polycrystal grains surfaces with corresponding crystallographic orientations are compared.

Keep in mind that precise determination of a grain surface crystallographic orientation is challenging as they are rather randomly oriented. Hence, the defined low indices are a close approximation of the actual crystallographic orientation.

In the end, the obtained results resolve whether a surface crystallographic orientation is a key factor controlling the behavior of HPF and platelets on rutile polycrystals. Consequently, it is possible to figure out whether produced in this study, polycrystalline substrates can be a promising tool for future studies of crystallographic orientation-dependent, biological processes. In addition, available engineering techniques allow for controlling the crystallographic orientation of exposed surfaces, to a large extent. As described in detail in a review by Barthes *et al.*, there is an opportunity to produce a

polycrystal with a high proportion of preferentially oriented grains to elicit a preferred biological response, and therefore engineer a highly efficient and biocompatible material for implants.<sup>23</sup>

So far, the HPF behavior on thermally etched rutile polycrystals (produced according to the method shown in [Figure 7.1.](#)) has been examined by Keller *et al.*<sup>194</sup> Observed crystallographic-dependent differences in HPF arrangement have been correlated with local differences in surface energy and wettability. However, in this study, the substantial faceting phenomenon being a side effect of thermal treatment was not excluded, which prevented a detailed evaluation of the crystallographic orientation of each facet wall.<sup>194</sup> Therefore, in the present study, thermal etching parameters were adjusted to allow observation of grain boundaries but simultaneously to induce minimal surface reconstructions. Electron backscatter diffraction (EBSD) method was used to determine the crystallographic orientations of grains surfaces, and then their topography was studied by atomic force microscopy (AFM). Afterward, a crystallographic orientation-dependent behavior of HPF and platelets was analyzed. Distribution of pre-adsorbed HPF molecules, an availability of specific platelet recognition sites in HPF molecules, and platelet activity were evaluated using specific antibodies detected by confocal microscopy. Platelet morphology was characterized using scanning electron microscopy (SEM). Finally, collected results were compared with observations reported using single crystals. This provided an opportunity to assess whether the use of thermally etched polycrystalline substrates may improve the process of designing biomaterial surfaces capable of inducing favorable protein conformations for desired biological reactions.

## **7.2. Materials and Methods**

### **7.2.1. Rutile polycrystals production and characterization methods**

The high-purity TiO<sub>2</sub> rutile powder (Sachleben THRP2, KRAHN Ceramics GmbH, Germany) was used to produce disc-shaped polycrystalline substrates with a diameter and height of about 10 mm and 5 mm, respectively. Powder was isostatically compacted in a cylindrical rubber form at 400 MPa. Then, obtained green bodies were sintered at 1450 °C (heating rate 10 °C/min until 1300 °C followed by 2 °C/min to 1450 °C) for 3 h in an ambient atmosphere and after cooling, cut into small discs. Surface of specimens was

mechanically ground using Buehler Ultra-Prep diamond grinding discs with up to 5  $\mu\text{m}$  abrasive size and subsequently polished using Buehler MetaDi diamond suspensions with up to 1  $\mu\text{m}$  abrasive size and suspension for final polishing (Buehler GmbH, Düsseldorf, Germany). Before microscopic observation of grain boundaries, substrates were subjected to thermal etching. Slight parameters i.e., temperature 1300 °C maintained for 15 min (heating rate 10 °C/min), were used to minimize the level of faceting and keep the surface roughness as low as possible.

Wettability of polycrystals was determined based on static water contact angle measured by the sessile drop method and DSA10 drop shape analysis system (Kruss GmbH, Hamburg, Germany).

The EBSD method was applied to analyze the crystallographic orientation of grains (Auriga 60® CrossBeam Workstation, Oxford Nordlys EBSD Detector, Carl Zeiss Jena GmbH, Jena, Germany). The step size was 6  $\mu\text{m}$ . Determined (hkl) Miller indices refer to the plane lying within the macroscopic polycrystal surface. A color-code crystallographic orientation map and corresponding inverse pole figure were generated, where each color is ascribed to the given (hkl) Miller indices.

Surface roughness of selected grains was determined using AFM (JPK BioAFM, Bruker, Berlin, Germany). Measurements were performed in at least three positions (800 x 800 nm) per grain and the same parameters as per characterization of single crystals (Chapter 5.2.4.) were applied. To target a strictly defined position on the polycrystal surface, AFM was coupled with an optical microscope, which was used to find a grain of interest. Then, the position of the AFM tip was calibrated by choosing the proper offset in a way, that an observed sample area remains the same under an optical microscope and AFM.

An optical microscope was also used to confirm that the grain sizes of produced polycrystals significantly exceed the size of platelets. Since grain diameter is in the range of several tens of  $\mu\text{m}$ , therefore, produced polycrystals were suitable for biological studies.

### 7.2.2. Protein adsorption studies

To visualize single protein molecules on previously characterized grains, HPF was adsorbed on rutile polycrystals from solutions with a concentration of 0.01 mg/mL, for 5 min, according to a procedure described in Chapter 5.2.2. AFM imaging was performed under air conditions.

Coverage of grains surfaces by HPF was analyzed using fluorescently-labeled HPF (FITC-HPF, antibodies-online GmbH, Germany) detected by confocal microscopy. Polycrystals were incubated in 1 mg/mL FITC-HPF solution for 2 h at 37 °C, and then loosely bound proteins were removed by washing once in PBS and twice in water. Finally, polycrystals were examined using a confocal laser scanning microscope (LSM 510 Meta, Zeiss). Grain-dependent surface coverage with the fluorescent agent was analyzed using ImageJ software.

Availability of primary platelet binding sites ( $\gamma^{400-411}$ ) in HPF molecules was determined using  $\gamma$ -chain antibodies. For this experiment, protein-coated polycrystals were blocked with 1% BSA for 1 h at 37 °C and immersed in mouse monoclonal primary  $\gamma$ -chain antibody (diluted 1: 300 in PBS, Bio-Techne GmbH, Germany) for 1 h at  $T = 37$  °C. After washing five times in PBS, the secondary Alexa Fluor® 488 conjugated goat anti-mouse IgG antibody (diluted 1: 300 in PBS, Abcam, Cambridge) was added. Finally, samples were rinsed five times in PBS and visualized using confocal microscopy. At least three grains marked by the same color on a crystallographic orientation map were examined.

### 7.2.3. Platelet adhesion and activation analysis

Platelets adhesion was performed according to the procedure described in Chapter 6.2.2. Subsequently, samples were prepared for SEM visualization in the same way as single crystals (See Chapter 6.2.3.). Crystallographic orientation-dependent cell morphology was analyzed at an accelerating voltage of 5 kV.

The degree of platelet activation was determined by means of the P-selectin expression level visualized by confocal microscopy. The same procedure as for the detection of HPF  $\gamma$ -chain was applied, however, the P-selectin antibody (diluted 1:300 in PBS, antibodies-online GmbH) was used as a primary antibody.



Note that presented results refer to at least three grains marked by the same color on the crystallographic orientation map.

#### 7.2.4. Statistical analysis

Results are presented as mean values with  $\pm$  standard deviations. Statistical analysis in a given group was performed by One-Way analysis (ANOVA) with Turkey test ( $p < 0.05$ ) using Origin software.

### 7.3. Results and Discussion

#### 7.3.1. Characterization of TiO<sub>2</sub> (rutile) polycrystals

Before biological experiments, produced rutile polycrystals were characterized. Optical microscope images (Figure 7.2.) showed, that applied thermal etching revealed grain boundaries, which enabled the differentiation of individual grains. Measured grain sizes are in the range of a few tens up to hundreds of microns, which eliminates the influence of grain boundaries on the behavior of cells analyzed later.

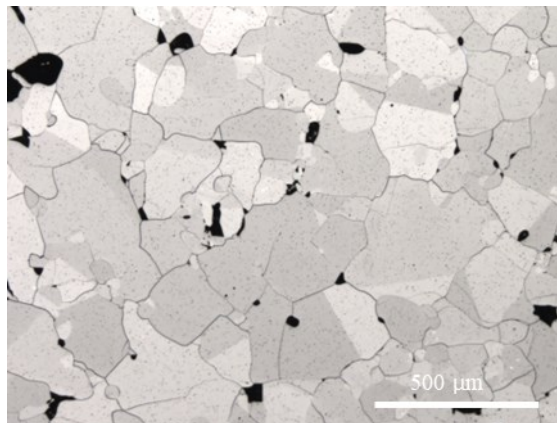


**Figure 7.2.** Optical microscope image of a thermally etched TiO<sub>2</sub> (rutile) polycrystal surface. Grain size exceeds several tens/hundreds of  $\mu\text{m}$  and grain boundaries are visible. Scale bar represents 500  $\mu\text{m}$ .

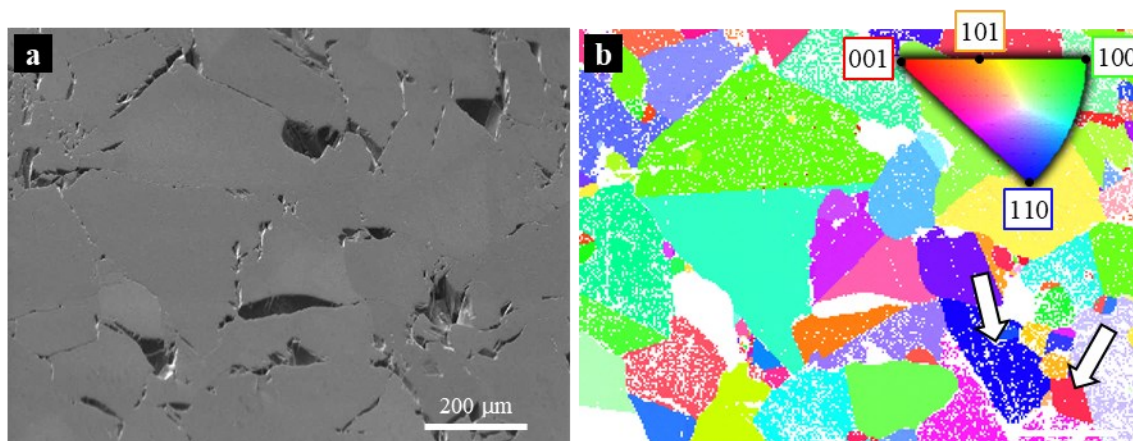


**Figure 7.3.** a) Representative SEM image of a thermally etched  $\text{TiO}_2$  (rutile) polycrystal surface in an exemplary position. b) EBSD image with a corresponding color-code inverse pole figure map in the inset. (hkl) Miller indices denote lattice planes lying in the macroscopic polycrystal surface. Arrows point to the grains with the (110) and (001) surface crystallographic orientation, which can be recognized in the EBSD image as deep blue and red color. Note, that estimated crystallographic orientations represent the closest approximation to the actual crystallographic orientation of a grain surface.

SEM image and corresponding crystallographic orientation map, in an exemplary position on a polycrystal surface, are presented in Figure 7.3. a) and b) respectively. Crystallographic orientations were expressed using (hkl) Miller indices of lattice planes lying within the macroscopic polycrystal surface. The inverse pole figure, in the inset of Figure 7.3. b), relates to a color code of these (hkl) Miller indices. Note, that an estimated surface crystallographic orientations of grains represent the closest approximation to actual crystallographic orientation. As predicted from the powder compression and sintering process, crystallographic orientation of the grain surfaces is rather random.

It is known that polycrystal surface is characterized by local, grain-dependent surface energy, which implies locally heterogeneous surface chemistry. To assess whether polycrystalline rutile displays variability in crystallographic orientation-dependent thrombogenic phenomena, HPF-mediated platelet adhesion was analyzed. Firstly, attention was devoted to grains with surface crystallographic orientation as close as possible to ideal (110) and (001) surfaces. Based on studies conducted on single crystals, these surfaces were assigned the most different physicochemical parameters among low-index surfaces, which resulted in their different degree of thrombogenicity (See Chapter 6). The (110) surface is characterized by a lower density of dangling bonds, lower surface energy, and thus higher stability compared to the (001) surface, which contains many undercoordinated atoms (Table 2.1.). Moreover, in the context of protein

adsorption, the (110) surface is considered hydrophobic, while the (001) surface is hydrophilic (Chapter 5).

On the crystallographic orientation map of polycrystals, the (110) grain surface is denoted in blue, while the (001) surface in red, as indicated by arrows in [Figure 7.3. b](#)). Surface topography of both grain types has been investigated by AFM and images are presented in [Figure 7.4](#).

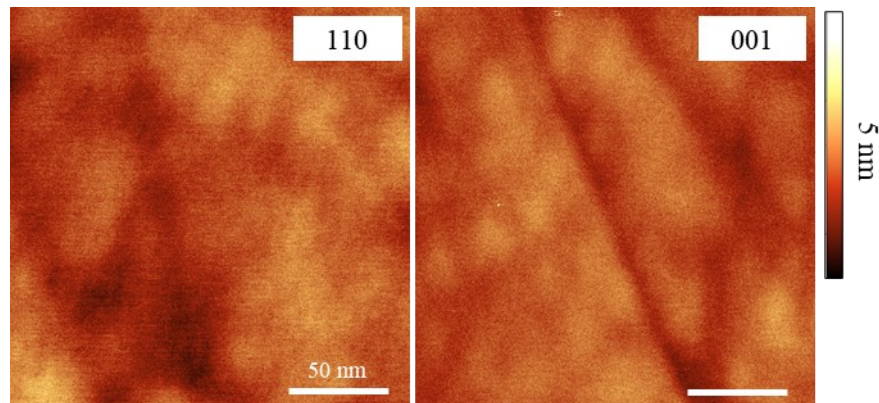


**Figure 7.4.** Topographic AFM images (200 nm x 200 nm) of bare (110) and (001) grain surface of TiO<sub>2</sub> (rutile) polycrystal.

Despite the thermal etching-induced, surface reconstructions, which are dependent on the thermodynamic stability of a grain surface, the short processing time allowed to maintain a relatively low and comparable surface roughness of both grains i.e., root mean square ( $R_q$ ) roughness was  $0.55 \pm 0.09$  nm and  $0.42 \pm 0.05$  nm for (110) and (001) surfaces, respectively. This implies only the beginning of the faceting process on an atomic scale. To some extent, roughness may also be a residue from the polycrystal polishing.<sup>221</sup> In the literature such surfaces are considered flat. Although the roughness is  $\sim 5$  times higher compared to single crystals, it should be still negligible from a protein adsorption point of view.<sup>38,125</sup>

### **7.3.2. Crystallographic orientation-dependent platelet adhesion and activation on rutile polycrystal surface**

To analyze how the crystallographic orientation of a grain surface affects the platelet adhesion process, rutile polycrystals were immersed in platelet pooled plasma (PPP), which contains a certain amount of HPF, as was mentioned in Chapter 6.3.1. After

120 min of incubation, the grain-dependent amount and activation state of platelets were evaluated. To confirm the reproducibility of the results, analysis was performed on at least three grains marked with a given color.

Based on SEM images of the (110) and (001) grains surfaces, presented in [Figure 7.5. a\)](#) and [b\)](#), rather low platelet adhesion was detected regardless of crystallographic orientation. Moreover, no differences in the platelet morphology were observed, which were mostly in a round or dendritic state. Based on the Goodman theory described in Chapter 6.3.1., this morphology indicates a low level of cell activation.

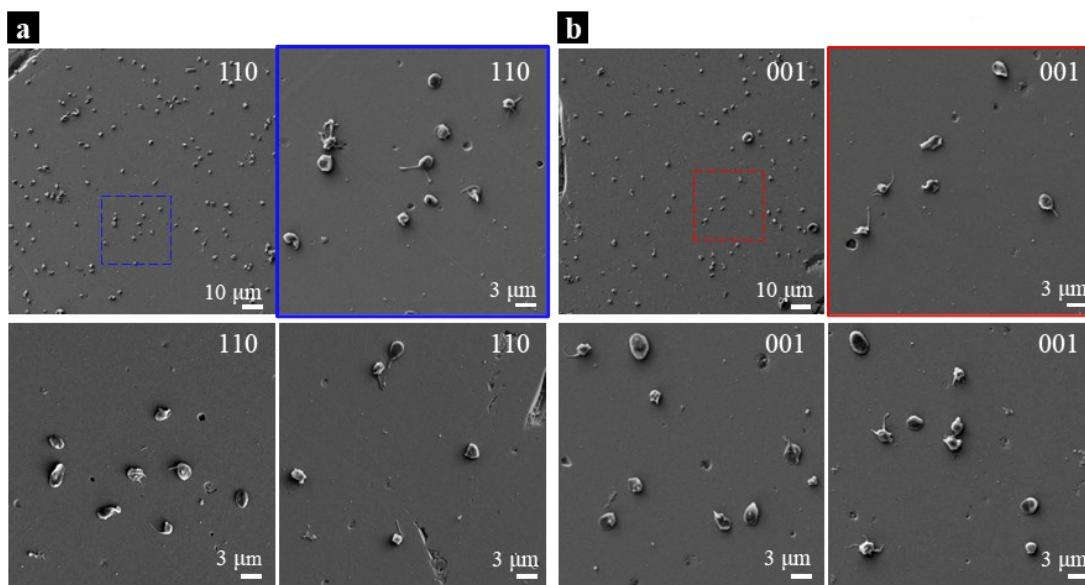


**Figure 7.5.** SEM images of a) (110) and b) (001) grains surfaces of TiO<sub>2</sub> (rutile) polycrystal exposed to platelets for 120 min under static conditions, taken on three grains marked by the same color, however in various surface positions. Upper images refer to the same grain but show different magnifications.

These findings are supported by the confocal microscopic visualization of the P-selectin expression level, which is a component released into the platelet membrane only during platelet activation.<sup>210</sup> [Figure 7.6.](#) shows the surface coverage by P-selectin conjugated fluorescent agent, which is  $6.03 \pm 0.11\%$  and  $6.46 \pm 0.14\%$  for (110) and (001) grains surfaces, respectively. P-selectin is detectable at a similar level, which indicates a similar platelets activation regardless of crystallographic orientation.

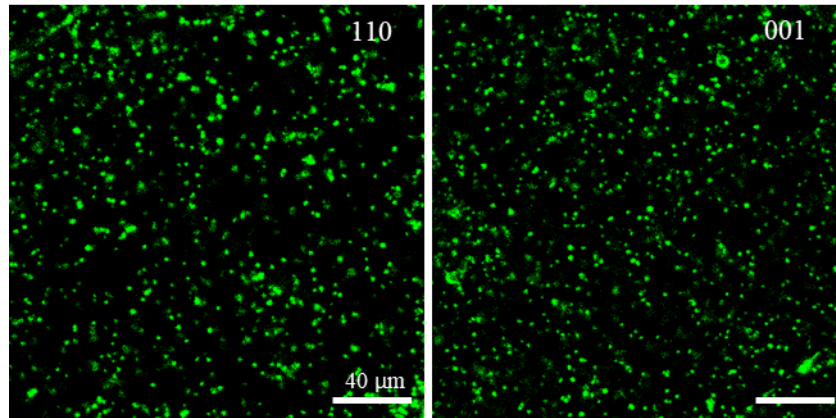


**Figure 7.6.** Confocal microscope images of expressed P-selectin on (110) and (001) grain surfaces after 120 min exposition of rutile polycrystal for PPP under static conditions.

If rutile single crystals were used as a substrate (Chapter 6), strong adhesion and morphological changes of platelets i.e., an increase in platelet size and formation of pseudopods were observed on the hydrophilic (001) surface with the highest surface energy. This was not observed on the hydrophobic (110) surface with the lower surface energy, where platelets were round and in a resting state. On rutile polycrystal, platelets did not manifest crystallographic orientation-dependent behavior, and their morphology was similar to that observed on the (110) surface of single crystal, indicating low thrombogenicity of both (110) and (001) grain surfaces.

In the next step, platelet morphology was also analyzed on other two low-index i.e., (100) and (101) surfaces (as in the case of single crystals) as well as a high-index surface, which are assigned green, orange, and light-yellow colors, respectively. SEM images are shown in [Figure 7.7](#). The amount and morphology of platelets on all examined grains were comparable to those observed on (110) and (001) grains surfaces. This indicates a similar degree of cell activation and non-thrombogenicity of those grains. Although such platelet behavior has often been observed on numerous polycrystalline grains, it does not imply that there are no places where platelets will be active.



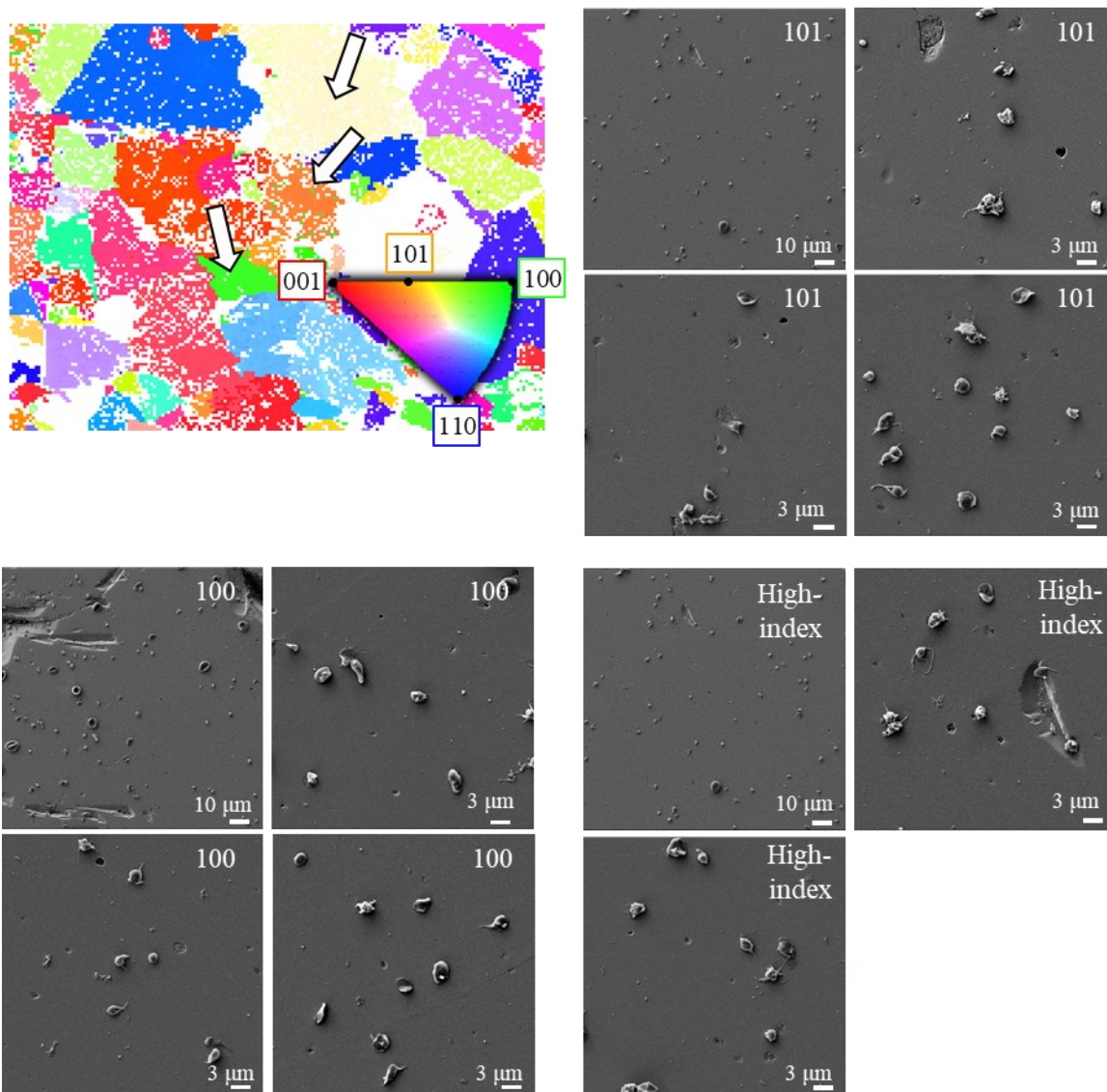


**Figure 7.7.** EBSD map of  $\text{TiO}_2$  (rutile) polycrystal surface in a second exemplary position. As indicated by arrows, the (100), (101), and high-index grains surfaces can be recognized in the EBSD image as green, orange, and bright yellow, respectively. Note, that estimated crystallographic orientations of grains surfaces represent the closest approximation to the actual crystallographic orientation. SEM images of (100), (101), and high-index surfaces exposed to platelets for 120 min under static conditions were taken on two/three grains marked by the same color, however in various surface positions. Upper images refer to the same grain but show different magnifications.

### 7.3.3. HPF conformation on thermally etched $\text{TiO}_2$ (rutile) polycrystal

For a better understanding of different platelet responses to single- and polycrystalline rutile, a grain-dependent HPF adsorption behavior was determined. HPF mediates platelet

adhesion to a material surface and its conformation directs the visibility of platelet binding sites.<sup>155</sup>

Confocal microscopy of fluorescently labeled HPF (Figure 7.8.) revealed a similar level of HPF adsorption on both (110) and (001) grains surfaces. Moreover, proteins were rather concentrated in a few isolated spots randomly distributed on the surface, which may suggest a high extent of the protein-protein interactions and formation of assemblies characteristic of HPF in trinodular conformation.<sup>199</sup> Lack of any significant changes in the distribution of HPF conjugated fluorescence agent on both grains can be attributed to the same amount and conformational state of protein molecules.<sup>222</sup>

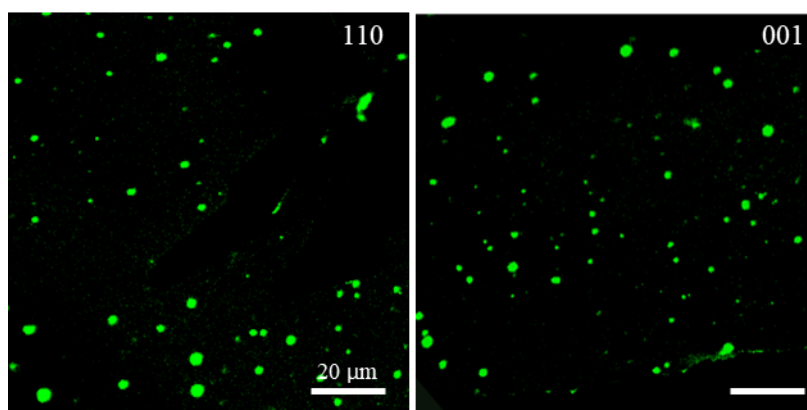


**Figure 7.8.** Distribution of fluorescently-labeled HPF on (110) and (001) grains surfaces of TiO<sub>2</sub> (rutile) polycrystal imaged by confocal microscopy.

Assumption was confirmed by AFM visualization of single protein molecules, as shown in Figure 7.9. a) and b). Three domains of HPF could be distinguished on both types of grain surfaces. The total lengths of HPF molecules adsorbed on the surface of the (110) and (001) grains were  $43.1 \pm 1.7$  nm and  $42.6 \pm 3.8$  nm, respectively. This is close to the trinodular HPF structure found on the hydrophobic (110) single crystal i.e.,  $45.5 \pm 3.6$  nm.

Moreover, the crystallographic orientation-dependent availability of  $\gamma^{400-411}$  platelet binding sites in HPF molecules was assessed by confocal microscopy and is visualized in Figure 7.9. b). The expression of fluorescently labeled sequences of  $\gamma$ -chain was low and at a similar level on both grain types, which is related to the same HPF conformation observed by AFM. As described in chapter 6.3.2, trinodular conformation of HPF observed on hydrophobic (110) rutile single crystal hindered the visibility of  $\gamma^{400-411}$ ,

which is also observed on investigated grains of rutile polycrystals. This also explains the lack of platelet activation reported in this study, regardless of crystallographic orientation.

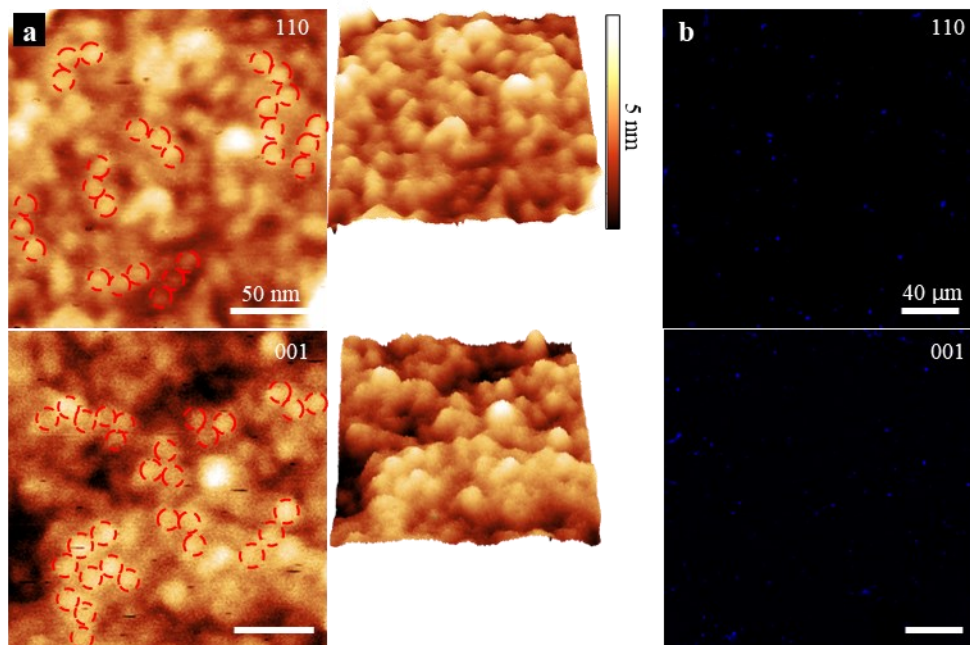


**Figure 7.9.** a) AFM images of (110) and (001) grain surfaces of TiO<sub>2</sub> (rutile) polycrystal coated by HPF ( $C = 0.01$  mg/mL,  $t = 5$  min) taken under air conditions. Images show trinodular HPF irrespective of surface crystallographic orientation. b) Confocal microscopy images of available  $\gamma^{400-411}$  on polycrystal grains i.e., sequences available to bind platelets.

While crystallographic orientation-dependent HPF conformational changes have been observed on rutile single crystals, as explained by water contact angle below or above Berg limit, i.e.,  $\Theta \sim 60 - 65^\circ$  (Table 5.1. and Figure 5.3.), in the case of polycrystals, it is not possible to accurately measure surface wettability of each grain. Instead, the measured value refers to the macroscopic polycrystal surface. For thermally etched rutile polycrystals investigated in this study, the water contact angle was  $62.10 \pm 2.09^\circ$ . Polycrystals are a combination of differently oriented grains, therefore this value includes local crystallographic orientation-dependent surface wettability variations. Since measured values are in the mentioned above transition range for proteins, therefore, one possible explanation for HPF adsorption in trinodular conformation, regardless of the surface crystallographic orientation, may be the hydrophobicity of examined grains i.e.,  $\Theta \geq 65^\circ$ . It is widely recognized that surface wettability is strictly correlated with surface energy and more precisely, hydrophobic surfaces are usually characterized by low surface



energy.<sup>223-225</sup> Furthermore, it is known that thermal etching creates reconstructed surfaces with lowered surface energies.<sup>26</sup> HPF unfolding was also observed in the study by Keller *et al.*, on a flat surface of high-index rutile polycrystal grain surfaces, exhibiting low free surface energy.<sup>194</sup>

The second possible explanation is surface non-stoichiometry (O/Ti ratio) induced by thermal treatment or contaminants in produced polycrystals related to the substrates fabrication processes e.g. coming from components used for polishing.<sup>26,189</sup>

The aim of our future research will be a detailed characterization of produced polycrystals and verification that their production method can be adapted to induce similar crystallographic orientation-dependent platelets behavior as single crystals, thus allowing for its usage in biological studies.

## **7.4. Conclusion**

This chapter describes the thrombogenicity of TiO<sub>2</sub> (rutile) polycrystals and their utility in the assessment of crystallographic orientation-dependent biological response, which is possible with the use of more expensive single crystals. Any significant differences in the behavior of platelets and HPF on different grains of polycrystals have not been observed despite local properties changes. Irrespective of surface crystallographic orientation, low platelets adhesion in a resting state was observed, as evidenced by their spherical morphology and low P-selectin expression to the cell membrane. This was correlated with the trinodular conformation of a pre-adsorbed HPF visualized by AFM, which had a direct impact on the poor visibility of  $\gamma^{400-411}$  platelet binding sites. On the one hand, these results indicate that the produced rutile polycrystals have a high probability of being highly biocompatible, however, they cannot be used as a universal tool to study the crystallographic orientation-dependent biological phenomena occurring at biomaterial - blood interface. A detailed explanation of the inconsistencies between observations collected on single crystals and polycrystals requires a more thorough characterization of polycrystals used in this study. The next task will be an improvement of the polycrystal production method.

## 8. Summary

This work addresses thrombogenic phenomena that still occur during patients' treatment as a result of contact between implants or medical devices and blood. A review of the current state of the art has led to the recognition of HPF as the main mediator of platelets adhesion, which is clot-building cells. This motivated the investigation of whether the adjustment of a material surface crystallographic orientation allows for HPF conformation control in a way to limit the availability of platelet binding sites and therefore minimizes their adhesion and activation.

The behavior of HPF and sequentially attaching platelets was investigated on TiO<sub>2</sub> in rutile form, one of the most common biomedical interfaces. Firstly, studies were performed on four well-defined rutile single crystals with (110), (100), (101), and (001) crystallographic orientations. Structure unfolding and therefore trinodular conformation of HPF was observed on the (110) surface, which limited visibility of the  $\gamma$ -chain and resulted in low adsorption of platelets in a resting state. In contrast, HPF in a more native-like conformation i.e., globular, on the (001) surface, exposed  $\gamma$ -chains, which stimulated increased platelet adhesion and activation. On the other two single crystals, HPF appeared in various spatial arrangements with a predominance of the globular one, and an intermediate platelets adhesion between that observed on (110) and (001) surfaces was found. It can be stated that the probability of clot formation increases with the frequency of HPF adsorption in the globular conformation. The determinant of HPF conformation-dependent platelets behavior is the crystallographic orientation of rutile single crystals, and thus arrangement and coordination number of the Ti and O atoms on the surface (density of dangling bonds), which dictates its physico-chemical properties such as surface energy and wettability. The most stable (110) surface with the lowest energy exhibits hydrophobicity in the context of protein adsorption, while the others, especially the (001) surface, are more energetic and hydrophilic.

Furthermore, AFM-based force measurements confirmed that the surface energy of a material changes after protein adsorption according to the adopted conformation. Since it is associated with exposure to the medium of protein regions characterized by different hydrophilicity/hydrophobicity, it facilitated the identification of HPF conformational changes adsorbed on rutile surfaces. In addition, these observations suggest the possibility of controlling subsequent surface energy-dependent biological processes that occur at the

biomaterial - blood interface. The observed differences in intermolecular forces between the AFM tip and protein-coated surface, or AFM tip and bare rutile surface enabled also the adhesion forces mapping, which supported the visual detection of adsorbed protein molecules.

Presented results suggest that the probability of pathological clot formation is the lowest on the (110) surface. Therefore, rutile with the (110) crystallographic orientation is a potential material that can be used to engineer highly biocompatible and hemocompatible implants used in medicine.

Nevertheless, the production of a whole implant from a single crystal is challenging. Therefore, it was evaluated whether the same conclusions could be drawn by studying rutile polycrystals, which are much cheaper to produce, and current technology allows control over the growth of preferentially oriented grains. In addition, due to the presence of many differently oriented grains on one sample, studies on polycrystals may improve an experimental procedure of crystallographic orientation-dependent biological processes.

The HPF-mediated platelets behavior was analyzed on multiple grains of polycrystals produced by powder compaction, sintering, and polishing. However, grain-specific changes in local surface properties did not affect either HPF adsorption or platelet adhesion, inconsistent with results obtained on single crystals. A detailed explanation of these contradictory findings requires a more detailed characterization of polycrystals, which is the scope of our future research. It is anticipated that this may be due to a reduction of surface energy and therefore hydrophobicity of a polycrystal surface induced by thermal etching. Other possible explanations are impurities or non-stoichiometry of the produced in this study substrates.

To conclude, a new direction in the development of highly biocompatible material surfaces has been proposed in this dissertation by combining materials science and biomedical knowledge. Evidence has been provided that allows to take a step forward, toward the design of safe implants and medical devices that effectively perform their functions.

## References

- (1) Domingues Goncalves, A.; Balestri, W.; Reinwald, Y. Biomedical Implants for Regenerative Therapies. In *Biomaterials*; IntechOpen, 2020. <https://doi.org/10.5772/intechopen.91295>.
- (2) Leali, P. T.; Merolli, A. Fundamentals of Biomaterials. In *Biomaterials in Hand Surgery*; Springer Milan: Milano, 2009; pp 1–11. [https://doi.org/10.1007/978-88-470-1195-3\\_1](https://doi.org/10.1007/978-88-470-1195-3_1).
- (3) Biomaterial-Tissue Interfaces: Proceedings of the Ninth European Conference on Biomaterials, Chester, UK, September 9-11. **1991**.
- (4) Burke, C. J.; Steadman, B. L.; Volkin, D. B.; Tsai, P.-K.; Bruner, M. W.; Middaugh, C. R. The Adsorption of Proteins to Pharmaceutical Container Surfaces. *International Journal of Pharmaceutics* **1992**, *86* (1), 89–93. [https://doi.org/10.1016/0378-5173\(92\)90034-Y](https://doi.org/10.1016/0378-5173(92)90034-Y).
- (5) Tang, L.; Thevenot, P.; Hu, W. Surface Chemistry Influences Implant Biocompatibility. *Current topics in medicinal chemistry* **2008**, *8* (4), 270–280. <https://doi.org/10.2174/156802608783790901>.
- (6) Shahali, H.; Jaggessar, A.; Yarlagadda, P. K. Recent Advances in Manufacturing and Surface Modification of Titanium Orthopaedic Applications. *Procedia Engineering* **2017**, *174*, 1067–1076. <https://doi.org/10.1016/j.proeng.2017.01.259>.
- (7) Kaur, M. Review on Titanium and Titanium Based Alloys as Biomaterials for Orthopaedic Applications. *Materials Science* **2019**, *102*, 844–862. <https://doi.org/10.1016/j.msec.2019.04.064>.
- (8) Brunette, D. M.; Tengvall, P.; Textor, M.; Thomsen, P. *Titanium in Medicine: Material Science, Surface Science, Engineering, Biological Responses and Medical Applications*; Engineering Materials; Springer Berlin Heidelberg: Berlin, Heidelberg, 2001. <https://doi.org/10.1007/978-3-642-56486-4>.
- (9) Johnson, B.; Starks, I.; Bancroft, G.; Roberts, P. J. The Effect of Care Bundle Development on Surgical Site Infection after Hemiarthroplasty: An 8-Year Review. *Journal of Trauma and Acute Care Surgery* **2012**, *72* (5), 1375–1379. <https://doi.org/10.1097/TA.0b013e318245267c>.
- (10) Liu, X.; Yuan, L.; Li, D.; Tang, Z.; Wang, Y.; Chen, G.; Chen, H.; Brash, J. L. Blood Compatible Materials: State of the Art. *Journal of Materials Chemistry B* **2014**, *2* (35), 5718–5738. <https://doi.org/10.1039/C4TB00881B>.
- (11) Ruggeri, Z. M. Mechanisms Initiating Platelet Thrombus Formation. *Thrombosis and haemostasis* **2018**, *78* (07), 611–616. <https://doi.org/10.1055/s-0038-1657598>.
- (12) Sivaraman, B.; Latour, R. A. The Relationship between Platelet Adhesion on Surfaces and the Structure versus the Amount of Adsorbed Fibrinogen. *Biomaterials* **2010**, *31* (5), 832–839. <https://doi.org/10.1016/j.biomaterials.2009.10.008>.
- (13) Hess, H. Muscle on Demand. *Nature Materials* **2021**, *20* (8), 1040–1041. <https://doi.org/10.1038/s41563-021-01069-1>.
- (14) Walkowiak-Przybyło, M.; Klimek, L.; Okrój, W.; Jakubowski, W.; Chwiłka, M.; Czajka, A.; Walkowiak, B. Adhesion, Activation, and Aggregation of Blood

- Platelets and Biofilm Formation on the Surfaces of Titanium Alloys Ti6Al4V and Ti6Al7Nb. *Journal of Biomedical Materials Research Part A* **2012**, *100A* (3), 768–775. <https://doi.org/10.1002/jbm.a.34006>.
- (15) Özcan, M.; Hämmerle, C. Titanium as a Reconstruction and Implant Material in Dentistry: Advantages and Pitfalls. *Materials* **2012**, *5* (9), 1528–1545. <https://doi.org/10.3390/ma5091528>.
  - (16) Oldani, C.; Dominguez, A. Titanium as a Biomaterial for Implants. In *Recent Advances in Arthroplasty*; InTech, 2012. <https://doi.org/10.5772/27413>.
  - (17) Elias, C. N.; Lima, J. H. C.; Valiev, R.; Meyers, M. A. Biomedical Applications of Titanium and Its Alloys. *The Journal of The Minerals, Metals & Materials Society* **2008**, *60*, 46–49. <https://doi.org/10.1007/s11837-008-0031-1>.
  - (18) Sarraf, M.; Rezvani Ghomi, E.; Alipour, S.; Ramakrishna, S.; Liana Sukiman, N. A State-of-the-Art Review of the Fabrication and Characteristics of Titanium and Its Alloys for Biomedical Applications. *Bio-Design and Manufacturing* **2022**, *5* (2), 371–395. <https://doi.org/10.1007/s42242-021-00170-3>.
  - (19) Lupi, S. M.; Albini, B.; Rodriguez Y. Baena, A.; Lanfrè, G.; Galinetto, P. Anatase Forming Treatment without Surface Morphological Alteration of Dental Implant. *Materials* **2020**, *13* (22), 5280. <https://doi.org/10.3390/ma13225280>.
  - (20) Vergara, L. I.; Passeggi, M. C. G.; Ferrón, J. The Role of Passivation in Titanium Oxidation: Thin Film and Temperature Effects. *Applied Surface Science* **2002**, *187* (3–4), 199–206. [https://doi.org/10.1016/S0169-4332\(01\)00986-2](https://doi.org/10.1016/S0169-4332(01)00986-2).
  - (21) Pantaroto, H. N.; Cordeiro, J. M.; Pereira, L. T.; de Almeida, A. B.; Nociti Junior, F. H.; Rangel, E. C.; Azevedo Neto, N. F.; da Silva, J. H. D.; Barão, V. A. R. Sputtered Crystalline TiO<sub>2</sub> Film Drives Improved Surface Properties of Titanium-Based Biomedical Implants. *Materials Science and Engineering: C* **2021**, *119*, 111638. <https://doi.org/10.1016/j.msec.2020.111638>.
  - (22) Jackson, M. J.; Ahmed, W. Titanium Dioxide Coatings in Medical Device Applications. In *Surface Engineered Surgical Tools and Medical Devices*; Springer US: Boston, MA, 2007; pp 49–63. [https://doi.org/10.1007/978-0-387-27028-9\\_3](https://doi.org/10.1007/978-0-387-27028-9_3).
  - (23) Barthes, J.; Ciftci, S.; Ponzio, F.; Knopf-Marques, H.; Pelyhe, L.; Gudima, A.; Kientzl, I.; Bognár, E.; Weszl, M.; Kzhyshkowska, J.; Vrana, N. E. Review: The Potential Impact of Surface Crystalline States of Titanium for Biomedical Applications. *Critical Reviews in Biotechnology* **2018**, *38* (3), 423–437. <https://doi.org/10.1080/07388551.2017.1363707>.
  - (24) Leng, Y. X.; Chen, J. Y.; Yang, P.; Sun, H.; Huang, N. The Microstructure and Properties of Titanium Dioxide Films Synthesized by Unbalanced Magnetron Sputtering. *Nuclear Instruments and Methods in Physics Research Section B: Beam Interactions with Materials and Atoms* **2007**, *257* (1–2), 451–454. <https://doi.org/10.1016/j.nimb.2007.01.096>.
  - (25) Diebold, U. The Surface Science of Titanium Dioxide. *Surface Science Reports* **2003**, *48* (5–8), 53–229. [https://doi.org/10.1016/S0167-5729\(02\)00100-0](https://doi.org/10.1016/S0167-5729(02)00100-0).
  - (26) Ramamoorthy, M.; Vanderbilt, D.; King-Smith, R. D. First-Principles Calculations of the Energetics of Stoichiometric TiO<sub>2</sub> Surfaces. *Physical Review B* **1994**, *49* (23), 16721–16727. <https://doi.org/10.1103/PhysRevB.49.16721>.

- (27) Momma, K.; Izumi, F. *VESTA 3 for Three-Dimensional Visualization of Crystal, Volumetric and Morphology Data*. *Journal of Applied Crystallography* **2011**, *44* (6), 1272–1276. <https://doi.org/10.1107/S0021889811038970>.
- (28) Perron, H.; Domain, C.; Roques, J.; Drot, R.; Simoni, E.; Catalette, H. Optimisation of Accurate Rutile TiO<sub>2</sub> (110), (100), (101) and (001) Surface Models from Periodic DFT Calculations. *Theoretical Chemistry Accounts* **2007**, *117* (4), 565–574. <https://doi.org/10.1007/s00214-006-0189-y>.
- (29) Wei, B.; Tielens, F.; Calatayud, M. Understanding the Role of Rutile TiO<sub>2</sub> Surface Orientation on Molecular Hydrogen Activation. *Nanomaterials* **2019**, *9* (9), 1199. <https://doi.org/10.3390/nano9091199>.
- (30) Barbosa, M. de A.; Fabris, G. da S. L.; Ferrer, M. M.; Azevedo, D. H. M. de; Sambrano, J. R. Computational Simulations of Morphological Transformations by Surface Structures: The Case of Rutile TiO<sub>2</sub> Phase. *Materials Research* **2017**, *20* (4), 920–925. <https://doi.org/10.1590/1980-5373-mr-2016-0709>.
- (31) De Nardo, L.; Raffaini, G.; Ebramzadeh, E.; Ganazzoli, F. Titanium Oxide Modeling and Design for Innovative Biomedical Surfaces: A Concise Review. *The International Journal of Artificial Organs* **2012**, *35* (9), 629–641. <https://doi.org/10.5301/ijao.5000040>.
- (32) Barnard, A. S.; Zapol, P.; Curtiss, L. A. Modeling the Morphology and Phase Stability of TiO<sub>2</sub> Nanocrystals in Water. *Journal of Chemical Theory and Computation* **2005**, *1* (1), 107–116. <https://doi.org/10.1021/ct0499635>.
- (33) Zhao, Z.-Y. Single Water Molecule Adsorption and Decomposition on the Low-Index Stoichiometric Rutile TiO<sub>2</sub> Surfaces. *The Journal of Physical Chemistry C* **2014**, *118* (8), 4287–4295. <https://doi.org/10.1021/jp500177n>.
- (34) Kavathekar, R. S.; Dev, P.; English, N. J.; MacElroy, J. M. D. Molecular Dynamics Study of Water in Contact with the TiO<sub>2</sub> Rutile-110, 100, 101, 001 and Anatase-101, 001 Surface. *Molecular Physics* **2011**, *109* (13), 1649–1656. <https://doi.org/10.1080/00268976.2011.582051>.
- (35) Hong, J.; Andersson, J.; Nilsson Ekdahl, K.; Elgue, G.; Axén, N.; Larsson, R.; Nilsson, B. Titanium Is a Highly Thrombogenic Biomaterial: Possible Implications for Osteogenesis. *Thrombosis and Haemostasis* **1999**, *82* (07), 58–64. <https://doi.org/10.1055/s-0037-1614630>.
- (36) Lotfi, A.; Reejhsinghani, R. Prevention of Stent Thrombosis: Challenges and Solutions. *Vascular Health and Risk Management* **2015**, *93*. <https://doi.org/10.2147/VHRM.S43357>.
- (37) Brown, J.; O'Brien, C. C.; Lopes, A. C.; Kolandaivelu, K.; Edelman, E. R. Quantification of Thrombus Formation in Malapposed Coronary Stents Deployed in Vitro through Imaging Analysis. *Journal of Biomechanics* **2018**, *71*, 296–301. <https://doi.org/10.1016/j.jbiomech.2018.01.044>.
- (38) Cacciafesta, P.; Humphris, A. D. L.; Jandt, K. D.; Miles, M. J. Human Plasma Fibrinogen Adsorption on Ultraflat Titanium Oxide Surfaces Studied with Atomic Force Microscopy. *Langmuir* **2000**, *16* (21), 8167–8175. <https://doi.org/10.1021/la000362k>.
- (39) Hong, J. K.; Gao, L.; Singh, J.; Goh, T.; Ruhoff, A. M.; Neto, C.; Waterhouse, A. Evaluating Medical Device and Material Thrombosis under Flow: Current and

- Emerging Technologies. *Biomater. Sci.* **2020**, *8* (21), 5824–5845. <https://doi.org/10.1039/D0BM01284J>.
- (40) Schulman, S. Advantages and Limitations of the New Anticoagulants. *Journal of Internal Medicine* **2014**, *275* (1), 1–11. <https://doi.org/10.1111/joim.12138>.
- (41) Radke, D.; Jia, W.; Sharma, D.; Fena, K.; Wang, G.; Goldman, J.; Zhao, F. Tissue Engineering at the Blood-Contacting Surface: A Review of Challenges and Strategies in Vascular Graft Development. *Advanced Healthcare Materials* **2018**, *7* (15), 1701461. <https://doi.org/10.1002/adhm.201701461>.
- (42) Labarrere, C. A.; Dabiri, A. E.; Kassab, G. S. Thrombogenic and Inflammatory Reactions to Biomaterials in Medical Devices. *Frontiers in Bioengineering and Biotechnology* **2020**, *8*, 123. <https://doi.org/10.3389/fbioe.2020.00123>.
- (43) Missirlis, Y. F.; Wautier, J.-L.; Ordinas, A.; Escolar, G.; White, J. G. Ultrastructure of Platelets and Platelet-Surface Interactions. In *The Role of Platelets in Blood-Biomaterial Interactions*; Springer Netherlands: Dordrecht, 1993; pp 3–13. [https://doi.org/10.1007/978-94-011-1745-6\\_1](https://doi.org/10.1007/978-94-011-1745-6_1).
- (44) Gregg, D.; Goldschmidt-Clermont, P. J. Platelets and Cardiovascular Disease. *Circulation* **2003**, *108* (13). <https://doi.org/10.1161/01.CIR.0000086897.15588.4B>.
- (45) Jung, F.; Braune, S. Thrombogenicity and Hemocompatibility of Biomaterials. *Biointerphases* **2016**, *11* (2), 029601. <https://doi.org/10.1116/1.4938557>.
- (46) Kieffer, N. Platelet Membrane Glycoproteins: Functions in Cellular Interactions. *Annual review of cell biology* **1990**, *6*, 329–357. <https://doi.org/10.1146/annurev.cb.06.110190.001553>.
- (47) Saboor, M.; Ayub, Q.; Ilyas, S.; Moinuddin, . Platelet Receptors: An Instrumental of Platelet Physiology. *Pakistan Journal of Medical Sciences* **2013**, *29* (3). <https://doi.org/10.12669/pjms.293.3497>.
- (48) Goodman, S. L.; Cooper, S. L.; Albrecht, R. M. Integrin Receptors and Platelet Adhesion to Synthetic Surfaces. *Journal of Biomedical Materials Research* **1993**, *27* (5), 683–695. <https://doi.org/10.1002/jbm.820270516>.
- (49) Savage, B.; Ruggeri, Z. M. Selective Recognition of Adhesive Sites in Surface-Bound Fibrinogen by Glycoprotein IIb-IIIa on Nonactivated Platelets. *Journal of Biological Chemistry* **1991**, *266* (17), 11227–11233. [https://doi.org/10.1016/S0021-9258\(18\)99152-0](https://doi.org/10.1016/S0021-9258(18)99152-0).
- (50) Siedlecki, C. A. *Hemocompatibility of Biomaterials for Clinical Applications*; Elsevier: Oxford, UK, 2018. <https://doi.org/10.1016/C2014-0-04140-8>.
- (51) Grunkemeier, J. M.; Tsai, W. B.; McFarland, C. D.; Horbett, T. A. The Effect of Adsorbed Fibrinogen, Fibronectin, von Willebrand Factor and Vitronectin on the Procoagulant State of Adherent Platelets. *Biomaterials* **2000**, *21* (22), 2243–2252. [https://doi.org/10.1016/S0142-9612\(00\)00150-2](https://doi.org/10.1016/S0142-9612(00)00150-2).
- (52) Nygren, H.; Tengvall, P.; Lundström, I. The Initial Reactions of TiO<sub>2</sub> with Blood. *Journal of Biomedical Materials Research* **1997**, *34* (4), 487–492. [https://doi.org/10.1002/\(SICI\)1097-4636\(19970315\)34:4<487::AID-JBM9>3.0.CO;2-G](https://doi.org/10.1002/(SICI)1097-4636(19970315)34:4<487::AID-JBM9>3.0.CO;2-G).

- (53) Horbett, T. A.; Brash, J. L. Proteins at Interfaces II: Fundamentals and Applications. In *Proteins at Interfaces II: Fundamentals and Applications*; ACS Symposium Series; American Chemical Society: Washington, DC, 1995; Vol. 602. <https://doi.org/10.1021/bk-1995-0602>.
- (54) Brash, J. L.; Horbett, T. A.; Latour, R. A.; Tengvall, P. The Blood Compatibility Challenge. Part 2: Protein Adsorption Phenomena Governing Blood Reactivity. *Acta Biomaterialia* **2019**, *94*, 11–24. <https://doi.org/10.1016/j.actbio.2019.06.022>.
- (55) Courtney, J. M.; Lamba, N. M. K.; Sundaram, S.; Forbes, C. D. Biomaterials for Blood-Contacting Applications. *Biomaterials* **1994**, *15* (10), 737–744. [https://doi.org/10.1016/0142-9612\(94\)90026-4](https://doi.org/10.1016/0142-9612(94)90026-4).
- (56) Whitford, D. In *Proteins: structure and function*; John Wiley & Sons, 2013.
- (57) Bouhallab, S.; Croguennec, T. Spontaneous Assembly and Induced Aggregation of Food Proteins. In *Polyelectrolyte Complexes in the Dispersed and Solid State II: Application Aspects*; Müller, M., Ed.; Springer Berlin Heidelberg: Berlin, Heidelberg, 2014; pp 67–101. [https://doi.org/10.1007/12\\_2012\\_201](https://doi.org/10.1007/12_2012_201).
- (58) Petsko, G. A.; Ringe, D. *Protein Structure and Function*; Primers in biology; New Science Press, 2004.
- (59) Kessel, A.; Ben-Tal, N. *Introduction to Proteins: Structure, Function, and Motion*; Chapman & Hall/CRC mathematical biology and medicine series; CRC Press, Taylor & Francis Group, 2018.
- (60) Luensmann, D.; Jones, L. Albumin Adsorption to Contact Lens Materials: A Review. *Contact Lens and Anterior Eye* **2008**, *31* (4), 179–187. <https://doi.org/10.1016/j.clae.2008.05.004>.
- (61) Rabe, M.; Verdes, D.; Seeger, S. Understanding Protein Adsorption Phenomena at Solid Surfaces. *Advances in Colloid and Interface Science* **2011**, *162* (1–2), 87–106. <https://doi.org/10.1016/j.cis.2010.12.007>.
- (62) Haynes, C. A.; Norde, W. Structures and Stabilities of Adsorbed Proteins. *Journal of Colloid and Interface Science* **1995**, *169* (2), 313–328. <https://doi.org/10.1006/jcis.1995.1039>.
- (63) Stillwell, W. Membrane Biogenesis. In *An Introduction to Biological Membranes*; Elsevier, 2016; pp 315–329. <https://doi.org/10.1016/B978-0-444-63772-7.00014-2>.
- (64) Czeslik, C. Factors Ruling Protein Adsorption. *Zeitschrift für Physikalische Chemie* **2004**, *218*, 771–801. <https://doi.org/10.1524/zpch.218.7.771.35722>.
- (65) Kollman, J. M.; Pandi, L.; Sawaya, M. R.; Riley, M.; Doolittle, R. F. Crystal Structure of Human Fibrinogen. *Biochemistry* **2009**, *48* (18), 3877–3886. <https://doi.org/10.1021/bi802205g>.
- (66) Hedayati, M.; Neufeld, M. J.; Reynolds, M. M.; Kipper, M. J. The Quest for Blood-Compatible Materials: Recent Advances and Future Technologies. *Materials Science and Engineering: R: Reports* **2019**, *138*, 118–152. <https://doi.org/10.1016/j.mser.2019.06.002>.
- (67) Felgueiras, H. P.; Murthy, N. S.; Sommerfeld, S. D.; Brás, M. M.; Migonney, V.; Kohn, J. Competitive Adsorption of Plasma Proteins Using a Quartz Crystal



- Microbalance. *ACS Applied Materials & Interfaces* **2016**, *8* (21), 13207–13217. <https://doi.org/10.1021/acsami.5b12600>.
- (68) Canoa, P.; Simón-Vázquez, R.; Popplewell, J.; González-Fernández, Á. A Quantitative Binding Study of Fibrinogen and Human Serum Albumin to Metal Oxide Nanoparticles by Surface Plasmon Resonance. *Biosensors and Bioelectronics* **2015**, *74*, 376–383. <https://doi.org/10.1016/j.bios.2015.05.070>.
- (69) Hirsh, S. L.; McKenzie, D. R.; Nosworthy, N. J.; Denman, J. A.; Sezerman, O. U.; Bilek, M. M. M. The Vroman Effect: Competitive Protein Exchange with Dynamic Multilayer Protein Aggregates. *Colloids and Surfaces B: Biointerfaces* **2013**, *103*, 395–404. <https://doi.org/10.1016/j.colsurfb.2012.10.039>.
- (70) Tsai, W.-B.; Horbett, T. A. The Role of Fibronectin in Platelet Adhesion to Plasma Preadsorbed Polystyrene. *Journal of Biomaterials Science, Polymer Edition* **1999**, *10* (2), 163–181. <https://doi.org/10.1163/156856299X00117>.
- (71) Asch, E.; Podack, E. Vitronectin Binds to Activated Human Platelets and Plays a Role in Platelet Aggregation. *Journal of Clinical Investigation* **1990**, *85* (5), 1372–1378. <https://doi.org/10.1172/JCI114581>.
- (72) Lambrecht, L. K.; Youngl, B. R.; Staffordl, R. E.; Park, K.; Albrecht, R. M.; Mosher, D. F.; Cooper, S. L. The Influence of Preadsorbed Canine von Willebrand Factor, Fibronectin and Fibrinogen on Ex Vivo Artificial Surface-Induced Thrombosis. *Thrombosis research* **1986**, *41* (1), 19. [https://doi.org/10.1016/0049-3848\(86\)90283-5](https://doi.org/10.1016/0049-3848(86)90283-5).
- (73) Chiumiento, A.; Lamponi, S.; Barbucci, R. Role of Fibrinogen Conformation in Platelet Activation. *Biomacromolecules* **2007**, *8* (2), 523–531. <https://doi.org/10.1021/bm060664m>.
- (74) Bledzka, K.; Smyth, S. S.; Plow, E. F. Integrin AIIb $\beta$ 3: From Discovery to Efficacious Therapeutic Target. *Circulation Research* **2013**, *112* (8), 1189–1200. <https://doi.org/10.1161/CIRCRESAHA.112.300570>.
- (75) Tsai, W.-B.; Grunkemeier, J. M.; McFarland, C. D.; Horbett, T. A. Platelet Adhesion to Polystyrene-Based Surfaces Preadsorbed with Plasmas Selectively Depleted in Fibrinogen, Fibronectin, Vitronectin, or von Willebrand's Factor. *Journal of Biomedical Materials Research* **2002**, *60* (3), 348–359. <https://doi.org/10.1002/jbm.10048>.
- (76) Soman, P.; Siedlecki, C. A. Effects of Protein Solution Composition on the Time-Dependent Functional Activity of Fibrinogen on Surfaces. *Langmuir* **2011**, *27* (17), 10814–10819. <https://doi.org/10.1021/la201111r>.
- (77) Chinn, J. Baboon Fibrinogen Adsorption and Platelet Adhesion to Polymeric Materials. *Thrombosis and Haemostasis* **1991**, No. 65(05), 608–617. <https://doi.org/10.1055/s-0038-1648198>.
- (78) Collier, B. S. Blockade of Platelet GPIIb/IIIa Receptors as an Antithrombotic Strategy. *Circulation* **1995**, *92* (9), 2373–2380. <https://doi.org/10.1161/01.CIR.92.9.2373>.
- (79) Herrick, S.; Blanc-Brude, O.; Gray, A.; Laurent, G. Fibrinogen. *The International Journal of Biochemistry & Cell Biology* **1999**, *31* (7), 741–746. [https://doi.org/10.1016/S1357-2725\(99\)00032-1](https://doi.org/10.1016/S1357-2725(99)00032-1).

- (80) Weisel, J. W.; Stauffacher, C. V.; Bullitt, E.; Cohen, C. A Model for Fibrinogen: Domains and Sequence. *Science* **1985**, *230* (4732), 1388–1391. <https://doi.org/10.1126/science.4071058>.
- (81) Weisel, J. W. Fibrinogen and Fibrin. *Advances in Protein Chemistry* **2005**, *70*, 247–299. [https://doi.org/10.1016/S0065-3233\(05\)70008-5](https://doi.org/10.1016/S0065-3233(05)70008-5).
- (82) Gardlund, B.; Hessel, B.; Blomback, B.; Marguerie, G.; Murano, G. Primary Structure of Human Fibrinogen. Characterization of Disulfide-Containing Cyanogen-Bromide Fragments. *European Journal of Biochemistry* **1977**, *77* (3), 595–610. <https://doi.org/10.1111/j.1432-1033.1977.tb11704.x>.
- (83) Hyltegren, K.; Hulander, M.; Andersson, M.; Skepö, M. Adsorption of Fibrinogen on Silica Surfaces—The Effect of Attached Nanoparticles. *Biomolecules* **2020**, *10* (3), 413. <https://doi.org/10.3390/biom10030413>.
- (84) Retzinger, G. S.; DeAnglis, A. P.; Patuto, S. J. Adsorption of Fibrinogen to Droplets of Liquid Hydrophobic Phases: Functionality of the Bound Protein and Biological Implications. *Arteriosclerosis, Thrombosis, and Vascular Biology* **1998**, *18* (12), 1948–1957. <https://doi.org/10.1161/01.ATV.18.12.1948>.
- (85) Waldeck, H.; Kao, W. J. Protein Adsorption to Biomaterials. In *Biological Interactions on Materials Surfaces: Understanding and Controlling Protein, Cell, and Tissue Responses*; Springer US: New York, NY, 2009; pp 1–18. [https://doi.org/10.1007/978-0-387-98161-1\\_1](https://doi.org/10.1007/978-0-387-98161-1_1).
- (86) Grunkemeier, J. M.; Horbett, T. A. Fibrinogen Adsorption to Receptor-like Biomaterials Made by Pre-Adsorbing Peptides to Polystyrene Substrates. *Journal of molecular recognition: JMR* **1996**, *9* (3), 247–257. [https://doi.org/10.1002/\(sici\)1099-1352\(199605\)9:3<247::aid-jmr336>3.0.co;2-h](https://doi.org/10.1002/(sici)1099-1352(199605)9:3<247::aid-jmr336>3.0.co;2-h).
- (87) Farrell, D. H.; Thiagarajan, P.; Chung, D. W.; Davie, E. W. Role of Fibrinogen  $\alpha$  and  $\gamma$  Chain Sites in Platelet Aggregation. *Biochemistry* **1992**, *89*, 10729–10732. <https://doi.org/10.1073%2Fpnas.89.22.10729>.
- (88) Zamarron, C.; Ginsberg, M. H.; Plow, E. F. A Receptor-Induced Binding Site in Fibrinogen Elicited by Its Interaction with Platelet Membrane Glycoprotein IIb-IIIa. *Journal of Biological Chemistry* **1991**, *266* (24), 16193–16199. [https://doi.org/10.1016/S0021-9258\(18\)98534-0](https://doi.org/10.1016/S0021-9258(18)98534-0).
- (89) Norde, W. My Voyage of Discovery to Proteins in Flatland ...and Beyond. *Colloids and Surfaces B: Biointerfaces* **2008**, *61* (1), 1–9. <https://doi.org/10.1016/j.colsurfb.2007.09.029>.
- (90) Gray, J. J. The Interaction of Proteins with Solid Surfaces. *Current Opinion in Structural Biology* **2004**, *14* (1), 110–115. <https://doi.org/10.1016/j.sbi.2003.12.001>.
- (91) Firkowska-Boden, I.; Zhang, X.; Jandt, K. D. Controlling Protein Adsorption through Nanostructured Polymeric Surfaces. *Advanced Healthcare Materials* **2018**, *7* (1), 1700995. <https://doi.org/10.1002/adhm.201700995>.
- (92) Latour, R. A. Fundamental Principles of the Thermodynamics and Kinetics of Protein Adsorption to Material Surfaces. *Colloids and Surfaces B: Biointerfaces* **2020**, *191*, 110992. <https://doi.org/10.1016/j.colsurfb.2020.110992>.
- (93) Tanaka, M.; Motomura, T.; Kawada, M.; Anzai, T.; Yuu Kasori; Shiroya, T.; Shimura, K.; Onishi, M.; Akira Mochizuki. Blood Compatible Aspects of Poly(2-

- Methoxyethylacrylate) (PMEA)—Relationship between Protein Adsorption and Platelet Adhesion on PMEA Surface. *Biomaterials* **2000**, *21* (14), 1471–1481. [https://doi.org/10.1016/S0142-9612\(00\)00031-4](https://doi.org/10.1016/S0142-9612(00)00031-4).
- (94) Ishihara, K.; Fukumoto, K.; Iwasaki, Y.; Nakabayashi, N. Modification of Polysulfone with Phospholipid Polymer for Improvement of the Blood Compatibility. Part 2. Protein Adsorption and Platelet Adhesion. *Biomaterials* **1999**, 1553–1559. [https://doi.org/10.1016/s0142-9612\(98\)00206-3](https://doi.org/10.1016/s0142-9612(98)00206-3).
- (95) Hylton, D. M.; Shalaby, S. W.; Latour, R. A. Direct Correlation between Adsorption-Induced Changes in Protein Structure and Platelet Adhesion. *Journal of Biomedical Materials Research Part A* **2005**, *73A* (3), 349–358. <https://doi.org/10.1002/jbm.a.30295>.
- (96) Podolnikova, N. P.; Yermolenko, I. S.; Fuhrmann, A.; Lishko, V. K.; Magonov, S.; Bowen, B.; Enderlein, J.; Podolnikov, A. V.; Ros, R.; Ugarova, T. P. Control of Integrin  $\alpha_{IIb}\beta_3$  Outside-In Signaling and Platelet Adhesion by Sensing the Physical Properties of Fibrin(ogen) Substrates. *Biochemistry* **2010**, *49* (1), 68–77. <https://doi.org/10.1021/bi9016022>.
- (97) Chen, H.; Yuan, L.; Song, W.; Wu, Z.; Li, D. Biocompatible Polymer Materials: Role of Protein–Surface Interactions. *Progress in Polymer Science* **2008**, *33* (11), 1059–1087. <https://doi.org/10.1016/j.progpolymsci.2008.07.006>.
- (98) Lu, D. R.; Park, K. Effect of Surface Hydrophobicity on the Conformational Changes of Adsorbed Fibrinogen. *Journal of Colloid and Interface Science* **1991**, *144* (1), 271–281. [https://doi.org/10.1016/0021-9797\(91\)90258-A](https://doi.org/10.1016/0021-9797(91)90258-A).
- (99) Ishihara, K.; Takai, M. Bioinspired Interface for Nanobiodevices Based on Phospholipid Polymer Chemistry. *Journal of The Royal Society Interface* **2009**, *6* (suppl\_3). <https://doi.org/10.1098/rsif.2008.0335>.
- (100) Tunc, S.; Maitz, M. F.; Steiner, G.; Vázquez, L.; Pham, M. T.; Salzer, R. In Situ Conformational Analysis of Fibrinogen Adsorbed on Si Surfaces. *Colloids and Surfaces B: Biointerfaces* **2005**, *42* (3–4), 219–225. <https://doi.org/10.1016/j.colsurfb.2005.03.004>.
- (101) Xiao, K.; Wen, L.; Jiang, L. Bioinspired Superwettability Materials. In *Kirk-Othmer Encyclopedia of Chemical Technology*; John Wiley & Sons Inc, Ed.; John Wiley & Sons, Inc.: Hoboken, NJ, USA, 2016; pp 1–34. <https://doi.org/10.1002/0471238961.koe00013>.
- (102) Yoon, R.-H.; Flinn, D. H.; Rabinovich, Y. I. Hydrophobic Interactions between Dissimilar Surfaces. *Journal of Colloid and Interface Science* **1997**, *185* (2), 363–370. <https://doi.org/10.1006/jcis.1996.4583>.
- (103) Xu, L.-C.; Siedlecki, C. A. Effects of Surface Wettability and Contact Time on Protein Adhesion to Biomaterial Surfaces. *Biomaterials* **2007**, *28* (22), 3273–3283. <https://doi.org/10.1016/j.biomaterials.2007.03.032>.
- (104) Berg, J. M.; Eriksson, L. G. T.; Claesson, P. M.; Borve, K. G. N. Three-Component Langmuir-Blodgett Films with a Controllable Degree of Polarity. *Langmuir* **1994**, *10* (4), 1225–1234. <https://doi.org/10.1021/la00016a041>.
- (105) Tsapikouni, T. S.; Missirlis, Y. F. Protein–Material Interactions: From Micro-to-Nano Scale. *Materials Science and Engineering: B* **2008**, *152* (1–3), 2–7. <https://doi.org/10.1016/j.mseb.2008.06.007>.

- (106) Chapman, R. G.; Ostuni, E.; Takayama, S.; Holmlin, R. E.; Yan, L.; Whitesides, G. M. Surveying for Surfaces That Resist the Adsorption of Proteins. *Journal of the American Chemical Society* **2000**, *122* (34), 8303–8304. <https://doi.org/10.1021/ja000774f>.
- (107) Ostuni, E.; Chapman, R. G.; Holmlin, R. E.; Takayama, S.; Whitesides, G. M. A Survey of Structure–Property Relationships of Surfaces That Resist the Adsorption of Protein. *Langmuir* **2001**, *17* (18), 5605–5620. <https://doi.org/10.1021/la010384m>.
- (108) Holmlin, R. E.; Chen, X.; Chapman, R. G.; Takayama, S.; Whitesides, G. M. Zwitterionic SAMs That Resist Nonspecific Adsorption of Protein from Aqueous Buffer. *Langmuir* **2001**, *17* (9), 2841–2850. <https://doi.org/10.1021/la0015258>.
- (109) Siegismund, D.; Keller, T. F.; Jandt, K. D.; Rettenmayr, M. Fibrinogen Adsorption on Biomaterials - A Numerical Study: Fibrinogen Adsorption on Biomaterials - A Numerical Study. *Macromolecular Bioscience* **2010**, *10* (10), 1216–1223. <https://doi.org/10.1002/mabi.201000120>.
- (110) Andrade, J. D.; Hlady, V. Protein Adsorption and Materials Biocompatibility: A Tutorial Review and Suggested Hypotheses. In *Biopolymers/Non-Exclusion HPLC*; Advances in Polymer Science; Springer Berlin Heidelberg: Berlin, Heidelberg, 1986; Vol. 79, pp 1–63. [https://doi.org/10.1007/3-540-16422-7\\_6](https://doi.org/10.1007/3-540-16422-7_6).
- (111) Vogler, E. A. Structure and Reactivity of Water at Biomaterial Surfaces. *Advances in Colloid and Interface Science* **1998**, *74* (1–3), 69–117. [https://doi.org/10.1016/S0001-8686\(97\)00040-7](https://doi.org/10.1016/S0001-8686(97)00040-7).
- (112) Yoon, J.-Y.; Kim, J.-H.; Kim, W.-S. Interpretation of Protein Adsorption Phenomena onto Functional Microspheres. *Colloids and Surfaces B: Biointerfaces* **1998**, *12* (1), 15–22. [https://doi.org/10.1016/S0927-7765\(98\)00045-9](https://doi.org/10.1016/S0927-7765(98)00045-9).
- (113) Sit, P. S.; Marchant, R. Surface-Dependent Conformations of Human Fibrinogen Observed by Atomic Force Microscopy under Aqueous Conditions. *Thrombosis and Haemostasis* **1999**, *82* (09), 1053–1060. <https://doi.org/10.1055/s-0037-1614328>.
- (114) Isoshima, K.; Ueno, T.; Arai, Y.; Saito, H.; Chen, P.; Tsutsumi, Y.; Hanawa, T.; Wakabayashi, N. The Change of Surface Charge by Lithium Ion Coating Enhances Protein Adsorption on Titanium. *Journal of the Mechanical Behavior of Biomedical Materials* **2019**, *100*, 103393. <https://doi.org/10.1016/j.jmbbm.2019.103393>.
- (115) Yang; Tsou; Hsiao; Cheng; Liu; Huang; Peng; Liu; Yung; Hsu. Electrochemical Polymerization of PEDOT–Graphene Oxide–Heparin Composite Coating for Anti-Fouling and Anti-Clotting of Cardiovascular Stents. *Polymers* **2019**, *11* (9), 1520. <https://doi.org/10.3390/polym11091520>.
- (116) Sivaraman, B.; Fears, K. P.; Latour, R. A. Investigation of the Effects of Surface Chemistry and Solution Concentration on the Conformation of Adsorbed Proteins Using an Improved Circular Dichroism Method. *Langmuir* **2009**, *25* (5), 3050–3056. <https://doi.org/10.1021/la8036814>.
- (117) Zheng, K.; Kapp, M.; Boccaccini, A. R. Protein Interactions with Bioactive Glass Surfaces: A Review. *Applied Materials Today* **2019**, *15*, 350–371. <https://doi.org/10.1016/j.apmt.2019.02.003>.

- (118) Evans-Nguyen, K. M.; Tolles, L. R.; Gorkun, O. V.; Lord, S. T.; Schoenfisch, M. H. Interactions of Thrombin with Fibrinogen Adsorbed on Methyl-, Hydroxyl-, Amine-, and Carboxyl-Terminated Self-Assembled Monolayers. *Biochemistry* **2005**, *44* (47), 15561–15568. <https://doi.org/10.1021/bi0514358>.
- (119) Chuang, W.-H.; Lin, J.-C. Surface Characterization and Platelet Adhesion Studies for the Mixed Self-Assembled Monolayers with Amine and Carboxylic Acid Terminated Functionalities. *Journal of Biomedical Materials Research Part A* **2007**, *82A* (4), 820–830. <https://doi.org/10.1002/jbm.a.31193>.
- (120) Rodrigues, S. N.; Gonçalves, I. C.; Martins, M. C. L.; Barbosa, M. A.; Ratner, B. D. Fibrinogen Adsorption, Platelet Adhesion and Activation on Mixed Hydroxyl-/Methyl-Terminated Self-Assembled Monolayers. *Biomaterials* **2006**, *27* (31), 5357–5367. <https://doi.org/10.1016/j.biomaterials.2006.06.010>.
- (121) Fernández-Montes Moraleda, B.; Román, J. S.; Rodríguez-Lorenzo, L. M. Influence of Surface Features of Hydroxyapatite on the Adsorption of Proteins Relevant to Bone Regeneration. *Journal of Biomedical Materials Research Part A* **2013**, *101A* (8), 2332–2339. <https://doi.org/10.1002/jbm.a.34528>.
- (122) Lim, J. Y.; Hansen, J. C.; Siedlecki, C. A.; Runt, J.; Donahue, H. J. Human Foetal Osteoblastic Cell Response to Polymer-Demixed Nanotopographic Interfaces. *Journal of The Royal Society Interface* **2005**, *2* (2), 97–108. <https://doi.org/10.1098/rsif.2004.0019>.
- (123) Kristensen, S. H.; Pedersen, G. A.; Nejsum, L. N.; Sutherland, D. S. Protein Adsorption at Nanopatterned Surfaces Studied by Quartz Crystal Microbalance with Dissipation and Surface Plasmon Resonance. *The Journal of Physical Chemistry B* **2013**, *117* (36), 10376–10383. <https://doi.org/10.1021/jp4038528>.
- (124) Han, M.; Sethuraman, A.; Kane, R. S.; Belfort, G. Nanometer-Scale Roughness Having Little Effect on the Amount or Structure of Adsorbed Protein. *Langmuir* **2003**, *19* (23), 9868–9872. <https://doi.org/10.1021/la030132g>.
- (125) Cai, K.; Bossert, J.; Jandt, K. D. Does the Nanometre Scale Topography of Titanium Influence Protein Adsorption and Cell Proliferation? *Colloids and Surfaces B: Biointerfaces* **2006**, *49* (2), 136–144. <https://doi.org/10.1016/j.colsurfb.2006.02.016>.
- (126) Rechendorff, K.; Hovgaard, M. B.; Foss, M.; Zhdanov, V. P.; Besenbacher, F. Enhancement of Protein Adsorption Induced by Surface Roughness. *Langmuir* **2006**, *22* (26), 10885–10888. <https://doi.org/10.1021/la0621923>.
- (127) Dolatshahi-Pirouz, A.; Pennisi, C. P.; Skeldal, S.; Foss, M.; Chevallier, J.; Zachar, V.; Andreasen, P.; Yoshida, K.; Besenbacher, F. The Influence of Glancing Angle Deposited Nanorough Platinum Surfaces on the Adsorption of Fibrinogen and the Proliferation of Primary Human Fibroblasts. *Nanotechnology* **2009**, *20* (9), 095101. <https://doi.org/10.1088/0957-4484/20/9/095101>.
- (128) Lord, M. S.; Whitelock, J. M.; Simmons, A.; Williams, R. L.; Milthorpe, B. K. Fibrinogen Adsorption and Platelet Adhesion to Silica Surfaces with Stochastic Nanotopography. *Biointerphases* **2014**, *9* (4), 041002. <https://doi.org/10.1116/1.4900993>.

- (129) Li, D.; Zheng, Q.; Wang, Y.; Chen, H. Combining Surface Topography with Polymer Chemistry: Exploring New Interfacial Biological Phenomena. *Polymer Chemistry* **2014**, *5* (1), 14–24. <https://doi.org/10.1039/C3PY00739A>.
- (130) Wenzel, R. N. Surface Roughness and Contact Angle. *The Journal of Physical and Colloid Chemistry* **1949**, *53* (9), 1466–1467. <https://doi.org/10.1021/j150474a015>.
- (131) Ye, X.; Shao, Y.; Zhou, M.; Li, J.; Cai, L. Research on Micro-Structure and Hemo-Compatibility of the Artificial Heart Valve Surface. *Applied Surface Science* **2009**, *255* (13–14), 6686–6690. <https://doi.org/10.1016/j.apsusc.2009.02.068>.
- (132) Koc, Y.; de Mello, A. J.; McHale, G.; Newton, M. I.; Roach, P.; Shirtcliffe, N. J. Nano-Scale Superhydrophobicity: Suppression of Protein Adsorption and Promotion of Flow-Induced Detachment. *Lab on a Chip* **2008**, *8* (4), 582. <https://doi.org/10.1039/b716509a>.
- (133) Vroman, L.; Adams, A. L. Adsorption of Proteins out of Plasma and Solutions in Narrow Spaces. *Journal of Colloid and Interface Science* **1986**, *111* (2), 391–402. [https://doi.org/10.1016/0021-9797\(86\)90042-1](https://doi.org/10.1016/0021-9797(86)90042-1).
- (134) Rothstein, J. P. Slip on Superhydrophobic Surfaces. *Annual Review of Fluid Mechanics* **2010**, *42* (1), 89–109. <https://doi.org/10.1146/annurev-fluid-121108-145558>.
- (135) Huang, Q.; Yang, Y.; Zheng, D.; Song, R.; Zhang, Y.; Jiang, P.; Vogler, E. A.; Lin, C. Effect of Construction of TiO<sub>2</sub> Nanotubes on Platelet Behaviors: Structure-Property Relationships. *Acta Biomaterialia* **2017**, *51*, 505–512. <https://doi.org/10.1016/j.actbio.2017.01.044>.
- (136) Lindon, J.; McManama, G.; Kushner, L.; Merrill, E.; Salzman, E. Does the Conformation of Adsorbed Fibrinogen Dictate Platelet Interactions with Artificial Surfaces? *Blood* **1986**, *68* (2), 355–362. <https://doi.org/10.1182/blood.V68.2.355.355>.
- (137) Wu, Y.; Simonovsky, F. I.; Ratner, B. D.; Horbett, T. A. The Role of Adsorbed Fibrinogen in Platelet Adhesion to Polyurethane Surfaces: A Comparison of Surface Hydrophobicity, Protein Adsorption, Monoclonal Antibody Binding, and Platelet Adhesion. *Journal of biomedical materials research. Part A* **2005**, *74A* (4), 722–738. <https://doi.org/10.1002/jbm.a.30381>.
- (138) Michael, K. E.; Vernekar, V. N.; Keselowsky, B. G.; Meredith, J. C.; Latour, R. A.; García, A. J. Adsorption-Induced Conformational Changes in Fibronectin Due to Interactions with Well-Defined Surface Chemistries. *Langmuir* **2003**, *19* (19), 8033–8040. <https://doi.org/10.1021/la034810a>.
- (139) Firkowska-Boden, I.; Helbing, C.; Dauben, T. J.; Jandt, K. D. How Nanotopography-Induced Conformational Changes of Fibrinogen Affect Platelet Adhesion and Activation. *Langmuir* **2020**, *36* (39), 11573–11580.
- (140) Song, S.; Ravensbergen, K.; Alabanza, A.; Soldin, D.; Hahm, J. Distinct Adsorption Configurations and Self-Assembly Characteristics of Fibrinogen on Chemically Uniform and Alternating Surfaces Including Block Copolymer Nanodomains. *ACS Nano* **2014**, *8* (5), 5257–5269. <https://doi.org/10.1021/nm5013397>.

- (141) Thyparambil, A. A.; Wei, Y.; Latour, R. A. Experimental Characterization of Adsorbed Protein Orientation, Conformation, and Bioactivity. *Biointerphases* **2015**, *10* (1), 019002. <https://doi.org/10.1116/1.4906485>.
- (142) Siedlecki, C. A.; Marchant, R. E. Atomic Force Microscopy for Characterization of the Biomaterial Interface. *Biomaterials* **1998**, *19* (4–5), 441–454. [https://doi.org/10.1016/S0142-9612\(97\)00222-6](https://doi.org/10.1016/S0142-9612(97)00222-6).
- (143) Chinn, J. A.; Posso, S. E.; Horbett, T. A.; Ratner, B. D. Postadsorptive Transition in Fibrinogen Adsorbed to Polyurethanes: Changes in Antibody Binding and Sodium Dodecyl Sulfate Elutability. *Journal of Biomedical Materials Research* **1992**, *26* (6), 757–778. <https://doi.org/10.1002/jbm.820260606>.
- (144) Horbett, T. A.; Cooper, K. W.; Lew, K. R.; Ratner, B. D. Rapid Postadsorptive Changes in Fibrinogen Adsorbed from Plasma to Segmented Polyurethanes. *Journal of Biomaterials Science, Polymer Edition* **1998**, *9* (10), 1071–1087. <https://doi.org/10.1163/156856298X00334>.
- (145) Shahryari, A.; Azari, F.; Vali, H.; Omanovic, S. The Response of Fibrinogen, Platelets, Endothelial and Smooth Muscle Cells to an Electrochemically Modified SS316LS Surface: Towards the Enhanced Biocompatibility of Coronary Stents. *Acta Biomaterialia* **2010**, *6* (2), 695–701. <https://doi.org/10.1016/j.actbio.2009.07.007>.
- (146) Tzoneva, R.; Heuchel, M.; Groth, T.; Altankov, G.; Albrecht, W.; Paul, D. Fibrinogen Adsorption and Platelet Interactions on Polymer Membranes. *Journal of Biomaterials Science, Polymer Edition* **2002**, *13* (9), 1033–1050. <https://doi.org/10.1163/156856202760319171>.
- (147) Ahmed, F.; Choudhury, N. R.; Dutta, N. K.; Brito e Abreu, S.; Zannettino, A.; Duncan, E. Interaction of Platelets with Poly(Vinylidene Fluoride- Co - Hexafluoropropylene) Electrospun Surfaces. *Biomacromolecules* **2014**, *15* (3), 744–755. <https://doi.org/10.1021/bm4015396>.
- (148) Zhao, A.; Wang, Z.; Zhou, S.; Xue, G.; Wang, Y.; Ye, C.; Huang, N. Titanium Oxide Films with Vacuum Thermal Treatment for Enhanced Hemocompatibility. *Surface Engineering* **2015**, *31* (12), 898–903. <https://doi.org/10.1179/1743294414Y.0000000367>.
- (149) Hu, Y.; Jin, J.; Liang, H.; Ji, X.; Yin, J.; Jiang, W. PH Dependence of Adsorbed Fibrinogen Conformation and Its Effect on Platelet Adhesion. *Langmuir* **2016**, *32* (16), 4086–4094. <https://doi.org/10.1021/acs.langmuir.5b04238>.
- (150) Zhang, L.; Casey, B.; Galanakis, D. K.; Marmorat, C.; Skoog, S.; Vorvolakos, K.; Simon, M.; Rafailovich, M. H. The Influence of Surface Chemistry on Adsorbed Fib.Pdf. *Acta Biomaterialia* **2017**, *54*, 164–174. <https://doi.org/10.1016/j.actbio.2017.03.002>.
- (151) Koo, J.; Galanakis, D.; Liu, Y.; Ramek, A.; Fields, A.; Ba, X.; Simon, M.; Rafailovich, M. H. Control of Anti-Thrombogenic Properties: Surface-Induced Self-Assembly of Fibrinogen Fibers. *Biomacromolecules* **2012**, *13* (5), 1259–1268. <https://doi.org/10.1021/bm2015976>.
- (152) Marchin, K. L.; Berrie, C. L. Conformational Changes in the Plasma Protein Fibrinogen upon Adsorption to Graphite and Mica Investigated by Atomic Force Microscopy. *Langmuir* **2003**, *19* (23), 9883–9888.

- (153) Cihova, M.; Müller, E.; Chandorkar, Y.; Thorwarth, K.; Fortunato, G.; Maniura-Weber, K.; Löffler, J. F.; Rottmar, M. Palladium-Based Metallic Glass with High Thrombogenic Resistance for Blood-Contacting Medical Devices. *Advanced Functional Materials* **2022**, *32* (4), 2108256. <https://doi.org/10.1002/adfm.202108256>.
- (154) Zhao, A.; Wang, Z.; Zhu, X.; Maitz, M. F.; Huang, N. Real-Time Characterization of Fibrinogen Interaction with Modified Titanium Dioxide Film by Quartz Crystal Microbalance with Dissipation. *Chinese Journal of Chemical Physics* **2014**, *27* (3), 355–360. <https://doi.org/10.1063/1674-0068/27/03/355-360>.
- (155) Zhang, X.; Helbing, C.; Arras, M. M. L.; Jandt, K. D.; Firkowska-Boden, I. *Langmuir* **2017**, *33* (26), 6563–6571. <https://doi.org/10.1021/acs.langmuir.7b01365>.
- (156) Xu, L.-C.; Bauer, J. W.; Siedlecki, C. A. Proteins, Platelets, and Blood Coagulation at Biomaterial Interfaces. *Colloids and Surfaces B: Biointerfaces* **2014**, *124*, 49–68. <https://doi.org/10.1016/j.colsurfb.2014.09.040>.
- (157) Helbing, C.; Stoeßel, R.; Hering, D. A.; Arras, M. M. L.; Bossert, J.; Jandt, K. D. PH-Dependent Ordered Fibrinogen Adsorption on Polyethylene Single Crystals. *Langmuir* **2016**, *32* (45), 11868–11877. <https://doi.org/10.1021/acs.langmuir.6b03110>.
- (158) Yamamoto, S.; Tanaka, M.; Sunami, H.; Arai, K.; Takayama, A.; Yamashita, S.; Morita, Y.; Shimomura, M. Relationship between Adsorbed Fibronectin and Cell Adhesion on a Honeycomb-Patterned Film. *Surface Science* **2006**, *600* (18), 3785–3791. <https://doi.org/10.1016/j.susc.2006.01.085>.
- (159) Vertegel, A. A.; Siegel, R. W.; Dordick, J. S. Silica Nanoparticle Size Influences the Structure and Enzymatic Activity of Adsorbed Lysozyme. *Langmuir* **2004**, *20* (16), 6800–6807. <https://doi.org/10.1021/la0497200>.
- (160) Lundqvist, M.; Sethson, I.; Jonsson, B.-H. Protein Adsorption onto Silica Nanoparticles: Conformational Changes Depend on the Particles' Curvature and the Protein Stability. *Langmuir* **2004**, *20* (24), 10639–10647. <https://doi.org/10.1021/la0484725>.
- (161) Shaw, C. P.; Middleton, D. A.; Volk, M.; Lévy, R. Amyloid-Derived Peptide Forms Self-Assembled Monolayers on Gold Nanoparticle with a Curvature-Dependent  $\beta$ -Sheet Structure. *ACS Nano* **2012**, *6* (2), 1416–1426. <https://doi.org/10.1021/nn204214x>.
- (162) Hulander, M.; Lundgren; Berglin; Ohrlander; Lausmaa; Elwing. Immune Complement Activation Is Attenuated by Surface Nanotopography. *International Journal of Nanomedicine* **2011**, 2653. <https://doi.org/10.2147/IJN.S24578>.
- (163) Roach, P.; Farrar, D.; Perry, C. C. Surface Tailoring for Controlled Protein Adsorption: Effect of Topography at the Nanometer Scale and Chemistry. *Journal of the American Chemical Society* **2006**, *128* (12), 3939–3945. <https://doi.org/10.1021/ja056278e>.
- (164) Visalakshan, R. M.; Cavallaro, A. A.; MacGregor, M. N.; Lawrence, E. P.; Koynov, K.; Hayball, J. D.; Vasilev, K. Nanotopography-Induced Unfolding of Fibrinogen Modulates Leukocyte Binding and Activation. *Advanced Functional Materials* **2019**, *29* (14), 1807453. <https://doi.org/10.1002/adfm.201807453>.



- (165) Klein, J. Probing the Interactions of Proteins and Nanoparticles. *Proceedings of the National Academy of Sciences* **2007**, *104* (7), 2029–2030. <https://doi.org/10.1073/pnas.0611610104>.
- (166) Treuel, L.; Nienhaus, G. U. Toward a Molecular Understanding of Nanoparticle–Protein Interactions. *Biophysical Reviews* **2012**, *4* (2), 137–147. <https://doi.org/10.1007/s12551-012-0072-0>.
- (167) Wang, H.; Akcora, P. Confinement Effect on the Structure and Elasticity of Proteins Interfacing Polymers. *Soft Matter* **2017**, *13* (8), 1561–1568. <https://doi.org/10.1039/C6SM02179D>.
- (168) Sutherland, D. S.; Broberg, M.; Nygren, H.; Kasemo, B. Influence of Nanoscale Surface Topography and Chemistry on the Functional Behaviour of an Adsorbed Model Macromolecule. *Macromolecular Bioscience* **2001**, *1*, 270–273.
- (169) Nandakumar, D.; Bendavid, A.; Martin, P. J.; Harris, K. D.; Ruys, A. J.; Lord, M. S. Fabrication of Semiordeed Nanopatterned Diamond-like Carbon and Titania Films for Blood Contacting Applications. *ACS Applied Materials & Interfaces* **2016**, *8* (11), 6802–6810. <https://doi.org/10.1021/acsami.5b11614>.
- (170) Smith, B. S.; Yoriya, S.; Grissom, L.; Grimes, C. A.; Popat, K. C. Hemocompatibility of Titania Nanotube Arrays. *Journal of Biomedical Materials Research Part A* **2010**, *95A* (2), 350–360. <https://doi.org/10.1002/jbm.a.32853>.
- (171) Bai, L.; Yang, Y.; Mendhi, J.; Du, Z.; Hao, R.; Hang, R.; Yao, X.; Huang, N.; Tang, B.; Xiao, Y. The Effects of TiO<sub>2</sub> Nanotube Arrays with Different Diameters on Macrophage/Endothelial Cell Response and *Ex Vivo* Hemocompatibility. *Journal of Materials Chemistry B* **2018**, *6* (39), 6322–6333. <https://doi.org/10.1039/C8TB01675E>.
- (172) Jia, E.; Zhao, X.; Lin, Y.; Su, Z. Protein Adsorption on Titanium Substrates and Its Effects on Platelet Adhesion. *Applied Surface Science* **2020**, *529*, 146986. <https://doi.org/10.1016/j.apsusc.2020.146986>.
- (173) Curtis, A.; Wilkinson, C. Topographical Control of Cells. *Biomaterials* **1997**, *18* (24), 1573–1583. [https://doi.org/10.1016/S0142-9612\(97\)00144-0](https://doi.org/10.1016/S0142-9612(97)00144-0).
- (174) Hulander, M.; Lundgren, A.; Faxälv, L.; Lindahl, T. L.; Palmquist, A.; Berglin, M.; Elwing, H. Gradients in Surface Nanotopography Used to Study Platelet Adhesion and Activation. *Colloids and Surfaces B: Biointerfaces* **2013**, *110*, 261–269. <https://doi.org/10.1016/j.colsurfb.2013.04.010>.
- (175) Lim, J. Y.; Donahue, H. J. Cell Sensing and Response to Micro- and Nanostructured Surfaces Produced by Chemical and Topographic Patterning. *Tissue Engineering* **2007**, *13* (8), 1879–1891. <https://doi.org/10.1089/ten.2006.0154>.
- (176) Koh, L. B.; Rodriguez, I.; Venkatraman, S. S. The Effect of Topography of Polymer Surfaces on Platelet Adhesion. *Biomaterials* **2010**, *31* (7), 1533–1545. <https://doi.org/10.1016/j.biomaterials.2009.11.022>.
- (177) Pham, T. T.; Wiedemeier, S.; Maenz, S.; Gastrock, G.; Settmacher, U.; Jandt, K. D.; Zanow, J.; Lüdecke, C.; Bossert, J. Hemodynamic Aspects of Reduced Platelet Adhesion on Bioinspired Microstructured Surfaces. *Colloids and Surfaces B: Biointerfaces* **2016**, *145*, 502–509. <https://doi.org/10.1016/j.colsurfb.2016.05.022>.

- (178) Minelli, C.; Kikuta, A.; Tsud, N.; Ball, M. D.; Yamamoto, A. A Micro-Fluidic Study of Whole Blood Behaviour on PMMA Topographical Nanostructures. *Journal of Nanobiotechnology* **2008**, *6* (1), 3. <https://doi.org/10.1186/1477-3155-6-3>.
- (179) Koh, L. B.; Rodriguez, I.; Venkatraman, S. S. A Novel Nanostructured Poly(Lactic-Co-Glycolic-Acid)–Multi-Walled Carbon Nanotube Composite for Blood-Contacting Applications: Thrombogenicity Studies. *Acta Biomaterialia* **2009**, *5* (9), 3411–3422. <https://doi.org/10.1016/j.actbio.2009.06.003>.
- (180) Milner, K. R.; Siedlecki, C. A.; Snyder, A. J. Development of Novel Submicron Textured Polyether(Urethane Urea) for Decreasing Platelet Adhesion. *ASAIO Journal* **2005**, *51* (5), 578–584. <https://doi.org/10.1097/01.mat.0000171594.44974.89>.
- (181) Sun, T.; Tan, H.; Han, D.; Fu, Q.; Jiang, L. No Platelet Can Adhere—Largely Improved Blood Compatibility on Nanostructured Superhydrophobic Surfaces. *Small* **2005**, *1* (10), 959–963. <https://doi.org/10.1002/sml.200500095>.
- (182) Ding, Y.; Leng, Y.; Huang, N.; Yang, P.; Lu, X.; Ge, X.; Ren, F.; Wang, K.; Lei, L.; Guo, X. Effects of Microtopographic Patterns on Platelet Adhesion and Activation on Titanium Oxide Surfaces. *Journal of Biomedical Materials Research Part A* **2013**, *101A* (3), 622–632. <https://doi.org/10.1002/jbm.a.34361>.
- (183) Minelli, C.; Kikuta, A.; Yamamoto, A. Blood Interaction with Nano-Topography. In *2006 International Conference on Nanoscience and Nanotechnology*; IEEE: Brisbane, QLD, Australia, 2006; p 4143382. <https://doi.org/10.1109/ICONN.2006.340602>.
- (184) Bui, V.-C.; Medvedev, N.; Apte, G.; Chen, L.-Y.; Denker, C.; Greinacher, A.; Nguyen, T.-H. Response of Human Blood Platelets on Nanoscale Groove Patterns: Implications for Platelet Storage. *ACS Applied Nano Materials* **2020**, *3* (7), 6996–7004. <https://doi.org/10.1021/acsnm.0c01326>.
- (185) Park, J. Y.; Gemmell, C. H.; Davies, J. E. Platelet Interactions with Titanium: Modulation of Platelet Activity by Surface Topography. *Biomaterials* **2001**, *22* (19), 2671–2682. [https://doi.org/10.1016/S0142-9612\(01\)00009-6](https://doi.org/10.1016/S0142-9612(01)00009-6).
- (186) Zhou, M.; Yang, J. H.; Ye, X.; Zheng, A. R.; Li, G.; Yang, P. F.; Zhu, Y.; Cai, L. Blood Platelet's Behavior on Nanostructured Superhydrophobic Surface. *Journal of Nano Research* **2008**, *2*, 129–136. <https://doi.org/10.4028/www.scientific.net/JNanoR.2.129>.
- (187) Drelich, J. W.; Boinovich, L.; Chibowski, E.; Della Volpe, C.; Hołysz, L.; Marmur, A.; Siboni, S. Contact Angles: History of over 200 Years of Open Questions. *Surface Innovations* **2020**, *8* (1–2), 3–27. <https://doi.org/10.1680/jsuin.19.00007>.
- (188) Wang, P.; Yu, Q.; Yuan, X.; Cui, Z.; Liu, Y.; Gao, N.; Jin, H.; Cheng, S.; Liu, J.; Li, H. Effect of Boron Doping Concentration on the Wettability and Surface Free Energy of Polycrystalline Boron-Doped Diamond Film. *Coatings* **2023**, *13* (2), 305. <https://doi.org/10.3390/coatings13020305>.
- (189) Tam, J.; Feng, B.; Ikuhara, Y.; Ohta, H.; Erb, U. Crystallographic Orientation–Surface Energy–Wetting Property Relationships of Rare Earth Oxides. *Journal of Materials Chemistry A* **2018**, *6* (38), 18384–18388. <https://doi.org/10.1039/C8TA04938F>.

- (190) Baszkin, A.; Lyman, D. J. The Interaction of Plasma Proteins with Polymers. I. Relationship between Polymer Surface Energy and Protein Adsorption/Desorption. *Journal of Biomedical Materials Research* **1980**, *14* (4), 393–403. <https://doi.org/10.1002/jbm.820140406>.
- (191) Michiardi, A.; Aparicio, C.; Ratner, B. D.; Planell, J. A.; Gil, J. The Influence of Surface Energy on Competitive Protein Adsorption on Oxidized NiTi Surfaces. *Biomaterials* **2007**, *28* (4), 586–594. <https://doi.org/10.1016/j.biomaterials.2006.09.040>.
- (192) Cai, Y.; Li, H.; Karlsson, M.; Leifer, K.; Engqvist, H.; Xia, W. Biomineralization on Single Crystalline Rutile: The Modulated Growth of Hydroxyapatite by Fibronectin in a Simulated Body Fluid. *RSC Advances* **2016**, *6* (42), 35507–35516. <https://doi.org/10.1039/C6RA04303H>.
- (193) Buchloh, S. Hepatocyte Performance on Different Crystallographic Faces of Rutile. *Biomaterials* **2003**, *24* (15), 2605–2610. [https://doi.org/10.1016/S0142-9612\(03\)00064-4](https://doi.org/10.1016/S0142-9612(03)00064-4).
- (194) Keller, T. F.; Reichert, J.; Thanh, T. P.; Adjiski, R.; Spiess, L.; Berzina-Cimdina, L.; Jandt, K. D.; Bossert, J. Facets of Protein Assembly on Nanostructured Titanium Oxide Surfaces. *Acta Biomaterialia* **2013**, *9* (3), 5810–5820. <https://doi.org/10.1016/j.actbio.2012.10.045>.
- (195) Yan, J.; Wu, G.; Guan, N.; Li, L.; Li, Z.; Cao, X. Understanding the Effect of Surface/Bulk Defects on the Photocatalytic Activity of TiO<sub>2</sub>: Anatase versus Rutile. *Physical Chemistry Chemical Physics* **2013**, *15* (26), 10978. <https://doi.org/10.1039/c3cp50927c>.
- (196) Moatti, A.; Bayati, R.; Narayan, J. Epitaxial Growth of Rutile TiO<sub>2</sub> Thin Films by Oxidation of TiN/Si{100} Heterostructure. *Acta Materialia* **2016**, *103*, 502–511. <https://doi.org/10.1016/j.actamat.2015.10.022>.
- (197) Watanabe, T.; Yoshida, N. Wettability Control of a Solid Surface by Utilizing Photocatalysis. *The Chemical Record* **2008**, *8* (5), 279–290. <https://doi.org/10.1002/tcr.20154>.
- (198) Bousnaki, M.; Koidis, P. Advances on Biomedical Titanium Surface Interactions. *Journal of Biomimetics, Biomaterials and Tissue Engineering* **2014**, *19*, 43–64. <https://doi.org/10.4028/www.scientific.net/JBBTE.19.43>.
- (199) Keller, T. F.; Schönfelder, J.; Reichert, J.; Tuccitto, N.; Licciardello, A.; Messina, G. M. L.; Marletta, G.; Jandt, K. D. How the Surface Nanostructure of Polyethylene Affects Protein Assembly and Orientation. *ACS Nano* **2011**, *5* (4), 3120–3131. <https://doi.org/10.1021/nn200267c>.
- (200) Agnihotri, A.; Siedlecki, C. A. Time-Dependent Conformational Changes in Fibrinogen Measured by Atomic Force Microscopy. *Langmuir* **2004**, *20* (20), 8846–88527.
- (201) Silva-Bermudez, P.; Muhl, S.; Rodil, S. E. A Comparative Study of Fibrinogen Adsorption onto Metal Oxide Thin Films. *Applied Surface Science* **2013**, *282*, 351–362. <https://doi.org/10.1016/j.apsusc.2013.05.133>.
- (202) Sommerfeld, J.; Richter, J.; Niepelt, R.; Kosan, S.; Keller, T. F.; Jandt, K. D.; Ronning, C. Protein Adsorption on Nano-Scaled, Rippled TiO<sub>2</sub> and Si Surfaces. *Biointerphases* **2012**, *7* (1), 55. <https://doi.org/10.1007/s13758-012-0055-5>.

- (203) Vogler, E. A. Water and the Acute Biological Response to Surfaces. *Journal of Biomaterials Science, Polymer Edition* **1999**, *10* (10), 1015–1045. <https://doi.org/10.1163/156856299X00667>.
- (204) Lindahl, C.; Borchardt, P.; Lausmaa, J.; Xia, W.; Engqvist, H. Studies of Early Growth Mechanisms of Hydroxyapatite on Single Crystalline Rutile: A Model System for Bioactive Surfaces. *Journal of Materials Science: Materials in Medicine* **2010**, *21* (10), 2743–2749. <https://doi.org/10.1007/s10856-010-4137-y>.
- (205) Ahmed, M.; Byrne, J. A.; McLaughlin, J. A. D. Glycine Adsorption onto DLC and N-DLC Thin Films Studied by XPS and AFM. *e-Journal of Surface Science and Nanotechnology* **2009**, *7*, 217–224. <https://doi.org/10.1380/ejsnt.2009.217>.
- (206) Kim, H. J.; Bae, I.-S.; Cho, S.-J.; Boo, J.-H.; Lee, B.-C.; Heo, J.; Chung, I.; Hong, B. Synthesis and Characteristics of NH<sub>2</sub>-Functionalized Polymer Films to Align and Immobilize DNA Molecules. *Nanoscale Research Letters* **2012**, *7* (1), 30. <https://doi.org/10.1186/1556-276X-7-30>.
- (207) Liu, W.; Wang, J.; Li, W.; Guo, X.; Lu, L.; Lu, X.; Feng, X.; Liu, C.; Yang, Z. A Shortcut for Evaluating Activities of TiO<sub>2</sub> Facets: Water Dissociative Chemisorption on TiO<sub>2</sub>-B (100) and (001). *Physical Chemistry Chemical Physics* **2010**, *12* (31), 8721. <https://doi.org/10.1039/b920128a>.
- (208) Harnett, E. M.; Alderman, J.; Wood, T. K. *Colloids and Surfaces B: Biointerfaces* **2007**, *55* (1), 90–97. <https://doi.org/10.1016/j.colsurfb.2006.11.021>.
- (209) Landoulsi, J.; Dupres, V. Direct AFM Force Mapping of Surface Nanoscale Organization and Protein Adsorption on an Aluminum Substrate. *Physical Chemistry Chemical Physics* **2013**, *15* (21), 8429. <https://doi.org/10.1039/c3cp00137g>.
- (210) Braune, S.; Fröhlich, G. M.; Lendlein, A.; Jung, F. Effect of Temperature on Platelet Adherence. *Clinical Hemorheology and Microcirculation* **2016**, *61* (4), 681–688. <https://doi.org/10.3233/CH-152028>.
- (211) Jones, M. I.; McColl, I. R.; Grant, D. M.; Parker, K. G.; Parker, T. L. Protein Adsorption and Platelet Attachment and Activation, on TiN, TiC, and DLC Coatings on Titanium for Cardiovascular Applications. **2000**, *52* (2), 413–421. [https://doi.org/10.1002/1097-4636\(200011\)52:2%3C413::aid-jbm23%3E3.0.co;2-u](https://doi.org/10.1002/1097-4636(200011)52:2%3C413::aid-jbm23%3E3.0.co;2-u).
- (212) Okpalugo, T. I. T.; Ogwu, A. A. DLC Thin Films for Implantable Medical Devices. In *Thin Film Coatings for Biomaterials and Biomedical Applications*; Elsevier, 2016; pp 261–287. <https://doi.org/10.1016/B978-1-78242-453-6.00011-0>.
- (213) Doolittle, R. F.; Goldbaum, D. M.; Doolittle, L. R. Designation of Sequences Involved in the “Coiled-Coil” Interdomainal Connections in Fibrinogen: Construction of an Atomic Scale Model. *Journal of Molecular Biology* **1978**, *120* (2), 311–325. [https://doi.org/10.1016/0022-2836\(78\)90070-0](https://doi.org/10.1016/0022-2836(78)90070-0).
- (214) Tsai, W.; Grunkemeier, J. M.; Horbett, T. A. Variations in the Ability of Adsorbed Fibrinogen to Mediate Platelet Adhesion to Polystyrene-Based Materials: A Multivariate Statistical Analysis of Antibody Binding to the Platelet Binding Sites of Fibrinogen. *Journal of Biomedical Materials Research Part A* **2003**, *67A* (4), 1255–1268. <https://doi.org/10.1002/jbm.a.20024>.

- (215) Kallas, P.; Valen, H.; Hulander, M.; Gadegaard, N.; Stormonth-Darling, J.; O'Reilly, P.; Thiede, B.; Andersson, M.; Haugen, H. J. Protein-Coated Nanostructured Surfaces Affect the Adhesion of *Escherichia Coli*. *Nanoscale* **2022**, *14* (20), 7736–7746. <https://doi.org/10.1039/D2NR00976E>.
- (216) Milisavljevic, I.; Wu, Y. Current Status of Solid-State Single Crystal Growth. *BMC Materials* **2020**, *2* (1), 2. <https://doi.org/10.1186/s42833-020-0008-0>.
- (217) Diebold, U. Specimen Treatments: Surface Preparation of Metal Compound Materials (Mainly Oxides). In *Specimen Handling, Preparation, and Treatments in Surface Characterization*; Springer US: Boston, MA, 2002; pp 145–171. [https://doi.org/10.1007/0-306-46913-8\\_5](https://doi.org/10.1007/0-306-46913-8_5).
- (218) Xin, T.; Wong, H. Grain-Boundary Grooving by Surface Diffusion with Strong Surface Energy Anisotropy. *Acta Materialia* **2003**, *51* (8), 2305–2317. [https://doi.org/10.1016/S1359-6454\(03\)00039-9](https://doi.org/10.1016/S1359-6454(03)00039-9).
- (219) Firment, L. E. Thermal Faceting of the Rutile TiO<sub>2</sub>(001) Surface. *Surface Science* **1982**, *116* (2), 205–216. [https://doi.org/10.1016/0039-6028\(82\)90428-9](https://doi.org/10.1016/0039-6028(82)90428-9).
- (220) Lowekamp, J. B.; Rohrer, G. S.; Morris Hotsenpiller, P. A.; Bolt, J. D.; Farneth, W. E. Anisotropic Photochemical Reactivity of Bulk TiO<sub>2</sub> Crystals. *The Journal of Physical Chemistry B* **1998**, *102* (38), 7323–7327. <https://doi.org/10.1021/jp982721e>.
- (221) Kubo, T.; Orita, H.; Nozoye, H. Surface Structures of Rutile TiO<sub>2</sub> (011). *Journal of the American Chemical Society* **2007**, *129* (34), 10474–10478. <https://doi.org/10.1021/ja072281h>.
- (222) Yang, Y.; Yu, M.; Böke, F.; Qin, Q.; Hübner, R.; Knust, S.; Schwiderek, S.; Grundmeier, G.; Fischer, H.; Keller, A. Effect of Nanoscale Surface Topography on the Adsorption of Globular Proteins. *Applied Surface Science* **2021**, *535*, 147671. <https://doi.org/10.1016/j.apsusc.2020.147671>.
- (223) Gessner, A.; Waicz, R.; Lieske, A.; Paulke, B.-R.; Mäder, K.; Müller, R. H. Nanoparticles with Decreasing Surface Hydrophobicities: Influence on Plasma Protein Adsorption. *International Journal of Pharmaceutics* **2000**, *196* (2), 245–249. [https://doi.org/10.1016/S0378-5173\(99\)00432-9](https://doi.org/10.1016/S0378-5173(99)00432-9).
- (224) Wu, Z.; Chen, H.; Huang, H.; Zhao, T.; Liu, X.; Li, D.; Yu, Q. A Facile Approach to Modify Polyurethane Surfaces for Biomaterial Applications. *Macromolecular Bioscience* **2009**, *9* (12), 1165–1168. <https://doi.org/10.1002/mabi.200900221>.
- (225) Comelles, J.; Estévez, M.; Martínez, E.; Samitier, J. The Role of Surface Energy of Technical Polymers in Serum Protein Adsorption and MG-63 Cells Adhesion. *Nanomedicine: Nanotechnology, Biology and Medicine* **2010**, *6* (1), 44–51. <https://doi.org/10.1016/j.nano.2009.05.006>.

## Acknowledgments

I would like to express my gratitude to Prof. Klaus D. Jandt for giving me the chance to work in his research group, for his kind support during PhD project, and most of all, for motivation to continue personal growth and broadening of horizons.

I would like to thank also Dr. Izabela Firkowska-Boden for her interest, valuable pieces of advice, and substantive pointers while working together on publications. Also, for lots of care and encouragement during hard moments.

Many thanks to all colleagues from Prof. Jandt's group, especially to Karl Scheuer, Jörg Boßert, Thomas Dauben, Christian Helbing, Inez Thiele, Heidrun Garlipp, and Ralf Wagner for their support during the experimental part of this work, patience and lots of kindness from the beginning of my stay in Jena.

In particular, I would like to thank my husband, Jakub Struczyński, who supported and motivated me throughout the entire duration of my PhD work. For hours spent listening to my ideas, helping with solving problems, and motivation to act in the most difficult moments. Your words: "Never give up, you can do anything!" will stay in my heart forever.

Finally, I would like to thank my parents, without whom I would not be the person I am Today. For continuous motivation and support throughout my education path.

Wreszcie, dziękuję moim Rodzicom. Bez nich nie byłabym tym, kim jestem dzisiaj. Za ich wsparcie, motywację na całej mojej drodze edukacji, od trudnych początków w szkole podstawowej aż do dzisiaj, kiedy to składam moją pracę doktorską

Thank You!

## Appendix

**Table A1.** Elemental composition on rutile single crystals surface after HPF adsorption

	Element	Position (eV)	Compound of reference	Band area (%)			
				(110)	(100)	(101)	(001)
CARBON (C 1s)							
C1	C-(C, H)	285.0	hydrocarbon, adventitious contamination	50	52	52	54
C2	C-N, C-O, (C=O)-O-C	286.5	amine, alcohol, ester	21	18	18	15
C3	C=O, O-C-O, (C=O)-N-C,	288.4	aldehyde, (hemi)acetal, amide, peptide link;	21	21	21	22
C4	(C=O)-O-R, (C=O)-OH	290.1	ester, carboxylic acid	8	9	9	9
NITROGEN (N 1s)							
N1	C-N/C-H	398.4	amine, imine	16	12	12	9
N2	(C=O)-NH	400.1	amide, peptide linked	74	73	73	72
N3	C-NH <sub>3</sub> <sup>+</sup>	401.2	protonated amine	10	15	15	19

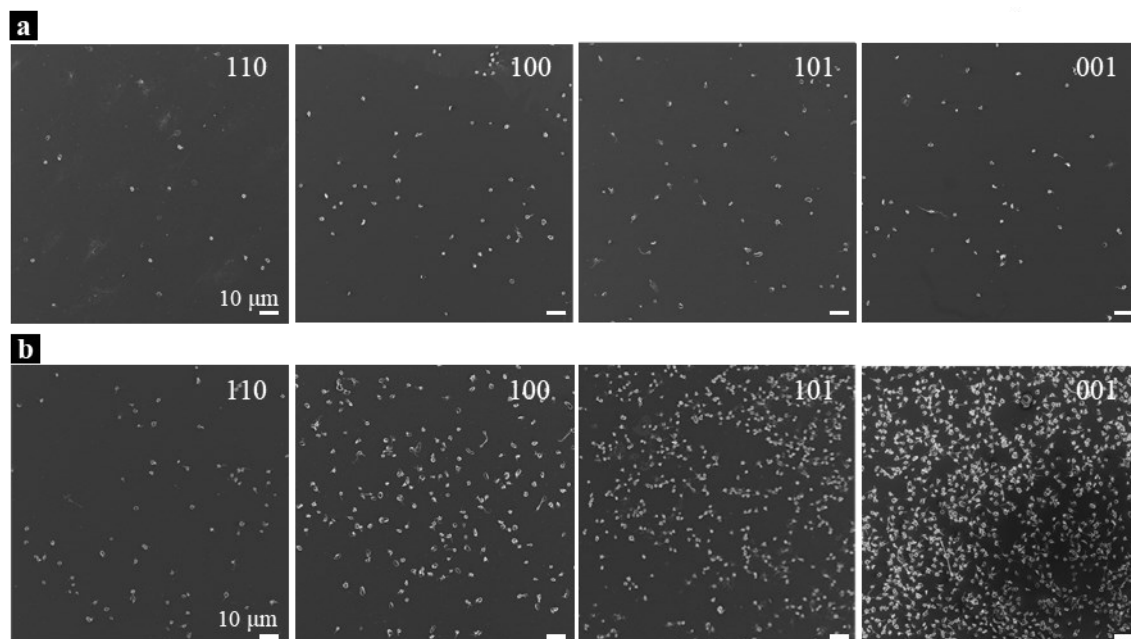


**Figure A1.** SEM images of rutile single crystals immersed for a) 5 min and b) 120 min in PPP under static conditions.